RĪGAS TEHNISKĀ UNIVERSITĀTE

Edvīns Ļetko

ZUDUMRADOŠU MODU REZONANSE INTEGRĒTAJĀ FOTONIKAS ČIPĀ

Promocijas darbs

LOSSY MODE RESONANCE PHENOMENON IN PHOTONIC INTEGRATED CIRCUITS

Doctoral Thesis

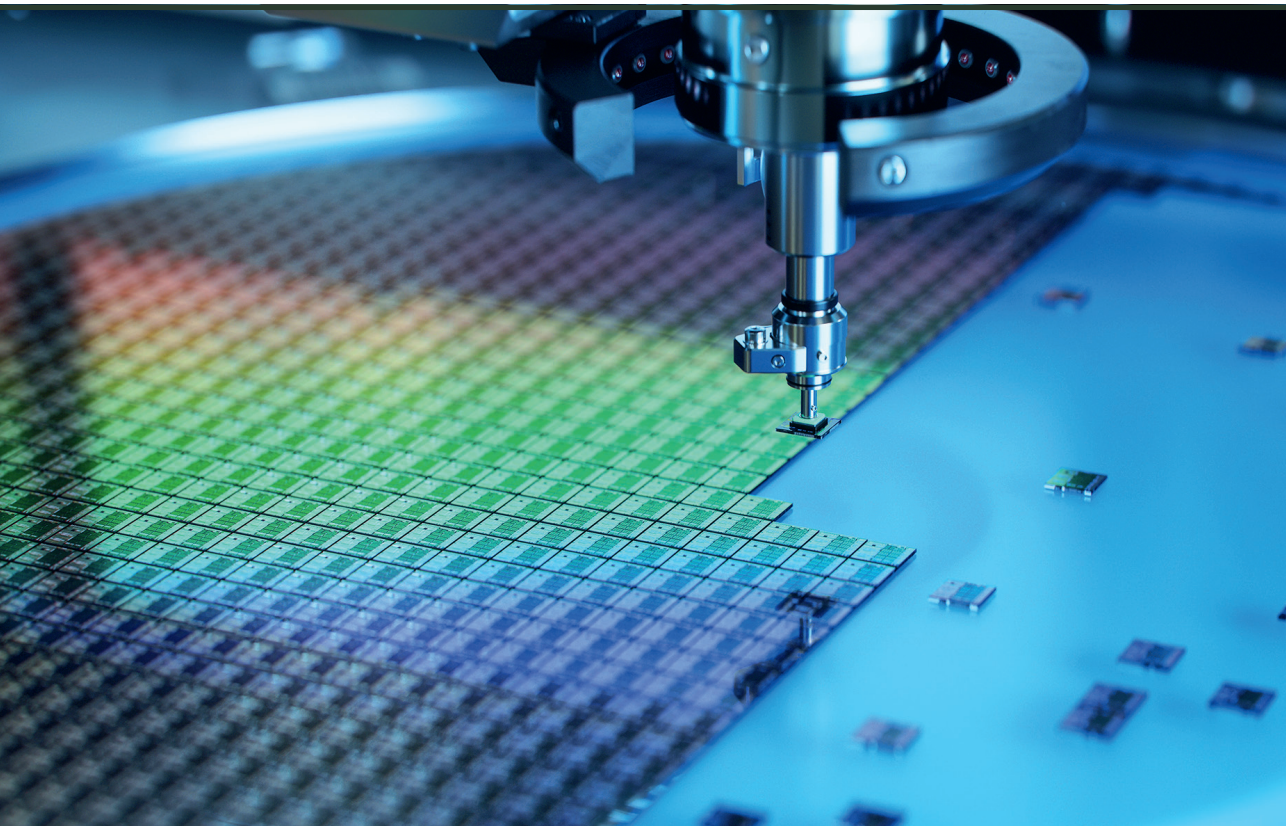

RTU Izdevniecība
RTU Press
Rīga 2025

RĪGAS TEHNISKĀ UNIVERSITĀTE
Dabaszinātņu un tehnoloģiju fakultāte
Tehniskās fizikas institūts

RIGA TECHNICAL UNIVERSITY
Faculty of Natural Sciences and Technology
Institute of Technical Physics

Edvīns Ļetko
Doktora studiju programmas "Ķīmija, materiālzinātne un tehnoloģijas" doktorants
Doctoral Student of the Study Program "Chemistry, Materials Science and Engineering"

ZUDUMRADOŠU MODU REZONANSE INTEGRĒTAJĀ FOTONIKAS ČIPĀ

Promocijas darbs

LOSSY MODE RESONANCE PHENOMENON IN PHOTONIC INTEGRATED CIRCUITS

Doctoral Thesis

Zinātniskie vadītāji / Scientific supervisors:
Dr. sc. ing. / Dr. sc. ing.
GATIS MOZOĻEVSKIS
asociētā profesore *Dr. phys.* / Associate Professor Dr. phys.
ILZE KLINCĀRE

RTU Izdevniecība / RTU Press

Rīga 2025 / Riga 2025

Ļetko, E. Zudumradošu modu rezonanse integrētajā fotonikas čipā. Promocijas darbs. – Rīga: RTU Izdevniecība, 2025. – 95 lpp.

Letko, E. Lossy Mode Resonance Phenomenon in Photonic Integrated Circuits. Doctoral Thesis. – Riga: RTU Press, 2025. – 95 p.

Iespiests saskaņā ar promocijas padomes "RTU P-02" 2025. gada 28. janvāra lēmumu, protokols Nr. 04030-9.2.2/1.

Published in accordance with the decision of the Promotion Council "RTU P-02" of 28 January 2025, Minutes No. 04030-9.2.2/1.

Promocijas darbs tika izstrādāts ar palīdzību no

- Eiropas Reģionālās attīstības fonda daļējo atbalstu projektā 1.1.1.1/20/A/045 un Eiropas Savienības Horizon 2020 programmas H2020-WIDESPREAD-01-2016-2017-TeamingPhase2 (projekta Nr. 739508, CAMART2);
- Nacionālās Pētījuma programmas (projekta Nr. VPPEM-FOTONIKA-2022/1-0001).

The Doctoral Thesis has been developed with the support from

- the European Regional Development Fund project "Development of a Novel Microfluidic Device for Label-Free Quantification of Prostate Cancer-Derived Extracellular Vesicles and Analysis of their RNA Content" (PROCEX) (1.1.1.1/20/A/045) and the European Union's Horizon 2020 Framework Program H2020-WIDESPREAD-01-2016-2017-TeamingPhase2 under grant agreement No. 739508, project CAMART2;
- the National Research Program "Smart Materials, Photonics, Technologies and Engineering Ecosystem" (project No. VPPEM-FOTONIKA-2022/1-0001).

PATEICĪBAS

Paldies maniem darba vadītājiem *Dr. sc. ing.* Gatim Mozoļevskim un asociētajai profesorei *Dr. phys.* Ilzei Klincārei par viņu ieguldījumu un nozīmīgo atbalstu visa darba tapšanas laikā! Vēlos pateikties arī savam kolēģim *Dr. phys.* Artūram Bundulim par lielo atbalstu un ieguldījumu visos ar darbu saistītajos pētījumos, kā arī *Dr. phys. Ignacio Del Villar* par noderīgajiem padomiem darba laikā.

Vislielākais paldies par finansiālo atbalstu, ko visa darba izstrādes laikā nodrošināja Cietvielu fizikas institūts, *Cellboxlabs Ltd.* un *CAMART2*! Paldies arī Rīgas Tehniskajai universitātei par sniegto atbalstu!

Edvīns Ļetko

ACKNOWLEDGEMENT

I extend my gratitude to my supervisors, Dr. sc. ing. Gatis Mozolevskis and Associate Professor Dr. phys. Ilze Klincāre, for their generous and invaluable support throughout the writing of the Thesis. Additionally, I would like to acknowledge my colleague Dr. phys. Arturs Bundulis for his extensive support and contribution to all research associated with the Thesis, as well as Dr. phys. Ignacio Del Villar for his helpful advice during the Thesis.

I am also deeply appreciate the financial support provided by the Institute of Solid State Physics, Cellboxlabs Ltd., and CAMART2 while writing the Thesis. Furthermore, I am grateful for the support from Riga Technical University.

Edvins Letko

SATURS

AUTORA IEGULDĪJUMS

Promocijas darba pamatā esošie zinātniskie raksti ir komandas darba rezultāts, un visu līdzautoru zināšanas dažādās jomās ir bijis nozīmīgs ieguldījums. Promocijas darba autora ieguldījums zinātniskajos rakstos apkopots 1. tabulā. Neviens no minētajiem rakstiem citos promocijas darbos nav iekļauts.

1. tabula

Autora ieguldījums, sagatavojot katru promocijas darbā iekļauto zinātnisko rakstu

1. publikācija	Polimēru viļņvadu izgatavošana, izmantojot fotolitogrāfiju. Zudumradošo pārklājumu nogulsnēšana uz integrētajiem viļņvadiem, izmantojot magnetrona putināšanu. Datu vizualizācija. Raksta sagatavošana. Autora procentuālais ieguldījums – 90 %.
2. publikācija	Ierīces simulācijas. Datu vizualizācija. Raksta sagatavošana. Autora procentuālais ieguldījums – 95 %.
3. publikācija	Zudumradošo pārklājumu nogulsnēšana, izmantojot magnetrona putināšanu. Datu vizualizācija. Raksta sagatavošana. Autora procentuālais ieguldījums – 90 %.
4. publikācija	Polimēru viļņvadu izgatavošana, izmantojot fotolitogrāfiju. Zudumradošo pārklājumu nogulsnēšana, izmantojot magnetrona putināšanu. Ierīces simulācijas. Datu vizualizācija. Raksta sagatavošana. Autora procentuālais ieguldījums – 85 %.

SAĪSINĀJUMI

CMOS	komplementārais metāla oksīda pusvadītājs
DC	līdzstrāva
FEM	galīgā elementu metode
FOM	labuma skaitlis
FWHM	pilnais platums pusminimumā
HB	gala cietināšana
ITO	indija alvas oksīds
LMR	zudumradošo modu rezonanse
MMF	daudzmodu šķiedra
PAA	poliakrilskābe
PAH	polialilamīna hidrohlorīds
PEB	pēc ekspozīcijas cietināšana
PIC	integrētās fotonikas čips
POC	pacienttuva
PSS	polinātrija stirensulfonāts
PVDF	polivinilidēnfluorīds
Q-factor	labums
RFOM	pieņemams labuma skaitlis
RH	relatīvais mitrums
RIU	laušanas koeficienta vienība
SB	pirms ekspozīcijas cietināšana
SEM	skenējošais elektronu mikroskops
SPR	virsmas plazmonu rezonanse
TE	šķērsvirziena elektriskā
TM	šķērsvirziena magnētiskā
UV	ultravioletais
VOC	gaistošs organisks savienojums
WG	viļņvads

DARBA VISPĀRĒJS RAKSTUROJUMS

Ievads

Zudumradošo modu rezonanses principi

Zudumradošo modu rezonanse (*LMR*) rodas, kad gaisma izplatās caur optisko šķiedru vai viļņvadu un mijiedarbojas ar plāno kārtiņu, kuras dielektriskās caurlaidības reālā komponente ir lielāka pēc absolūtās vērtības gan par pašas kārtiņas dielektriskās caurlaidības imagināro komponenti, gan par šķiedras vai viļņvada dielektriskās caurlaidības reālo komponenti[1]. Šīs plānās kārtiņas esamība pa virsu optiskai šķiedrai vai viļņvadam rada zuduma līnijas caurlaidības spektrā. Šīs zuduma līnijas parādās, pateicoties mijiedarbībai starp serdes modām viļņvadā un zuduma modām plānā kārtiņā[2]. Šo zudumu līniju viļņa garumi ir atkarīgi no vairākiem ārējiem parametriem (piemēram, pH[3] vai mitruma[4]), tāpēc tie tiek izmantoti vairākos sensora lietojumos[5].

LMR piedāvā vairākas priekšrocības, salīdzinot ar citām šķiedru vai viļņvadu metodēm. Atšķirībā no virmas plazmonu rezonanses (*SPR*) un citām bieži izmantotām metodēm *LMR* ir spējīgs radīt vairākas rezonanses vienlaikus. Turklāt, salīdzinot ar *SPR*, *LMR* efekts tiek novērots gan ar šķērsvirziena elektrisku (*TE*) polarizāciju, gan ar šķērsvirziena magnētisku (*TM*) polarizāciju[5]. *LMR* var tikt sasniegts, izmantojot dažādus materiālus, piemēram, polimērus[3], pusvadītājus[6] un dielektriķus[7], tāpēc tas piedāvā lielāku lietojuma elastību un palīdz samazināt ierīču izgatavošanas izmaksas.

LMR parādības matemātiskais modelis

Viļņvadā vadītās gaismas mijiedarbība ar plāno kārtiņu var radīt konstruktīvu vai destruktīvu interferenci, rezultātā pastiprinot gaismas absorbciju pie noteiktiem viļņa garumiem. Šīs plānās kārtiņas esamība ievieš papildu fāzes nobīdi un maina vadītās modas efektīvo laušanas koeficientu, tādējādi ietekmējot interferences apstākļus. Tas kalpo kā pamata mehānisms *LMR* parādībai viļņvados ar plānās kārtiņas perturbācijām[8].

Kad gaisma izplatās cauri viļņvadam un krītošais leņķis θ_1 uz saskarnes robežas starp viņvadu un plāno kārtiņu ir pietiekami liels, tad tās apkārtnē notiek pilnīgā atstarošanās. Gaisma, kas izplatās, šajā gadījumā mijiedarbojas ar pārklājumu, pateicoties izdziestošajam laukam. Vienkāršotai parādības analīzei un raksturošanai tiek izmantota divu staru interferences aproksimācija (1. att.)[8].

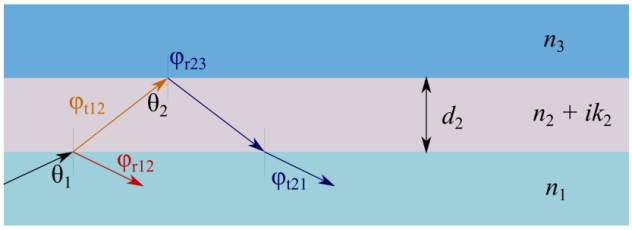

1. att. *LMR* parādības viļņvadā fizikālais modelis[8].

Izmantojot Freneļa vienādojumus un daudzstaru interferenču teoriju, var atvasināt vienādojumus, kas ar labu precizitāti apraksta *LMR* parādību. Situācijās, kad $\theta_1 \approx 90\,°$, kā tas parasti notiek viļņvadu un optisko šķiedru gadījumos, rezonanses viļņa garumu, pie kura notiek destruktīvā interference, var izteikt ar 1. vienādojumu[8]:

$$\lambda_{\mathrm{LMR}} = \frac{2\pi d_2 \sqrt{n_2^2 - n_1^2}}{m\pi + \arctan\left(\left(\frac{n_2^2}{n_3^2}\right)^s \frac{\sqrt{n_1^2 - n_3^2}}{\sqrt{n_2^2 - n_1^2}}\right)}, \tag{1}$$

kur λ_{LMR} – LMR viļņa garums, d_2 – pārklājuma biezums, m – interferenču kārta, n_1, n_2 un n_3 – attiecīgi viļņvada, pārklājuma un apkārtējās vides laušanas koeficienti. Parameters s 1. vienādojumā tiek definēts ar 2. vienādojumu[8] un ir atkarīgs no gaismas polarizācijas:

$$s = \begin{cases} 1 \text{ for TM mode} \\ 0 \text{ for TE mode} \end{cases}. \tag{2}$$

LMR_{TE} un LMR_{TM} demonstrē līdzīgas īpašības, izņemot atšķirīgus rezonanses viļņa garumus un jutību pret apkārtējās vides izmaiņām[8], līdz ar to turpmākā analīze koncentrēsies tikai uz *TM* polarizāciju. Jutību S pie tā paša krītošā leņķa θ_1 var izteikt ar 3. vienādojumu[8]:

$$S = \frac{2\pi n_2^2 d_2 \left(\frac{1}{n_3\sqrt{n_1^2 - n_3^2}} + \frac{2\sqrt{n_1^2 - n_3^2}}{n_3^2}\right)}{\arctan^2\left(\frac{\sqrt{n_1^2 - n_3^2}}{\sqrt{n_2^2 - n_1^2}}\right)\left(1 + \frac{n_2^4(n_1^2 - n_3^2)}{n_3^4(n_2^2 - n_1^2)}\right)}. \tag{3}$$

LMR parādības kontekstā tādi parametri kā pusminimuma platums (*FWHM*) un pīķa dziļums ir gandrīz tikpat būtiski kā rezonanses viļņa garums un jutība. *LMR* pīķa *FWHM* var noteikt, izmantojot 4. vienādojumu[8].

$$FWHM = \frac{4\pi d_2 \left(n_2^2 - n_1^2 + \lambda_{\mathrm{LMR}}\left(n_1 \left.\frac{\partial n_1}{\partial \lambda}\right|_{\lambda=\lambda_{\mathrm{LMR}}} - n_2 \left.\frac{\partial n_2}{\partial \lambda}\right|_{\lambda=\lambda_{\mathrm{LMR}}}\right)\right)}{\lambda_{\mathrm{LMR}}^2 \sqrt{n_2^2 - n_1^2}} \tag{4}$$

LMR pīķa dziļumu D var noteikt, izmantojot 5. vienādojumu[8].

$$D = \frac{4\sqrt{R_{12}R_{23}}(1-R_{12})(1-R_{23})}{(1-R_{12}R_{23})^2}, \quad (5)$$

kur R_{12} un R_{23} – atstarošanās spējas attiecīgi uz viļņvada un pārklājuma saskarnes robežvirsmas un pārklājuma un vides saskarnes robežvirsmas.

Galvenie lietojumi *LMR* jomā

Optisko šķiedru sensori, kuru pamatā ir *LMR* parādība, tiek plaši izmantoti fizikālo, ķīmisko un bioloģisko parametru mērīšanai. Šos sensorus izmanto pārtikas kvalitātes novērtēšanā, medicīniskajā diagnostikā un vides uzraudzībā. Turklāt *LMR* ierīces ir perspektīva platforma dažāda veida sensoru realizācijā, īpaši biosensoru jomā[9].

LMR parādības spēja noteikt relatīvo mitrumu (*RH*) ir pētīta literatūrā. Pētījumā[10] optiskās šķiedras, kas tika pārklātas ar TiO_2/PSS, tika izmantotas kā efektīvās ierīces *RH* noteikšanai. Paaugstināta mitruma klātbūtne izraisa ūdens plānās kārtiņas veidošanos kondensācijas rezultātā, kas savukārt ļauj noteikt *RH* līmeni gaisā. Rezonanses viļņa garuma nobīde gadījumā, kad *RH* mainās no 20 % līdz 90 %, redzama 2. attēlā.

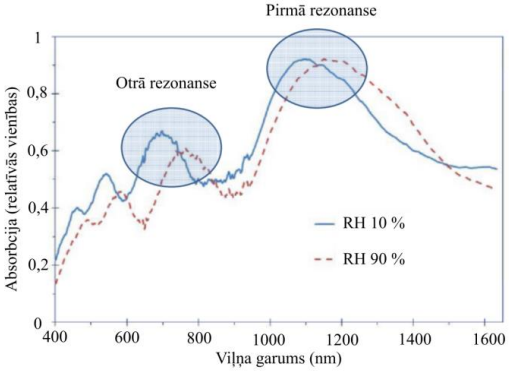

2. att. Ierīces spektrālā atbilde vidēs ar dažādiem *RH*[10].

Pētījumā[11] parādīta *LMR* efekta lietojamība sprieguma mērīšanā. Tas tika realizēts, izmantojot trīsslāņu struktūru uz optiskās šķiedras, kas sastāvēja no divām indijas alvas oksīda (*ITO*) kārtiņām un polivinilidēnfluorīda (PVDF) pārklājuma starp *ITO* kārtiņām. Iekšējā struktūras kārtiņa kalpoja gan kā *LMR* pārklājums, gan kā pirmais elektrods. PVDF šajā gadījumā pildīja elektrooptiskā materiāla funkciju, mainot savu laušanas koeficientu atkarībā no ārējā elektriskā lauka. Struktūras ārējā *ITO* plānā kārtiņa veidoja otro elektrodu. Ierīces uzbūve un mērītie caurlaidības spektri pie dažādiem pieliktiem spriegumiem redzami 3. attēlā.

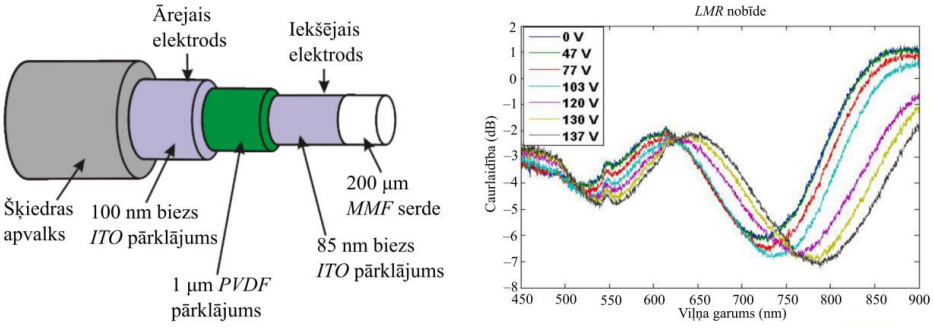

(a) (b)

3. att. Sprieguma mērītājs: (a) shematiska ierīces reprezentācija; (b) *LMR* pīķu nobīde pie pieliktiem ārējiem spriegumiem[11].

Plāno kārtiņu laušanas koeficienta izmaiņas atkarībā no temperatūras ir plaši izplatīta parādība. Pētījumā[12] optiskās šķiedras temperatūras sensors uz *LMR* parādības bāzes tika nodemonstrēts ar SnO_2 plāno kārtiņu. Rezonanses viļņa garuma nobīde otrai *LMR* kārtai atkarībā no sintētiskās smēreļļas temperatūras redzama 4. attēlā. Izstrādātā ierīce sasniedza jutību ap 2,2 nm/°C temperatūru diapazonā no 45 °C līdz 75 °C.

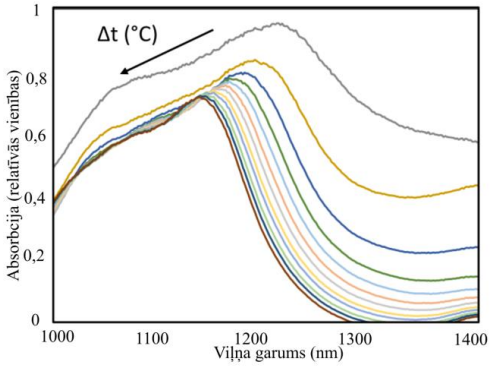

4. att. *LMR* spektri ierīcei ar SnO_2 pārklājumu, kad smēreļļas temperatūra mainās robežās no 45 °C līdz 75 °C[12].

PAH/PAA (polialilamīna hidrohlorīds/poliakrilskābe) polimēru plēves uzbriest un piepūšas, mainoties šķīduma pH līmenim[13]. Tas rada PAH/PAA polimēru plēvju laušanas koeficienta izmaiņas, kas savukārt izraisa *LMR* viļņa garuma nobīdi. Novērojumi (5. att.) parāda, ka pH izmaiņas PAH/PAA plēvēs rada *LMR* viļņa garuma nobīdi, parādot augstu jutību pret pH izmaiņām.

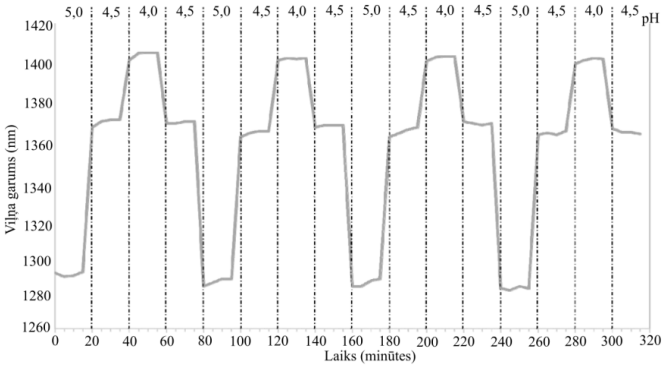

5. att. Sensora *LMR* viļņa garums, iegremdējot to šķīdumos ar dažādu pH[13].

LMR parādībā balstīti optisko šķiedru sensori sniedz iespēju noteikt gaistošos organiskos savienojumus (*VOCs*). Optiskās šķiedras, kas ir pārklātas ar PAH/PAA, ir spējīgas detektēt dažādas *VOC* gāzes, nodrošinot dažādus *LMR* viļņa garumus dažādām specifiskām *VOC* gāzēm, padarot to par selektīvu sensoru[14]. Rezonanses viļņa garums *LMR* sensoram ar PAH/PAA polimēru plēvēm ir demonstrējis lineāru atkarību no etanola, metanola un isopropanola koncentrācijām. Sensora veiktspēja tika novērtēta gan koncentrāciju palielinot, gan samazinot, demonstrējot minimālu histerēzi (6. att.).

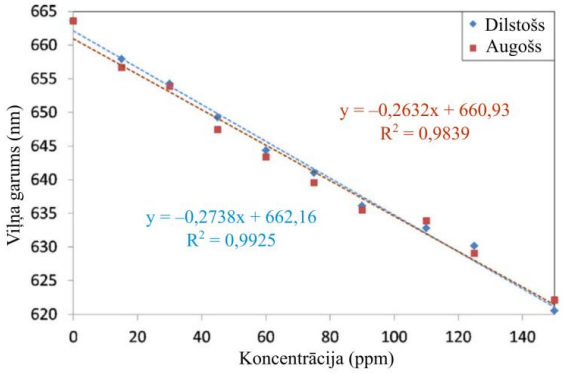

6. att. *LMR* viļņa garuma lineāra atkarība no etanola tvaika koncentrācijas[14].

Optiskās šķiedras biosensori, kas balstās *LMR* parādībās, nodrošina bezmarķiera noteikšanas platformu. Šajos biosensoros bioloģiskās reakcijas izraisa efektīvā laušanas koeficienta izmaiņas pārklājumā, kas rezultātā rada *LMR* pīķu viļņa garuma nobīdes. Kopīgs izaicinājums visiem biosensoriem ir specifisko molekulu noteikšana lielāku molekulu grupās. Optiskās šķiedras sensori, kas darbojas pēc *LMR* principa, piedāvā risinājumu šai problēmai, izmantojot jutīgā pārklājuma funkcionalizāciju, piemēram, ar aptamēriem[15]. Literatūrā ir aprakstīti vairāki

biosensori, kuru pamatā ir *LMR* parādība, piemēram, antigliadīna antivielu biosensori, C reaktīvā proteīna biosensori, imūnglobulīna G biosensori, trombīna biosensori, siekalu kortizola biosensori un citi[2].

LMR radītās rezonanses var izmantot, lai selektīvi atļautu vai aizliegtu noteikto gaismas viļņu garumu pārraidi, veicinot optisko filtrēšanas ierīču attīstību sakaru nolūkiem[16]. Pētījumā[17] aprakstīts optiskās šķiedras regulējams filtrs, kas balstās *LMR* parādībā. Šajā filtrā pirmais slānis (*ITO*) kalpo gan kā ierīces elektrods, gan kā *LMR* parādības ģenerators. Otrais slānis (PVDF) tiek izmantots filtra regulēšanai, savukārt ārējais slānis (*ITO*) darbojas kā otrs elektrods. Eksperimentālie rezultāti liecina, ka izgatavotais filtrs ir ļoti jutīgs pret pielikto ārējo spriegumu, nodrošinot *LMR* viļņa garuma izmaņu par 0,4 nm/V. Aprakstītais optiskais filtrs shematiski attēlots 7. attēlā.

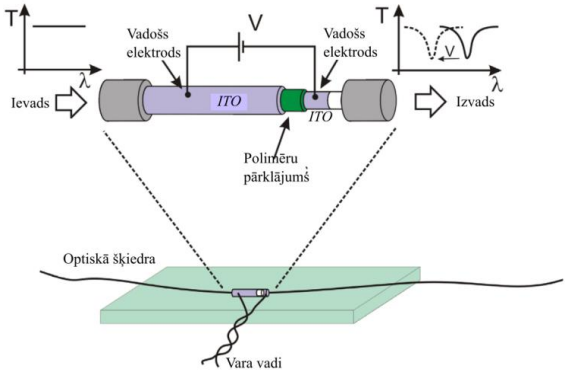

7. att. Elektrooptiskais viļņa garuma filtrs uz *LMR* parādības bāzes[17].

Galvenie izaicinājumi *LMR* jomā

Saskaņā ar avotā[8] sniegtajiem atklājumiem tika konstatēts, ka plānāki zuduma pārklājumi un lielāka laušanas koeficienta atšķirība starp viļņvada serdi un apkārtējo vidi rada mazāku *FWHM*. Tomēr šī pieeja izraisa arī ierīces jutības samazināšanos[8]. Šī nesakritība var būt viens no galvenajiem izaicinājumiem, lai izstrādātu sensoru uz *LMR* parādības bāzes, kam vienlaikus ir gan augsta jutība, gan šaurs *FWHM*.

Publikācijā[8] ir konstatēts, ka teorētiski *LMR* jutīgums var sasniegt bezgalību. Tomēr pastāv arī daži praktiski ierobežojumi, kas jāņem vērā. Pirmkārt, jutība ir proporcionāla rezonanses viļņa garumam, un, lai sasniegtu augstu jutību, bieži vien ir nepieciešams darboties pēc iespējas garāku viļņu garuma diapazonā, kas ir tuvu komerciāli pieejamo optisko spektrometru robežai. Lai gan pastāv daži specializēti instrumenti, kas spēj mērīt garākus viļņu garumus, tiem parasti ir zemāka izšķirtspēja, kā arī to izmantošana parasti ir dārgāka. Ņemot vērā minēto, galvenais *LMR* trūkums ir augstās izmaksas, lai iegūtu jutīgu spektrometru, kas spēj uztvert nepieciešamos viļņu garumus

atbilstošām *LMR* līnijām. Otrkārt, rezonanses līnijas pie garākiem viļņu garumiem bieži vien ir platākas, kas var negatīvi ietekmēt labuma skaitli (*FOM*) un *LMR* izšķirtspēju[18].

Rezonanses pīķa dziļums ir svarīgs parametrs, kas raksturo ierīces veiktspēju. Pīķa dziļums ietekmē tādu parametru kā pieņemams labuma skaitlis (*RFOM*), ko plaši izmanto integrēto sensoru salīdzināšanai. *RFOM* matemātiski definēts ar 6. vienādojumu.

$$RFOM = \frac{S \cdot D}{FWHM}. \tag{6}$$

Sasniegt pilnīgu absorbciju pie rezonanses viļņa garuma, kas atbilst 100 % rezonanses dziļumam, ir iespējams, ja abās robežvirsmās (starp viļņvadu un pārklājumu, kā arī starp pārklājumu un apkārtējo vidi) ir līdzvērtīga atstarošanās spēja. Tomēr praksē šos nosacījumus vienmēr izpildīt nav iespējams, līdz ar to zema absorbcija var sarežģīt *LMR* identifikāciju[8].

Visbeidzot, ir svarīgi atzīmēt, ka pašreizējos *LMR* sensoru prototipos galvenokārt tiek izmantotas optiskās šķiedras[6]. Tomēr šāda atkarība no optiskajām šķiedrām rada grūtības sasniegt vieglu ražošanas mērogojamību, jo nepieciešama manuāla apstrāde. *LMR* bāzēto optisko šķiedru sensoru ražošana ir sarežģīta lielo izmaksu dēļ, kas kavē produkta komercializācijas iespējas. Turklāt šādu optisko šķiedru ierīču integrēšana ar citiem fotoniskiem elementiem uz čipa ir komplicēta, kas papildus ietekmē *LMR* parādības komercializācijas potenciālu. Šāda integrācija var radīt unikālus produktus specifiskiem lietojumiem. Tas padara lētu *LMR* sensoru ražošanu sarežģītāku un kavē to integrēšanu ar citiem fotoniskiem elementiem integrētajā fotonikas čipā (*PIC*). Promocijas darba galvenais mērķis ir piedāvāt šīs problēmas atrisinājumu.

Fotonika uz polimēru bāzes

Polimēri ir kļuvuši par perspektīviem materiāliem integrēto viļņvadu ražošanā. Salīdzinot ar neorganiskiem materiāliem, polimēri piedāvā zemākas izmaksas *PIC* ražošanā, elastību un potenciālu pielāgoties, lai iegūtu vēlamās īpašības konkrētos fotonikas lietojumos[19]. Turklāt integrētās polimēru fotonikas izgatavošanas pamatā ir standarta komplementārā metāla oksīda pusvadītāja (*CMOS*) metodes. Tādējādi polimēru ierīču ražošanu var veikt jebkurās *CMOS* piemērotās tīrtelpās. Polimēri ir pievilcīgi arī hibrīdās organiskās-neorganiskās sistēmās, kurās tiek izstrādātas sarežģītas un lētas optoelektroniskās komponentes[20]. Tādējādi pāreja no silīcija integrētās fotonikas uz polimēru fotoniku ir loģisks solis integrētās fotonikas nozarē. Dažādas tehnoloģijas, piemēram, Brega režģa sensori[21], interferometriskie sensori[22] un mikrodobumu sensori[23], jau ir attīstītas polimēru fotonikā. Savukārt *LMR* parādība līdz šim bija demonstrēta tikai optiskajās šķiedrās un plakanajos viļņvados. Šajā kontekstā šo tehnoloģiju pārnešana uz polimēru fotonikas platformu sniegs būtiskas inovācijas šajā jomā.

Promocijas darba mērķi

1. Integrēt eksperimentālos rezultātus ar galīgo elementu simulācijām, lai uzlabotu fundamentālo izpratni par zudumradošās modu rezonanses parādību.

2. Izstrādāt darbplūsmu integrēto zudumradošās modu rezonanses ierīču izgatavošanai.
3. Demonstrēt zudumradošās modu rezonanses fenomenu integrētajā fotonikas čipā, sasniedzot jutību, kas ir salīdzināma ar tām, ko piedāvā alternatīvās konfigurācijas, piemēram, optiskās šķiedras un plakanie viļņvadi.

Aizstāvāmās tēzes

1. Integrētajos viļņvados, kas izgatavoti no dažādiem negatīviem fotorezistiem, ir iespējams novērot zudumradošās modu rezonanses parādību.
2. Integrētie zudumradošās modu rezonanses sensori var sasniegt 905 nm/*RIU* jutību, kas salīdzināma ar 829 nm/*RIU* jutību plaši izmantotajā plakano viļņvadu konfigurācijā.
3. Galīgo elementu metodi ir iespējams lietot, lai simulētu zudumradošās modu rezonanses parādību integrētajos polimēru viļņvados, panākot atbilstību eksperimentālajiem rezultātiem ar 1 % relatīvo kļūdu.

Zinātniskā novitāte

Promocijas darbs sniedz eksperimentālu pierādījumu koncepcijai par *LMR* parādības pāreju no optisko šķiedru un plakano viļņvadu konfigurācijām uz integrētiem čipiem. Tas demonstrē iepriekš nesasniegtu progresu un potenciālu integrēt šo jauno tehnoloģiju kopā ar citiem fotoniskajiem elementiem vienā čipā. Turklāt šajā darbā tiek novērtēti dažādi polimēri, kas ir pielāgoti *LMR* lietojumiem, un tiek piedāvāta inovatīva metode šo viļņvadu izgatavošanai.

Praktiskā nozīme

Lielākā praktiskā nozīme, *LMR* parādībai pārejot no optiskajām šķiedrām un plakanajiem viļņvadiem uz fotoniskiem čipiem, ir tās mērogojamība un komercializācijas potenciāls, īpaši ņemot vērā savietojamību ar *CMOS* tehnoloģiju. Papildus tam *PIC* galvenā priekšrocība ir tās spēja integrēt dažādus elementus vienā čipā, lai nodrošinātu unikālas funkcijas. Nākamais posms integrēto *LMR* sensoru attīstībā varētu ietvert to integrāciju ar spektrometriem un gaismas avotiem uz čipa, līdz ar to ievērojami samazinot ierīču izmaksas un veidojot būtisku virzību komerciālajiem lietojumiem.

Darba struktūra un apjoms

Promocijas darbs ir zinātnisko rakstu kopā, kas ir veltīti *LMR* parādības pētījumiem fotonikas integrētajos čipos. Promocijas darbs ir izstrādāts latviešu un angļu valodā. Tā rezultāti ir publicēti četrās zinātniskajās publikācijās, kas ir indeksētas *Scopus* datubāzē. Darba kopsavilkumā ir iekļauti 23 attēli. Kopējais *CiteScore* visiem iekļautajiem rakstiem promocijas darbā ir 16,4 (*Scopus* datubāzes dati). Rezultāti tika prezentēti trīs starptautiskās zinātniskās konferencēs.

Promocijas darba zinātniskās publikācijas

Zinātniskie raksti, kuros publicēti promocijas darba rezultāti

1. **E. Letko**, A. Bundulis, G. Mozolevskis, V. Vibornijs. Integrated Lossy Mode Resonance Sensor Based on SU-8 Waveguides. *Proceedings of SPIE – The international Society for Optical Engineering*. **2022**, 11998B, 1–6 (*Q4, Scopus CiteScore(2022)=0.7*).
2. **E. Letko**, A. Bundulis, G. Mozolevskis. Theoretical Development of Polymer-Based Integrated Lossy-Mode Resonance Sensor for Photonic Integrated Circuits. *Photonics*, **2022**, 9 (10), 764–773 (*Q3, Scopus CiteScore(2022)=2.3*).
3. **E. Letko**, A. Bundulis, G. Mozolevskis. Lossy Mode Resonance Sensors Based on Planar Waveguides: Theoretical and Experimental Comparison. *IEEE Photonics Journal*, **2024**, 16 (1), 1–7 (*Q2, Scopus CiteScore(2023)=4.5*).
4. **E. Letko**, A. Bundulis, E. Vanags, G. Mozolevskis. Lossy Mode Resonance in Photonic Integrated Circuits. *Optics and Lasers in Engineering*, **2024**, 181, 1–11 (*Q1, Scopus CiteScore(2023)=8.9*).

Citi promocijas darba izstrādes laikā publicētie zinātniskie raksti

1. A. Ozols, **E. Letko**, P. Augustovs, D. Saharovs, E. Zarins, V. Kokars. Photoinduced anisotropy of IWK-2D azobenzene molecular glassy films. *Key Engineering Materials*, **2018**, 762, 233–238. (*Q4, Scopus CiteScore(2018)=0.7*).
2. A. Medvids, S. Varnagiris, **E. Letko**, D. Milcius, L. Grase, S. Gaidukovs, A. Mychko, A. Pludons, P. Onufrijevs, H. Mimura. Phase transformation from rutile to anatase with oxygen ion dose in the TiO_2 layer formed on a Ti substrate. *Materials Science and Semiconductor Processing*, **2020**, 106, 104776, 1–6. (*Q1, Scopus CiteScore(2020)=5.9*).
3. A. Ozols, G. Mozolevskis, **E. Letko**, M. Rutkis, R. Zabels, E. Linina, I. Osmanis. Sputtered SiOxNy thin films – improving optical efficiency of liquid crystal diffuser elements in multi-focal near-to-eye display architecture. *Proceedings of SPIE – The international Society for Optical Engineering*, **2021**, 118720I, 1–5. (*Q4, Scopus CiteScore(2021)=0.9*).

Dalība konferencēs

1. Oral presentation in international conference “Proceeding of SPIE – The International Society for Optical Engineering”: **E. Letko**, A. Bundulis, G. Mozolevskis, V. Vibornijs. Integrated Lossy Mode Resonance Sensor Based on SU-8 Waveguides. San Francisco, USA, 22–27 January 2022.
2. Poster presentation in international conference “Nordic Nanolab User Meeting 2022**”: E. Letko**, A. Bundulis, V. Vibornijs, G. Mozolevskis. Fabrication of Lossy Mode Resonance Sensor Based on SU-8 Waveguides. Gothenburg, Sweden, 5–6 May 2022.
3. Poster presentation in international conference “Deep Tech Atelier 2023”: **E. Letko**, A. Bundulis, I. Del Villar, G. Mozolevskis. Development of Integrated Lossy Mode Resonance Sensor Based on Polymer Photonics. Riga, Latvia, 20–21 April 2023.

PROMOCIJAS DARBA GALVENIE REZULTĀTI

Integrētais *LMR* sensors SU-8 viļņvados (1. publikācija)

Pirmā publikācija ir pirmais mēģinājums realizēt *LMR* parādību fotonikas integrētajā čipā. Lai gan šis zinātniskais raksts deva sākotnēju ieskatu *LMR* parādībā, bija grūti novērtēt ierīces jutības veiktspēju rezonanses līniju platuma dēļ. Neskatoties uz šo izaicinājumu, pētījums būtiski veicināja sapratni par galvenajām problēmām, kas saistītas ar integrēto *LMR* sensoru izstrādi, un apsprieda potenciālos turpmākos lietojumus.

Galvenais mērķis 1. publikācijā bija veikt pirmos caurlaidības mērījumus integrētajā *LMR* ierīcē. Šim nolūkam noteiktie uzdevumi bija:

- izstrādāt mikroizgatavošanas darbplūsmu integrētai ierīcei no SU-8 viļņvadiem;
- novērtēt pārklājuma biezuma vienmērību uz SU-8 viļņvada;
- veikt caurlaidības mērījumus *LMR* viļņvados, kas pārklāti ar dažāda materiāla plānām kārtiņām.

Galvenie 1. publikācijas rezultāti redzami 8.–10. attēlā.

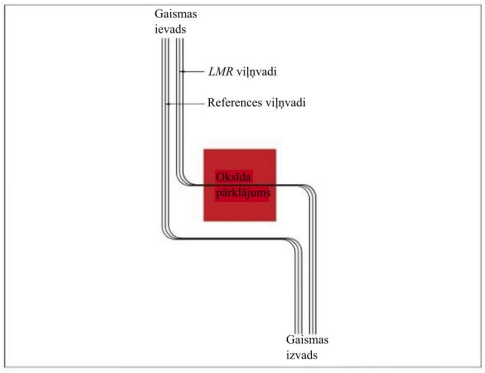

8. att. *LMR* ierīces dizains[24].

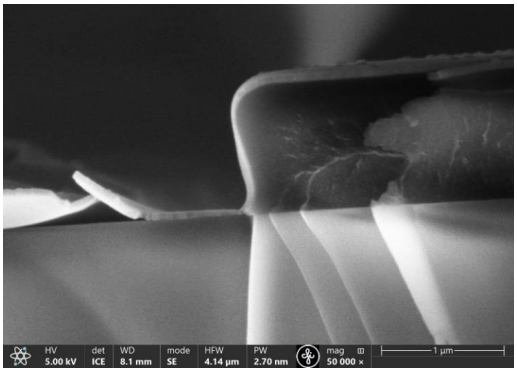

9. att. Viļņvada šķērsgriezums ar 65 nm biezu ZnO pārklājumu[24].

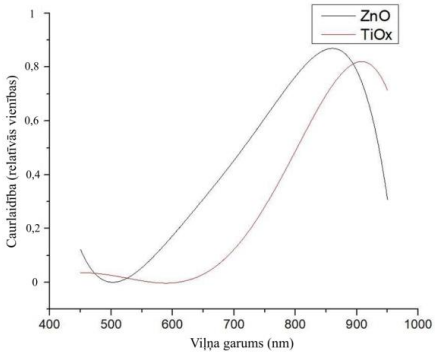

10. att. Caurlaidība SU-8 viļņvados, kas pārklāti ar ZnO un TiO_x plānajām kārtiņām[24].

1. publikācijas galvenie rezultāti un secinājumi

- Čipa dizainā tika izmantotas divas viļņvadu grupas – references viļņvadi gaismas avota spektra mērīšanai un *LMR* viļņvadi parādības novērošanai. Optimāla efektivitāte tika sasniegta, izmantojot izliektu viļņvada formu, lai mazinātu fona apgaismojumu (8. att.).
- ZnO un TiO_x materiāliem tika novērotas platas *LMR* līnijas. Novērotās *LMR* līnijas sakrita ar teorētiski paredzētajiem viļņa garumiem (10. att.).
- Magnetrona putināšana nodrošināja pilnīgu SU-8 viļņvada pārklājumu ar oksīdu (9. att.).

Uz polimēra bāzes integrētā *LMR* sensora teorētiskā izstrāde (2. publikācija)

Ņemot vērā 1. publikācijā minētos izaicinājumus, kas saistīti ar integrētās *LMR* ierīces izgatavošanu, kuras jutība būtu salīdzināma ar *LMR* sensoriem alternatīvās konfigurācijās, pētījums, kas aprakstīts 2. publikācijā, tika sākts, lai izpētītu teorētiskos dizaina risinājumus

integrētajām *LMR* ierīcēm un analizētu *LMR* parādības atkarību no kritiskām dimensijām. *LMR* parādība fotonikas integrētajā čipā iepriekš nebija pētīta, tāpēc bija svarīgi veikt teorētiskos aprēķinus un simulācijas, lai racionalizētu *LMR* tehnoloģijas pārnešanu no optiskajām šķiedrām un plakanajiem viļņvadiem uz integrēto fotoniku. Līdz ar to 2. publikācijas mērķis bija teorētiski parādīt *LMR* efekta sasniegšanas potenciālu integrētā čipa līmenī un noteikt optimālo SU-8 viļņvada ģeometriju un zudumu pārklājuma biezumu, lai uzlabotu sensora jutību.

2. publikācijas mērķi:

- izpētīt *LMR* parādības atkarību no SU-8 viļņvadu šķērsgriezuma ģeometrijas;
- izpētīt *LMR* atkarību no zuduma pārklājuma biezuma;
- izpētīt *LMR* parādības uzvedību atkarībā no izplatītām modām viļņvados;
- novērtēt izstrādātās ierīces jutības veiktspēju;
- izstrādātajā *LMR* čipā novērot vairākas rezonanses vienlaikus.

Galvenie 2. publikācijas rezultāti redzami 11.–13. attēlā.

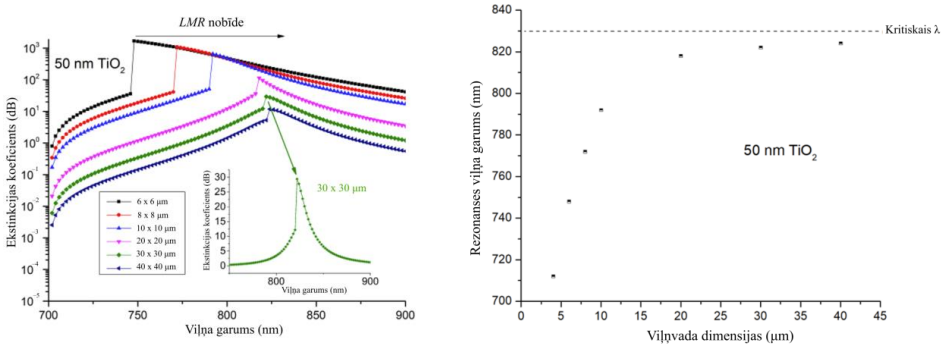

(a) (b)

11. att. Viļņvada izmēru ietekme uz *LMR* parādību: (a) normalizēti caurlaidības spektri dažādiem viļņvada izmēriem; (b) *LMR* viļņa garuma atkarība no viļņvada izmēriem[25].

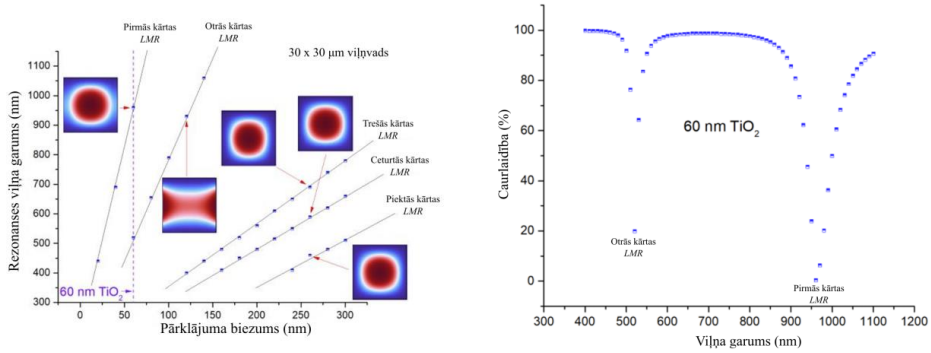

(a) (b)

12. att. *LMR* atkarībā no zuduma pārklājuma biezuma: (a) *LMR* viļņa garums kā funkcija no pārklājuma biezuma; (b) caurlaidības spektrs ierīcei ar 60 nm TiO_2 pārklājuma biezumu[25].

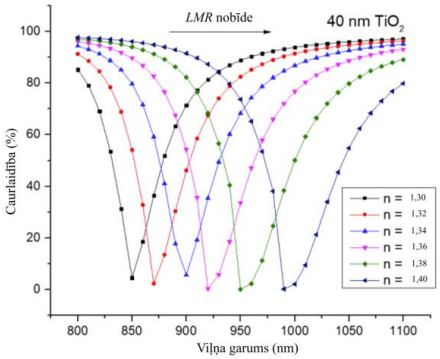

13. att. *LMR* nobīde atkarībā no vides laušanas koeficienta izmaiņām[25].

2. publikācijas galvenie rezultāti un secinājumi

- Teorētiskās simulācijas atklāja *LMR* parādības novērošanas iespējamību integrētajos SU-8 viļņvados, kas pārklāti ar TiO_2 zudumu pārklājumu.
- Tika konstatēts, ka *LMR* regulēšana ir iespējama, pielāgojot viļņvada ģeometriju, jo *LMR* viļņa garums reaģē uz viļņvada izmēriem ar augstu jutību (11. att.). Turklāt tika pierādīts, ka šī jutība ir izteiktāka mazākiem viļņvadiem, bet, sasniedzot noteiktus izmērus, *LMR* viļņa garums stabilizējas un novērojama minimāla nobīde (11. b att.).
- Tika nodemonstrēts, ka integrētajos SU-8 viļņvados, kas pārklāti ar TiO_2 zudumu pārklājumu, teorētiski var novērot vairākus *LMR*.
- Tika apstiprināts, ka gan *TE*, gan *TM* polarizācijai ir novērojams *LMR* efekts integrētajā ierīcē, un rezonanses viļņu garumi nedaudz atšķiras starp abām polarizācijām.
- Maksimālā jutība ap 1400 nm/*RIU* tika sasniegta ar 40 nm biezu TiO_2 pārklājumu, kas ir piemērots mērīšanai vidēs ar laušanas koeficientiem no 1,30 līdz 1,40 (13. att.).

Plakanos viļņvados balstīti *LMR* sensori – teorētisks un eksperimentāls salīdzinājums (3. publikācija)

Lielākajā daļā zinātniskās literatūras *LMR* parādība galvenokārt tiek pētīta no inženiertehniskā aspekta, kā rezultātā trūkst teorētiskā pamatojuma un izpratnes par fundamentālajiem procesiem. Šajā publikācijā padziļināti pētīta *LMR* parādība plakanajos viļņvados ar zudumu pārklājumiem, kas bieži tiek izmantoti *LMR* jomā. Pie šādiem pārklājumiem pieder TiO_2, SnO_2 un *ITO*. Iegūtie eksperimentālie rezultāti tika salīdzināti ar simulācijām, kas veiktas ar *FEM* rīkiem *COMSOL* vidē. Pētījuma īpašā novitāte ir eksperimentālo atklājumu un teorētisko aprēķinu apvienojums. Turklāt

no integrētā *LMR* sensora izstrādes viedokļa šis pētījums bija būtisks, jo tā mērķis bija noteikt optimālo zudumu pārklājuma materiālu turpmākiem pētījumiem un integrētās ierīces izstrādei.

3. publikācijas mērķi:

- eksperimentāli novērot *LMR* parādību sensoru ierīcēs ar TiO_2, SnO_2 un *ITO* pārklājumiem;
- izpētīt *LMR* parādības atkarību no dažāda biezuma zudumu pārklājumiem;
- noskaidrot nogulsnēto plāno kārtiņu elektrooptiskās īpašības, tostarp laušanas un ekstinkcijas koeficientus, lai uzlabotu simulācijas rezultātu precizitāti;
- visu izgatavoto paraugu caurlaidības spektrus salīdzināt ar teorētiski aprēķinātajiem spektriem, kas iegūti ar *FEM* simulācijas rīkiem;
- novērot *LMR*, ko izraisa gan *TE*, gan *TM* polarizācija;
- identificēt piemērotāko zudumu pārklājumu, pamatojoties uz *LMR* pīķa formu;
- novērtēt izgatavoto ierīču jutību, uzklājot šķidros analītus uz sensora jutīgās zonas;
- noteikt izgatavoto ierīču labumus, lai novērtētu to veiktspēju.

Galvenie 3. publikācijas rezultāti redzami 14.–17. attēlā.

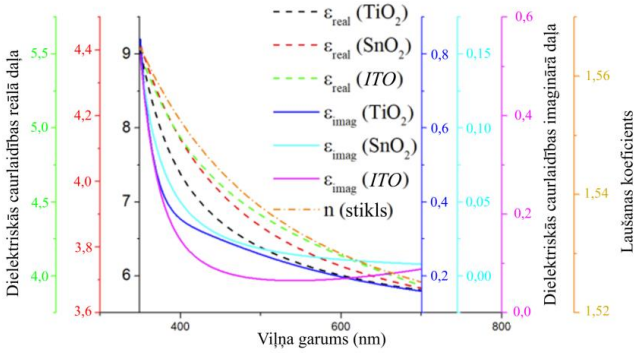

14. att. Dispersijas līknes stikla viļņvadam, TiO_2, SnO_2 un *ITO* plānām kārtiņām[26].

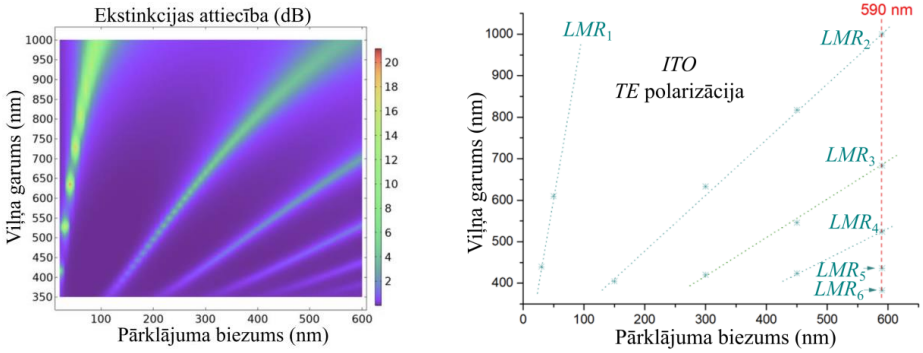

(a) (b)

15. att. *LMR* parādības uzvedība atkarībā no viļņa garuma un *ITO* biezuma *TE* polarizētai gaismai: (a) teorētiskais aprēķins; (b) eksperimentālie rezultāti[26].

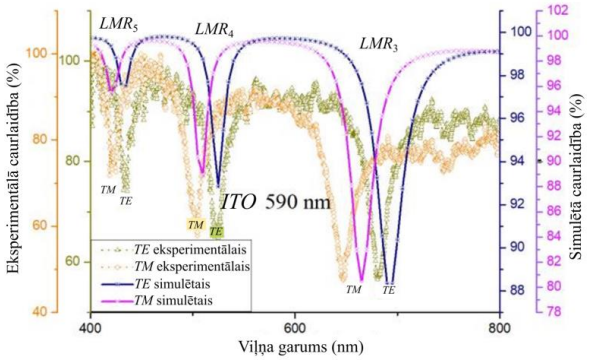

16. att. Caurlaidības spektri ierīcei ar 590 nm biezu *ITO* pārklājumu[26].

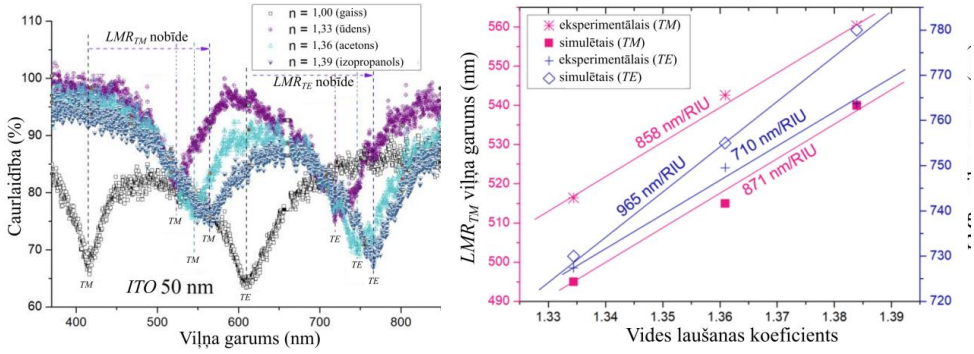

(a) (b)

17. att. Jutības veiktspēja paraugam ar 50 nm *ITO* pārklājumu: (a) eksperimentālā jutība dažādos šķidrumos; (b) *LMR* viļņa garums kā funkcija no apkārtējās vides laušanas koeficienta gan *TE*, gan *TM* polarizētai gaismai[26].

3. publikācijas galvenie rezultāti un secinājumi

- *ITO* pārklājums izrādījās vispiemērotākais *LMR* balstītiem sensoru lietojumiem, jo tas vienīgais radīja izteiktas rezonanses visā redzamās gaismas spektrā (16. att.). Šo rezultātu varētu skaidrot ar *ITO* nogulsnēšanas tehnoloģiju, kurā izmantota nereaktīvā magnetronu putināšana, savukārt citi oksīdi tika nogulsnēti reaktīvā procesā Ar/O_2 plazmā, veidojot kristāliskus graudus ar ierobežotu mijiedarbību ar garāka viļņa garuma gaismu. Alternatīvs skaidrojums balstās atšķirīgās ekstinkcijas koeficientu dispersijas līknēs *ITO* un citiem oksīda pārklājumiem.
- Salīdzinot teorētiskās simulācijas un eksperimentālos rezultātus, tika konstatēts, ka *FEM* kombinācijā ar iebūvēto modu analīzi precīzi apraksta *LMR* parādības pamatfiziku plakanajos viļņvados. Teorētiskie rezultāti rādīja pietiekamu sakritību ar eksperimentālajiem datiem visā pārklājuma biezuma diapazonā (15. att.). Dažas nelielas labumu atšķirības starp teorētiskajiem un eksperimentālajiem rezultātiem var būt saistītas ar plāno kārtiņu nevienmērību un mazāk precīzu teorētisko ievades datu pieejamību attiecībā uz vides optiskajām īpašībām un pārklājuma biezumiem.
- Mērījumu laikā izmantotais lineārais polarizators apstiprināja *LMR* parādības paredzamo polarizācijas atkarību (16.–17. att.).

LMR fotonikas integrētajā čipā (4. publikācija)

4. publikācijā aprakstīts promocijas darba noslēguma pētījums. Visi trīs iepriekšējie zinātniskie raksti (1. publikācija, 2. publikācija un 3. publikācija) sniedza ieskatu *LMR* parādībā un risināja konkrētus jautājumus par pirmā pilnībā integrētā *LMR* balstītā sensora izveidi. 1. publikācija palīdzēja izprast virzienu, kurā jādodas, lai izveidotu strādājošu prototipu. 2. publikācija sniedza ieskatu polimēru viļņvadu izmēru ierobežojumos. 3. publikācija nodrošināja pirmo reālo eksperimentālo pieredzi veiksmīgai *LMR* ģenerēšanai. 4. publikācijā pirmo reizi tika parādīts *LMR* efekts fotonikas integrētajos čipos ar jutību un *FOM* vērtību, kas ir salīdzināma ar optisko šķiedru un plakano viļņvadu konfigurācijām. Turklāt 4. publikācijā izpētīti dažādi polimēru materiāli integrēto viļņvadu izgatavošanai, tostarp *OrmoClear*, *OrmoCore* un SU-8 fotorezistus. Turklāt 4. publikācijā ieviesta jauna pieeja biezo polimēru viļņvadu izgatavošanā. Visbeidzot, šajā pētījumā eksperimentālie rezultāti tika salīdzināti ar simulācijas rezultātiem, kas iegūti, izmantojot *FEM* rīkus *COMSOL* vidē.

4. publikācijas mērķi:

- izstrādāt inovatīvu darbplūsmu biezo viļņvadu izgatavošanai;
- izveidot eksperimentālu mērījumu sistēmu integrēto fotonikas čipu testēšanai;
- samazināt gaismas ievadīšanas zudumus integrētajos viļņvados;

- izpētīt *LMR* parādības atkarību no taisnās un izliektās viļņvadu ģeometrijas;
- fotonikas integrētajā čipā novērot vairākas *LMR* rezonanses vienlaikus;
- salīdzināt dažādu polimēru izgatavoto viļņvadu caurlaidības spējas;
- salīdzināt eksperimentāli iegūtos spektrus ar teorētiski sagaidāmiem spektriem, izmantojot *FEM* simulācijas palīdzību;
- salīdzināt *LMR* parādības uzvedību integrētajā fotonikas čipa konfigurācijā ar vispāratzītām konfigurācijām kā plakanie viļņvadi;
- novērtēt integrēto ierīču jutības spējas, uzklājot šķidros analītus uz sensora jutīgajām zonām;
- noteikt izgatavoto ierīču *FOM*, lai novērtētu to veiktspēju.

Galvenie 4. publikācijas rezultāti redzami 18.–23. attēlā.

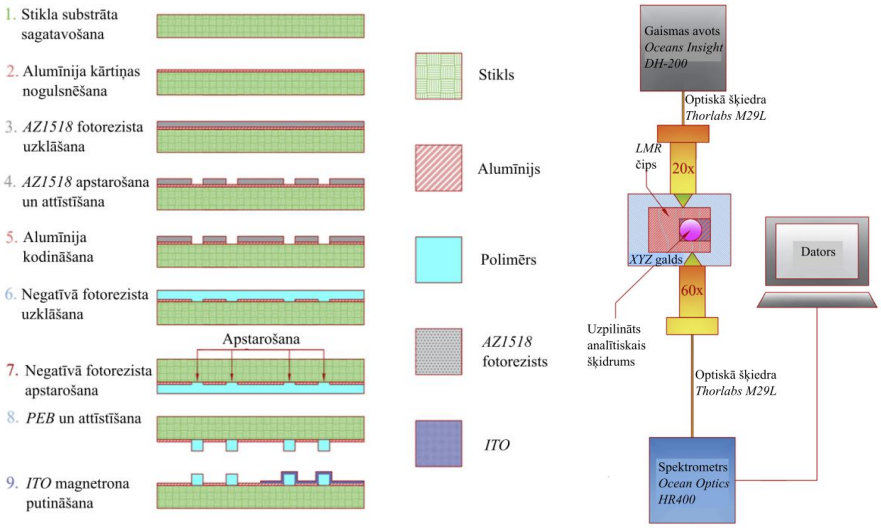

(a) (b)

18. att. *LMR* čips: (a) izgatavošanas darbplūsma; (b) testēšana[27].

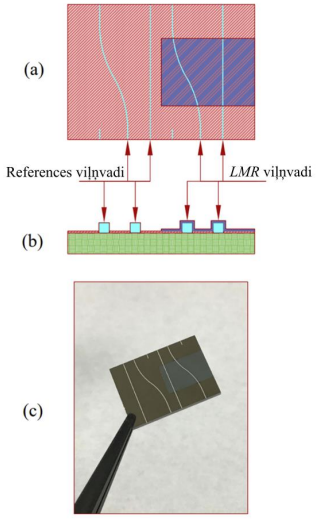

19. att. *LMR* čipa dizains: (a) skats no augšas; (b) šķērsgriezuma skats; (c) faktiskās ierīces fotoattēls[27].

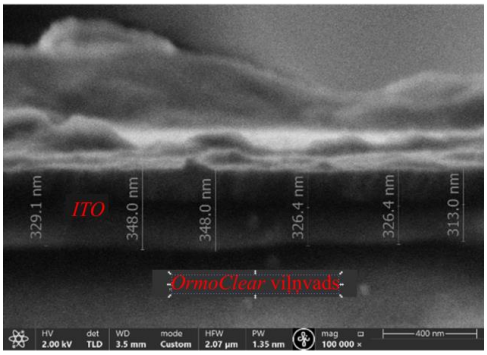

(a)

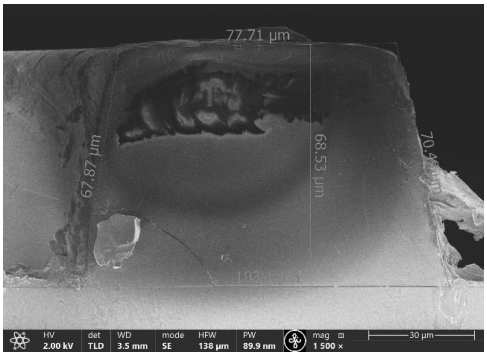

(b)

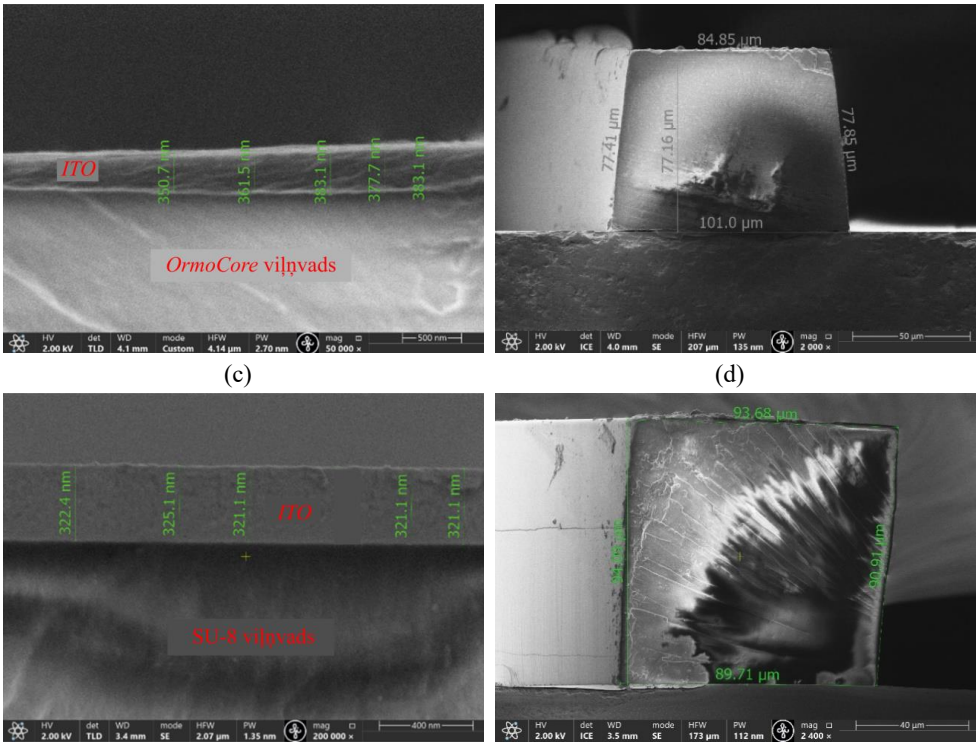

20. att. SEM analīze: (a) *ITO* uz *OrmoClear* viļņvada; (b) *OrmoClear* viļņvada šķērsgriezums; (c) *ITO* uz *OrmoCore* viļņvada; (d) *OrmoCore* viļņvada šķērsgriezums; (e) *ITO* uz SU-8 viļņvada; (f) SU-8 viļņvada šķērsgriezums[27].

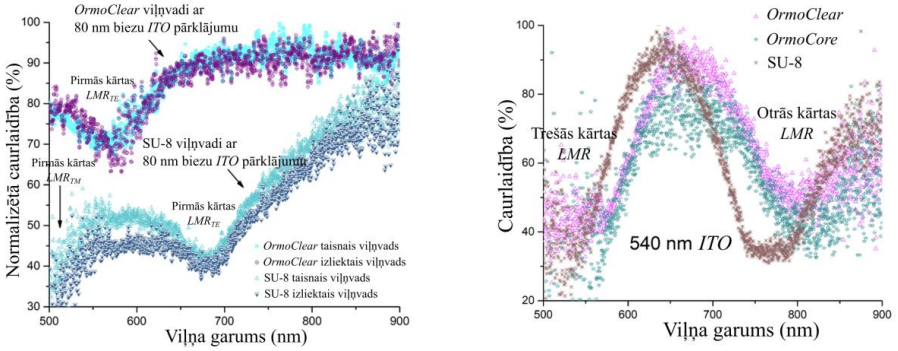

21. att. *LMR* parādības salīdzinājums dažāda veida viļņvados: (a) salīdzinājums taisnā un izliektā viļņvadā; (b) salīdzinājums dažādu polimēru viļņvados [27].

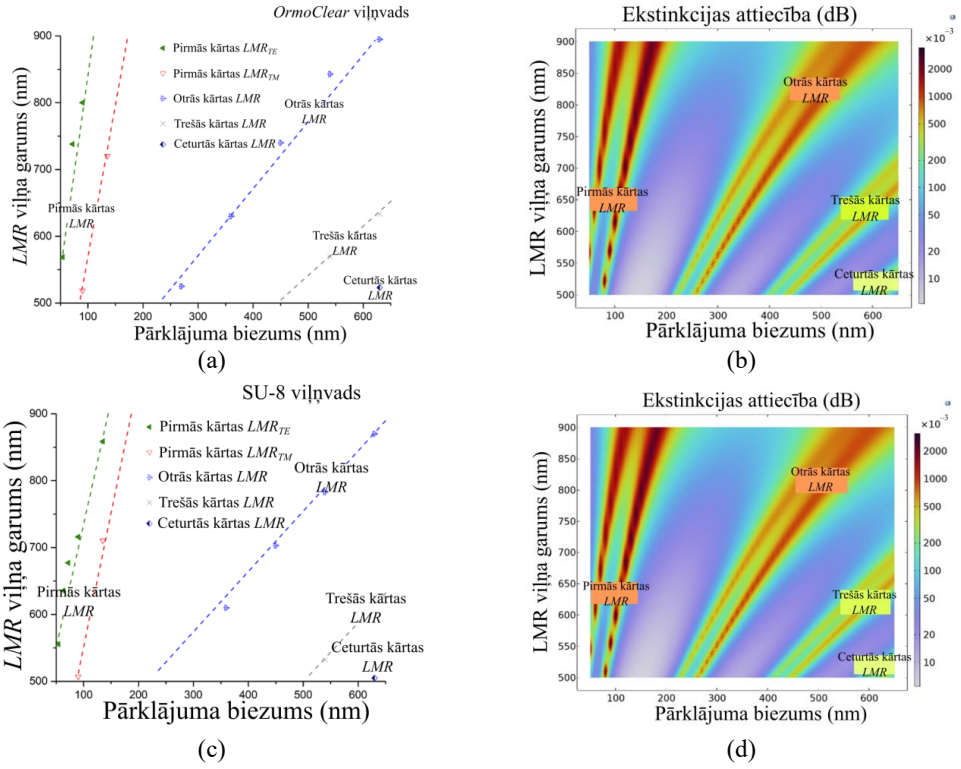

22. att. *LMR* parādība atkarībā no viļņa garuma un *ITO* biezuma: (a) eksperimentālie rezultāti *OrmoClear* viļņvadiem; (b) teorētiskie rezultāti *OrmoClear* viļņvadiem; (c) eksperimentālie rezultāti SU-8 viļņvadiem; (d) teorētiskie rezultāti SU-8 viļņvadiem[27].

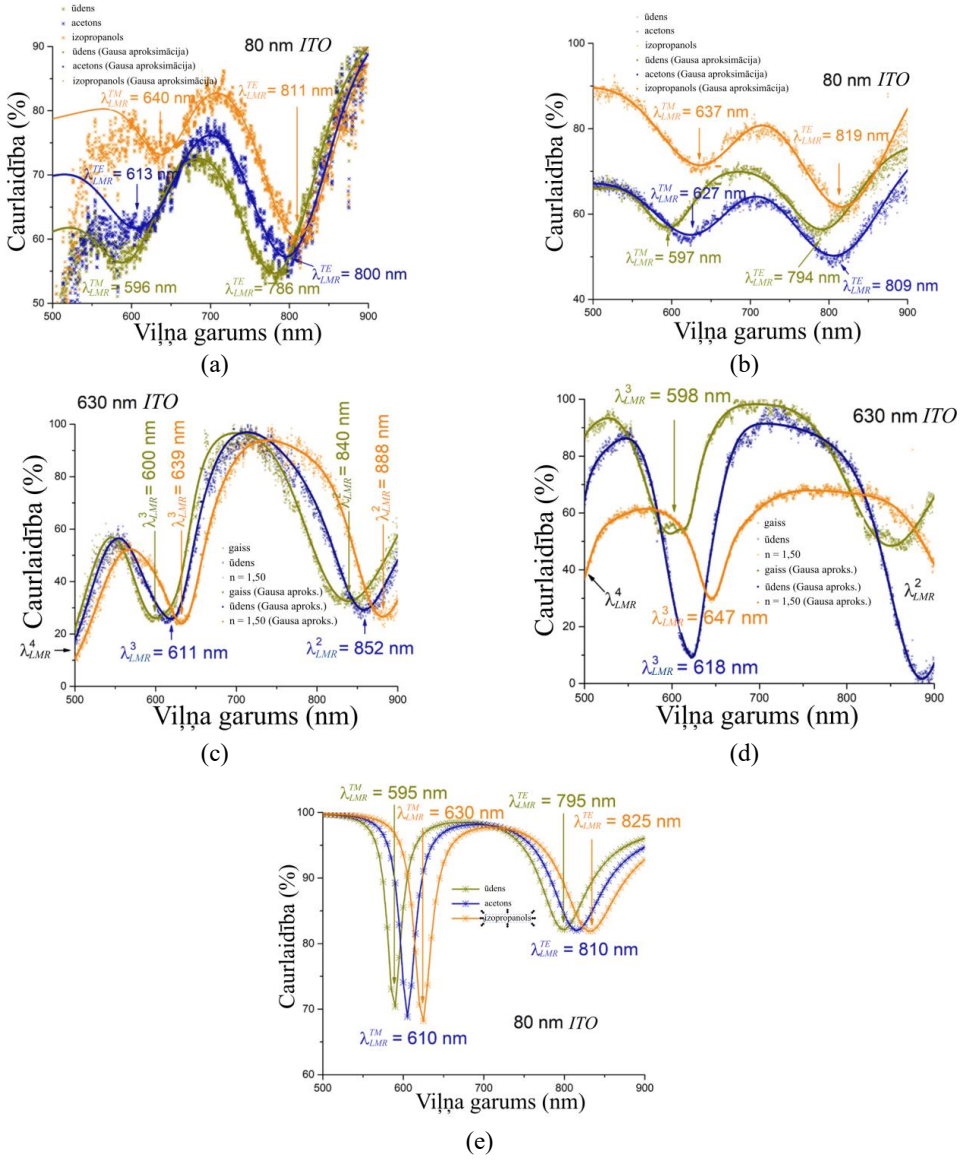

23. att. Eksperimentālā jutības atbilde dažādos šķidrumos: (a) pirmās kārtas *LMR* integrētā ierīcē, kuras pamatā ir SU-8 viļņvadi; (b) pirmās kārtas *LMR* plakanā stikla viļņvadā; (c) augstākās kārtas *LMR* integrētā ierīcē, kuras pamatā ir uz SU-8 viļņvadiem; (d) augstākas kārtas *LMR* plakanā stikla viļņvadā; (e) teorētiski aprēķināti pirmās kārtas *LMR* integrētā ierīcē, kuras pamatā ir SU-8 viļņvadi[27].

4. publikācijas galvenie rezultāti un secinājumi

- Lai pārbaudītu *LMR* parādību fotonikas integrētajos čipos, tika izveidota pielāgota mērīšanas sistēma, kas redzama 18. b attēlā.
- Gaismas zudumu ievadīšanas no optiskās šķiedras uz viļņvadiem samazināšanai tika izmantota ārpakalpojuma zāģēšanas tehnika, kas nodrošināja gludākas un plakanākas viļņvadu malas. Gaismu ievada no šķiedras uz viļņvadi, izmantojot objektīvu (18. b att.).
- Fotonikas čipos, kas izgatavoti no visiem pārbaudītajiem polimēriem (21. b att.), tika novērotas vairākas LMR rezonanses.
- Šis pētījums veiksmīgi parādīja *LMR* parādības ģenerēšanu integrētajos viļņvados ar dažādu ģeometriju. Attiecīgie spektri redzami 21. a attēlā.
- Starp pārbaudītajiem polimēriem, kas izmantoti viļņvadu izgatavošanai, vislabāk piemērotais polimērs visā redzamā gaismas spektra diapazonā izrādījās SU-8, sniedzot izteiktākus *LMR* efektus, salīdzinot ar citiem polimēriem.
- Tika pierādīts, ka viļņvada ģeometrijai ir minimāla ietekme uz *LMR* parādības uzvedību, izņemot gaismas intensitātes samazināšanos, kas novērojama izliektajos viļņvados lieces dēļ (21. a att.).
- Šis pētījums iepazīstina ar inovatīvu biezo viļņvadu izgatavošanas metodi, kas ietver ekspozīciju caur stikla pamatni un alumīnija masku, kas atrodas tieši uz čipa (18. a att.). Šāda pieeja ļauj izveidot augstas kvalitātes viļņvadus, kas spēj efektīvi izplatīt gaismu, lai novērotu *LMR* parādību, kas nav sasniedzama ar citām viļņvadu izgatavošanas metodēm.
- Integrētām ierīcēm un plakaniem viļņvadiem jutība un *FOM* sasniedza līdzīgas vērtības, kas apliecināja integrēto sistēmu potenciālu *LMR* jomā (23. att.). Relatīvā kļūda starp eksperimentāli iegūtajiem *LMR* viļņu garumiem (23. a att.) un simulācijās paredzētajiem viļņu garumiem (23. e att.) ir 1 %.
- Izņemot *OrmoCore*, katrs pārbaudītais polimēru materiāls parādīja *LMR* atkarību no pārklājuma biezuma un rezonanses viļņa garuma, kas saskanēja ar teorētiskajām prognozēm, kas veiktas, izmantojot *FEM* simulācijas rīkus *COMSOL* vidē (22. att.). Galvenās atšķirības bija saistītas ar mērījumu iestatījumiem, kur netika izmantots lineārs polarizators, kas ierobežoja iespējas novērot *TM* un *TE* modas atsevišķi augstākas kārtas *LMR* rezonansēs, kā to paredz teorētiskie aprēķini. Turklāt eksperimentāli iegūtais *FOM* labi saskanēja ar simulācijās iegūtajiem rezultātiem.

SECINĀJUMI

1. Pirmo reizi *LMR* parādība tika novērota integrētajos viļņvados, kas izgatavoti no dažādiem polimēriem, piemēram, *OrmoClear*, *OrmoCore* un SU-8 fotorezistiem.
2. Integrētie *LMR* sensori var sasniegt jutību ap 905 nm/*RIU*, kas ir salīdzināma ar citām *LMR* sensoru konfigurācijām. Lai to panāktu, integrētajā fotonikas čipā jāiekļauj SU-8 viļņvadi ar 100 × 100 µm šķērsgriezuma izmēriem un 80 nm biezu *ITO* zuduma pārklājumu.
3. Pirmo reizi *FEM* simulācijas metodoloģija tika pilnībā izstrādāta, lai modelētu *LMR* parādību integrētajos polimēru viļņvados, uzrādot atbilstību eksperimentāli iegūtajiem *LMR* viļņu garumiem ar 1 % relatīvo kļūdu. Šī metode ir spējīga optimizēt arī reālu ierīču dizainu, lai sasniegtu maksimālu jutības veiktspēju.

LITERATŪRAS SARAKSTS

(1) Del Villar, I.; Arregui, F. J.; Zamarreño, C. R.; Corres, J. M.; Bariain, C.; Goicoechea, J.; Elosua, C.; Hernaez, M.; Rivero, P. J.; Socorro, A. B.; Urrutia, A.; Sanchez, P.; Zubiate, P.; Lopez, D.; De Acha, N.; Ascorbe, J.; Matias, I. R. Optical Sensors Based on Lossy-Mode Resonances. *Sensors Actuators, B Chem.* **2017**, *240*, 174–185. https://doi.org/10.1016/j.snb.2016.08.126.

(2) Wang, Q.; Zhao, W. M. A Comprehensive Review of Lossy Mode Resonance-Based Fiber Optic Sensors. *Opt. Lasers Eng.* **2018**, *100* (July 2017), 47–60. https://doi.org/10.1016/j.optlaseng.2017.07.009.

(3) Zamarreño, C. R.; Hernáez, M.; Del Villar, I.; Matías, I. R.; Arregui, F. J. Optical Fiber PH Sensor Based on Lossy-Mode Resonances by Means of Thin Polymeric Coatings. *Sensors Actuators, B Chem.* **2011**, *155*(1), 290–297. https://doi.org/10.1016/j.snb.2010.12.037.

(4) Zamarreño, C. R.; Hernaez, M.; Del Villar, I.; Matias, I. R.; Arregui, F. J. Tunable Humidity Sensor Based on ITO-Coated Optical Fiber. *Sensors Actuators, B Chem.* **2010**, *146*(1), 414–417. https://doi.org/10.1016/j.snb.2010.02.029.

(5) Fuentes, O.; Goicoechea, J.; Corres, J. M.; Villar, I. Del; Ozcariz, A.; Matias, I. R. Generation of Lossy Mode Resonances with Different Nanocoatings Deposited on Coverslips. *Opt. Express* **2020**, *28*(1), 288. https://doi.org/10.1364/oe.28.000288.

(6) Arregui, F. J.; Villar, I. Del; Corres, J. M.; Goicoechea, J.; Carlos, R.; Elosua, C.; Hernaez, M.; Rivero, P. J.; Socorro, A. B.; Sanchez, P.; Zubiate, P.; Lopez, D.; Acha, N. De; Matias, I. R. Fiber-Optic Lossy Mode Resonance Sensors. *Procedia Eng.* **2014**, *87*, 3–8. https://doi.org/10.1016/j.proeng.2014.11.253.

(7) Refractometer, F.; Sudas, D. P.; Zakharov, L. Y.; Jitov, V. A.; Golant, K. M. Silicon Oxynitride Thin Film Coating to Lossy Mode Resonance. **2022**, 1–12.

(8) Zhao, W. M.; Wang, Q. Analytical Solutions to Fundamental Questions for Lossy Mode Resonance. *Laser Photonics Rev.* **2023**, *17*(1), 1–18. https://doi.org/10.1002/lpor.202200554.

(9) Razquin, L.; Zamarreno, C. R.; Munoz, F. J.; Matias, I. R.; Arregui, F. J. Thrombin Detection by Means of an Aptamer Based Sensitive Coating Fabricated onto LMR-Based Optical Fiber Refractometer. *Proc. IEEE Sensors* **2012**, 3–6. https://doi.org/10.1109/ICSENS.2012.6411186.

(10) Zamarreño, C. R.; Hernaez, M.; Sanchez, P.; Del Villar, I.; Matias, I. R.; Arregui, F. J. Optical Fiber Humidity Sensor Based on Lossy Mode Resonances Supported by TiO2/PSS Coatings. *Procedia Eng.* **2011**, *25*, 1385–1388. https://doi.org/10.1016/j.proeng.2011.12.342.

(11) Ascorbe, J.; Corres, J. M.; Arregui, F. J.; Matias, I. R. Low voltage transducer based on the changes in the wavelength of the attenuation band. *SENSORS, 2014 IEEE*, **2014**, 1–4. https://doi.org/10.1109/ICSENS.2014.6985404

(12) Sánchez, P.; Zamarreño, C. R.; Arregui, F. J.; Matías, I. R. LMR-Based Optical Fiber Refractometers for Oil Degradation Sensing Applications in Synthetic Lubricant Oils. *J. Light. Technol.* **2016**, *34*(19), 4537–4542. https://doi.org/10.1109/JLT.2016.2562701.

(13) Zubiate, P.; Zamarreno, C. R.; Del Villar, I.; Matias, I. R.; Arregui, F. J. D-Shape Optical Fiber PH Sensor Based on Lossy Mode Resonances (LMRs). *2015 IEEE SENSORS* -

Proc. **2015**, 1–4. https://doi.org/10.1109/ICSENS.2015.7370421.
(14) Elosúa, C.; Vidondo, I.; Arregui, F. J.; Bariain, C.; Luquin, A.; Laguna, M.; Matías, I. R. Lossy Mode Resonance Optical Fiber Sensor to Detect Organic Vapors. *Sensors Actuators, B Chem.* **2013**, *187*, 65–71. https://doi.org/10.1016/j.snb.2012.09.046.
(15) Zamarreño, C. R.; Ardaiz, I.; Ruete, L.; Muñoz, F. J.; Matias, I. R.; Arregui, F. J. C-Reactive Protein Aptasensor for Early Sepsis Diagnosis by Means of an Optical Fiber Device. *Proc. IEEE Sensors* **2013**, 4–7. https://doi.org/10.1109/ICSENS.2013.6688222.
(16) Paliwal, N.; John, J. Lossy Mode Resonance Based Fiber Optic Sensors. *Smart Sensors, Meas. Instrum.* **2017**, *21*(10), 31–50. https://doi.org/10.1007/978-3-319-42625-9_2.
(17) Corres, J. M.; Ascorbe, J.; Arregui, F. J.; Matias, I. R. Tunable Electro-Optic Wavelength Filter Based on Lossy-Guided Mode Resonances. *Opt. Express* **2013**, *21*(25), 31668. https://doi.org/10.1364/oe.21.031668.
(18) Chiavaioli, F.; Gouveia, C. A. J.; Jorge, P. A. S.; Baldini, F. Towards a Uniform Metrological Assessment of Grating-Based Optical Fiber Sensors: From Refractometers to Biosensors. *Biosensors* **2017**, *7*(2). https://doi.org/10.3390/bios7020023.
(19) Paquet, C.; Kumacheva, E. Polymers for Photonics. **2008**, *11*(4), 48–56.
(20) Sciences, O. Hybrid Organic-Inorganic for Low-Cost Photonics Integration. **2007**, *00*, 234–235.
(21) Sherman, S.; Zappe, H. Printable Bragg Gratings for Polymer-Based Temperature Sensors. *Procedia Technol.* **2014**, *15*, 702–709. https://doi.org/10.1016/j.protcy.2014.09.041.
(22) Jiang, L.; Wu, J.; Chen, K.; Zheng, Y.; Deng, G.; Zhang, X.; Li, Z.; Chiang, K. S. Polymer Waveguide Mach-Zehnder Interferometer Coated with Dipolar Polycarbonate for on-Chip Nitroaromatics Detection. *Sensors Actuators, B Chem.* **2020**, *305* (September 2019), 127406. https://doi.org/10.1016/j.snb.2019.127406.
(23) Wei, H.; Krishnaswamy, S. Polymer Micro-Ring Resonator Integrated with a Fiber Ring Laser for Ultrasound Detection. *Opt. Lett.* **2017**, *42*(13), 2655. https://doi.org/10.1364/ol.42.002655.
(24) Benítez, M.; Zubiate, P.; Del Villar, I.; Socorro-Leránoz, A. B.; Matías, I. R. Lossy Mode Resonance Based Microfluidic Platform Developed on Planar Waveguide for Biosensing Applications. *Biosensors* **2022**, *12*(6), 403. https://doi.org/10.3390/bios12060403.
(25) Letko, E.; Bundulis, A.; Mozolevskis, G.; Vibornijs, V. Integrated Lossy Mode Resonance Sensor Based on SU-8 Waveguides. **2022**, No. March 2022, 26. https://doi.org/10.1117/12.2607716.
(25) Letko, E.; Bundulis, A.; Mozolevskis, G. Theoretical Development of Polymer-Based Integrated Lossy-Mode Resonance Sensor for Photonic Integrated Circuits. *Photonics* **2022**, *9*(10). https://doi.org/10.3390/photonics9100764.
(27) Letko, E.; Bundulis, A.; Mozolevskis, G. Lossy Mode Resonance Sensors Based on Planar Waveguides: Theoretical and Experimental Comparison. *IEEE Photonics J.* **2024**, *16*(1), 1–7. https://doi.org/10.1109/JPHOT.2023.3348993.
(28) Letko, E.; Bundulis, A.; Vanags, E.; Mozolevskis, G. Lossy Mode Resonance in Photonic Integrated Circuits. *Opt. Lasers Eng.* **2024**, *181* (May). https://doi.org/10.1016/j.optlaseng.2024.108387.

TABLE OF CONTENTS

AUTHOR'S CONTRIBUTION

The articles that form the basis of this Thesis are the result of a team effort with important input from all co-authors with complementary expertise in different fields. The author's contribution to the articles is described in Table 1. None of the articles mentioned is included in other Theses.

Table 1

Author's Contribution to the Preparation of Each Paper Included in the Thesis

Paper I	Fabrication of polymer waveguides through photolithography. Application of lossy coatings via magnetron sputtering onto the integrated waveguides. Data visualization. Writing of the paper. Contribution percentage – 90 %.
Paper II	Device simulations. Data visualization. Writing of the paper. Contribution percentage – 95 %.
Paper III	Application of lossy coatings via magnetron sputtering. Device simulations. Data visualization. Writing of the paper. Contribution percentage – 90 %.
Paper IV	Fabrication of polymer waveguides through photolithography. Application of lossy coatings via magnetron sputtering onto the integrated waveguides. Device simulations. Data visualization. Writing of the paper. Contribution percentage – 85 %.

ABBREVIATIONS

CMOS	complementary metal-oxide-semiconductor
DC	direct current
FEM	finite element method
FOM	figure of merit
FWHM	the full width at half minimum
HB	hard bake
ITO	indium tin oxide
LMR	lossy mode resonance
MMF	multi-mode fiber
PAA	polyacrylic acid
PAH	poly-allylamine hydrochloride
PEB	post-exposure bake
PIC	photonic integrated circuits
POC	point of care
PSS	poly(sodium 4-styrenesulfonate)
PVDF	poly(vinylidene fluoride)
Q-factor	quality factor
RFOM	a reasonable figure of merit
RH	relative humidity
RIU	refractive index unit
SB	soft bake
SEM	scanning electron microscope
SPR	surface plasmon resonance
TE	transverse electric
TM	transverse magnetic
UV	ultraviolet
VOC	volatile organic compound
WG	waveguide

GENERAL OVERVIEW OF THE THESIS

Introduction

Lossy mode resonance principles

Lossy mode resonance (LMR) arises when light passes through an optical fiber or waveguide and interacts with thin films having positive real permittivity values greater in magnitude than both their own imaginary parts and the permittivity of the fiber or waveguide materials, leading to its observable occurrence.[1] The deposition of lossy coatings on optical fibers or waveguides results in the emergence of attenuation bands in the transmission spectra. These attenuation bands can be attributed to the coupling between the core and lossy modes of the dielectric-cladding thin film, providing an explanation for their occurrence.[2] The wavelengths of these attenuation bands are influenced by a wide range of external parameters (pH,[3] humidity,[4] etc.); therefore, they can be used as sensors in various applications.[5]

LMR offers several advantages over alternative sensing techniques based on optical fibers and waveguides. Unlike surface plasmon resonance (SPR) and other commonly employed methods, LMR can generate multiple resonances. Furthermore, in contrast to SPR, LMR can be observed using both transverse electric (TE) and transverse magnetic (TM) polarized light.[5] In addition, LMR offers practicality as it can be observed across a range of cladding materials, including polymer,[3] semiconductor,[6] and dielectric coatings.[7] This versatility allows for flexible and cost-effective fabrication of sensing devices.

Mathematical model for LMR phenomenon

The interaction between guided light within a waveguide and a thin film can lead to either constructive or destructive interference, resulting in enhanced absorption at specific wavelengths. The presence of a thin film introduces additional phase shifts and alters the effective refractive index of the guided mode, thereby influencing the interference conditions. This serves as the fundamental mechanism behind lossy mode resonance in waveguide-based structures with thin film perturbations.[8]

When light propagates through a medium, and the incident angle θ_1 on the waveguide-cladding interface is sufficiently large, total reflection occurs at the interface between the nanofilm and its surroundings. Consequently, the light interacts with the surrounding layer through the evanescent field. For a simplified analysis of this phenomenon, the two-beam interference approximation can be employed (see Fig. 1).[8]

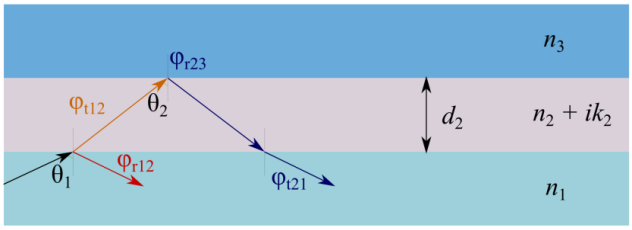

Fig. 1. The physical model of LMR in the waveguide.[8]

By employing Fresnel equations and the theory of multiple-beam interference, one can formulate equations describing the dynamics of the LMR phenomenon. In scenarios where $\theta_1 \approx 90°$, as typically encountered in the waveguide and optical fiber contexts, the resonance wavelength at which destructive interference occurs can be succinctly expressed as Eq. (1)[8]:

$$\lambda_{\mathrm{LMR}} = \frac{2\pi d_2 \sqrt{n_2^2 - n_1^2}}{m\pi + \arctan\left(\left(\frac{n_2^2}{n_3^2}\right)^s \frac{\sqrt{n_1^2 - n_3^2}}{\sqrt{n_2^2 - n_1^2}}\right)}, \tag{1}$$

where λ_{LMR} is the LMR wavelength, d_2 is the thickness of cladding, m is the interference order, n_1, n_2 and, n_3 are refractive indices of waveguide material, cladding material and surroundings, respectively. The parameter s in equation (1) is contingent upon the polarization of the guided light and is defined as Eq. (2)[8]:

$$s = \begin{cases} 1 \text{ for TM mode} \\ 0 \text{ for TE mode} \end{cases}. \tag{2}$$

$\mathrm{LMR_{TE}}$ and $\mathrm{LMR_{TM}}$ exhibit similar characteristics, with the exception of their distinct resonance wavelengths and surrounding sensitivity.[8] Consequently, the subsequent analysis will focus solely on the TM polarization. The sensitivity S for the same incident angle θ_1 can be expressed as Eq. (3)[8]:

$$S = \frac{2\pi n_2^2 d_2 \left(\frac{1}{n_3\sqrt{n_1^2 - n_3^2}} + \frac{2\sqrt{n_1^2 - n_3^2}}{n_3^2}\right)}{\arctan^2\left(\frac{\sqrt{n_1^2 - n_3^2}}{\sqrt{n_2^2 - n_1^2}}\right)\left(1 + \frac{n_2^4(n_1^2 - n_3^2)}{n_3^4(n_2^2 - n_1^2)}\right)}. \tag{3}$$

In the context of the LMR phenomenon, parameters such as the full width at half minimum (FWHM) and the depth of the peak are nearly as crucial as the resonance wavelength and sensitivity. The width of the LMR peak can be assessed utilizing Eq. (4)[8]:

$$\mathrm{FWHM} = \frac{4\pi d_2 \left(n_2^2 - n_1^2 + \lambda_{\mathrm{LMR}}\left(n_1 \frac{\partial n_1}{\partial \lambda}\Big|_{\lambda=\lambda_{\mathrm{LMR}}} - n_2 \frac{\partial n_2}{\partial \lambda}\Big|_{\lambda=\lambda_{\mathrm{LMR}}}\right)\right)}{\lambda_{\mathrm{LMR}}^2 \sqrt{n_2^2 - n_1^2}}. \tag{4}$$

The LMR peak depth D can be evaluated using Eq. (5)[8]:

$$D = \frac{4\sqrt{R_{12}R_{23}}(1 - R_{12})(1 - R_{23})}{(1 - R_{12}R_{23})^2}, \quad (5)$$

where R_{12} and R_{23} represent the reflectivity at the waveguide-cladding and cladding-surroundings interfaces, respectively.

Main applications in the LMR field

Fiber optic sensors based on LMRs have a wide range of applications in detecting physical, chemical, and biological parameters. These applications encompass areas such as food quality assessment, medical diagnostics, and environmental monitoring. Moreover, LMR-based refractometers serve as versatile platforms for various sensor types, with particular relevance to biosensing.[9]

The LMR phenomenon has been investigated for its potential in relative humidity (RH) sensing. In study[10], TiO_2/PSS coated LMR optical fibers were employed as effective devices for fabricating optical fiber humidity sensors. The presence of humidity causes the formation of a thin water layer on the coating and allows water to enter the pores, enabling the device to monitor RH levels. Fig. 2 illustrates the shift in resonance wavelength observed when the RH varies from 20 % to 90 %.

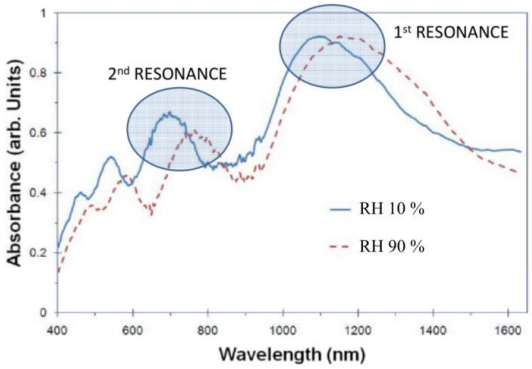

Fig. 2. Spectral response of the device for different external medium RH.[10]

In study,[11] the utilization of LMR-based fiber optic devices for voltage measurement is demonstrated. These devices incorporate poly(vinylidene fluoride) (PVDF) films and are designed with a three-layer thin film structure deposited onto the surface of a multimode optical fiber. The innermost film, indium tin oxide (ITO), serves as both the generator of LMR and the first electrode. The PVDF film, deposited onto the ITO layer, exhibits changes in the refractive index corresponding to the applied external voltage. The outer layer, ITO, forms the second electrode.

The structure of the described voltage measurement device and the measured transmittance spectra for various applied voltages are presented in Fig. 3.

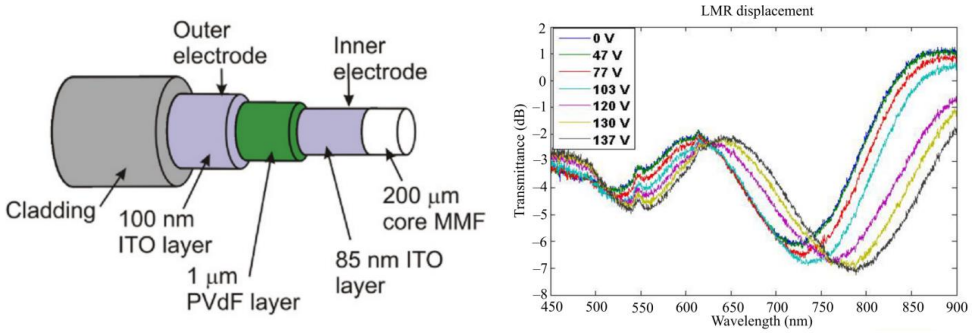

(a) (b)

Fig. 3. Voltage measurement device: (a) schematic representation of the multilayer structure, and (b) LMR peak shift produced by external voltage.[11]

The change in the refractive index of a thin film with temperature is a widely recognized phenomenon. In study,[12] a fiber optic temperature sensor based on LMR was implemented using a SnO_2 thin film coating. Figure 4 illustrates the wavelength shift of the second LMR of the SnO_2 coating as the temperature of the synthetic lubricant oil sample increases. The developed device exhibits a sensitivity of approximately 2.2 nm/°C within the temperature range of 45 °C and 75 °C.

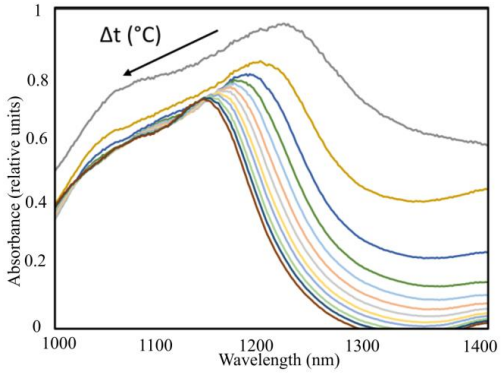

Fig. 4. Spectral response of the LMR device with SnO_2 coating when the temperature of the oil sample varies in the range from 45 °C to 75 °C.[12]

PAH/PAA (poly-allylamine hydrochloride/polyacrylic acid) polymeric films not only generate the LMR phenomenon but also swelling and deswelling behaviors in response to changes in the pH of the solution.[13] This means that the refractive index of PAH/PAA polymeric films undergoes changes, resulting in a shift in resonance wavelength. The observations in Fig. 5 validate that the

pH-induced LMRs generated by PAH/PAA coatings display high sensitivity to pH variations. Consequently, when the device is immersed in a pH solution, the LMR wavelength shift enables the accurate determination of pH levels in the surrounding environment.

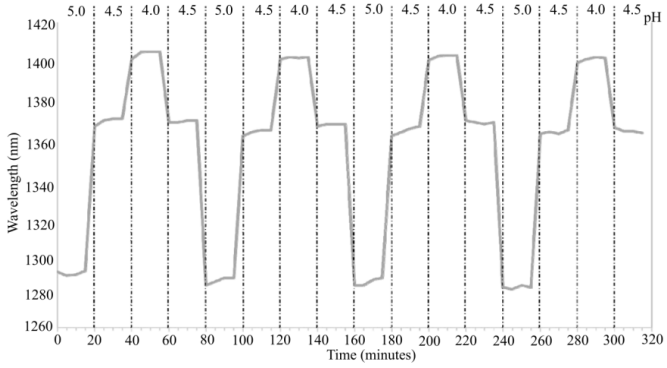

Fig. 5. The dynamic response of the sensor when immersed in various pH solutions.[13]

LMR-based optical fiber sensors offer the capability to detect volatile organic compounds (VOCs). Sensors coated with PAH/PAA are capable of detecting a range of VOC gases and exhibit wavelength shifts for different gases, making them suitable for distinguishing various VOCs.[14] The resonance wavelength of the LMR-based sensor, utilizing a PAH/PAA polymeric film, demonstrates a linear relationship with VOC concentration. Specific sensitivities for ethanol, methanol, and isopropanol were calculated through linear approximations. The sensor's performance was evaluated for both increasing and decreasing concentrations, demonstrating minimal hysteresis, as depicted in Fig. 6.

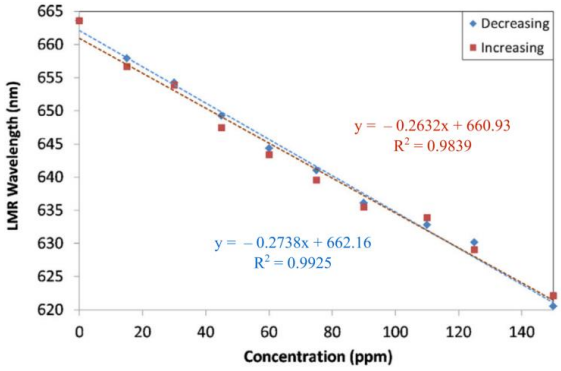

Fig. 6. Linear approximation of the LMR wavelength as a function of vapor concentration for ethanol.[14]

Optical fiber biosensors utilizing LMRs provide a label-free detection platform. These biosensors operate on the principle of exploiting biological reactions that induce changes in the refractive index of the coating, resulting in a shift in the resonance peaks.[2] In biosensing, one common challenge is the detection of specific molecules within a larger group of molecules. LMR-based optical fiber sensors address this issue by employing the functionalization of lossy coating with sensitive materials such as aptamers.[15] Various concrete applications of optical fiber biosensors based on LMRs have been demonstrated, including biosensors for anti-gliadin antibodies, C-reactive protein, immunoglobulin G, thrombin, salivary cortisol, and more.[2]

LMR-induced resonance can be utilized to selectively allow or hinder the transmission of specific wavelengths of light, facilitating the advancement of optical filtering devices for communication purposes.[16] Study[17] presents an optical fiber tunable filter that relies on LMR. In this filter, the first layer (ITO) serves both as the electrode and the generator of LMR. The second layer (PVDF) is employed for filter tuning, while the outer layer (ITO) acts as the other electrode. Experimental results have shown that the fabricated filter exhibits notable sensitivity to the applied voltage, leading to a wavelength shift of 0.4 nm/V. A schematic representation of the described optical filter is given in Fig. 7.

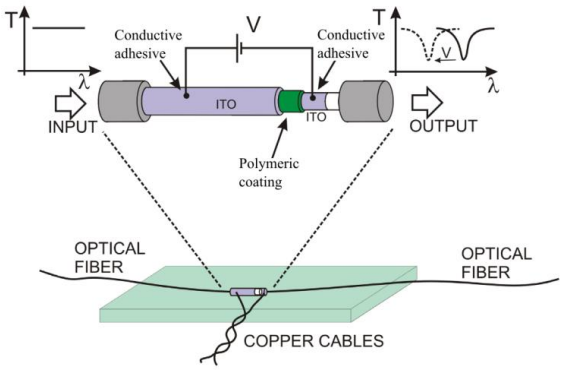

Fig. 7. Electro-optic wavelength filter based on LMR.[17]

Main challenges in the LMR field

According to findings,[8] it has been observed that thinner lossy coatings and a higher refractive index difference between the substrate and surrounding lead to a smaller FWHM. Interestingly, this approach contradicts the goal of increasing sensitivity, as indicated in the study.[8] This discrepancy may be one of the main challenges in achieving an LMR-based sensor with both high sensitivity and a narrow FWHM.

From article,[8] it was deduced that theoretically, the sensitivity of LMR can reach infinity. However, there are practical limitations that need to be taken into account. Firstly, the sensitivity is proportional to the resonance wavelength, and achieving high sensitivity often requires operating in a long wavelength range that is close to the limit of commercially available optical spectrum analyzers. While there are some specialized instruments capable of detecting such long wavelengths, their wavelength resolution is typically lower, and they tend to be more expensive to acquire. Therefore, the primary disadvantage of LMR lies in the cost of obtaining a sensitive spectrometer capable of detecting the required resonance attenuation bands. Secondly, the resonance spectrum tends to be broader at longer wavelengths, which can negatively impact the figure of merit (FOM) and detection resolution.[18]

The depth of the resonance peak is another crucial parameter in evaluating the reasonable figure of merit (RFOM). The RFOM can be mathematically defined as shown in Eq. (6):

$$\mathrm{RFOM} = \frac{S \cdot D}{\mathrm{FWHM}}. \tag{6}$$

Achieving an absolute absorbance at the resonance wavelength, which corresponds to a 100 % resonance depth, is possible when the equivalent reflectivity at both interfaces (substrate-coating and coating-surrounding) approaches 1.[8] However, in practice, this is not always straightforward to achieve, making it challenging to identify LMRs due to their low absorption.

Lastly, it is worth noting that the current prototypes of LMR-based sensors predominantly rely on optical fibers.[6] However, this reliance on optical fibers poses difficulties in terms of achieving easy production scalability due to the requirement for manual processing. As a result, the cost-effective production of LMR-based sensors becomes challenging, hindering the possibility of product commercialization. Additionally, integrating such fiber-based devices with other photonic integrated circuits (PICs) is complex, further impacting the commercialization potential of the LMR phenomenon. This integration could lead to the creation of unique products for specific applications. The primary objective of this Doctoral Thesis is to provide a solution to address this challenge.

Polymer-based photonics

Polymers have gained prominence as materials for the fabrication of waveguides. In comparison to inorganic materials, polymers offer cost-effectiveness, flexibility, and the ability to be functionalized to achieve desired properties for specific photonic applications.[19] Moreover, the fabrication of integrated polymer photonics relies on standard complementary metal-oxide-semiconductor (CMOS) techniques. Consequently, the production of polymer-based devices can be carried out in any CMOS-oriented cleanroom. Polymers are also attractive in hybrid organic-inorganic systems for the development of complex and cost-effective optoelectronic components.[20] Hence, the transition from silicon-based integrated photonics to polymer-based photonics

represents a logical progression in the photonic integrated circuits industry. Many technologies, such as grating-based sensors,[21] interferometric sensors,[22] and microcavity-based sensors,[23] have already been developed for polymer-based photonics. However, the LMR phenomenon has previously been demonstrated only in optical fibers[6] and planar waveguides,[24] and not even in inorganic photonic circuits. In this context, the introduction of this technology into integrated polymer-based photonics marks a significant innovation in the field of polymer photonics.

Aims of the Thesis

1. To integrate experimental results with finite element method simulations to enhance the fundamental understanding of lossy mode resonance.
2. To develop the fabrication workflow of integrated on-chip devices for lossy mode resonance applications.
3. To demonstrate the lossy mode resonance phenomenon in photonic integrated circuits, achieving sensing capabilities comparable to those found in alternatives such as optical fibers and planar waveguide configurations.

Statements to be defended

1. The lossy mode resonance phenomenon can be observed in integrated waveguides made from various negative photoresists.
2. Integrated lossy mode resonance sensors can achieve a sensing performance of 905 nm/RIU, which is comparable to the 829 nm/RIU sensitivity observed in established planar waveguide configurations.
3. The finite element method can be applied to simulate the lossy mode resonance phenomenon in integrated waveguides, achieving experimental agreement with a relative error of 1 %.

Scientific novelty

The Thesis provides experimental proof-of-concept for transitioning the LMR phenomenon from setups using optical fibers and planar waveguides to PICs, representing a previously unattained advancement with the potential capability to integrate this new technology alongside other photonic elements on a single chip. Additionally, the Thesis assesses different polymers for manufacturing integrated waveguides customized for LMR applications and introduces an innovative fabrication method for these waveguides.

Practical significance

The primary practical significance of transitioning the LMR phenomenon from optical fibers and planar waveguides to PICs lies in its scalability and potential for commercialization, particularly due to its compatibility with CMOS technology. Moreover, a key advantage of PICs lies in their ability to integrate diverse elements on a single chip to deliver unique functionalities. The next stage in the development of integrated LMR sensors could involve integrating them with spectrometers and on-chip light sources, thereby significantly reducing device costs and marking a significant breakthrough in terms of commercial applications.

Structure of the Thesis

The Doctoral Thesis is a collection of scientific articles dedicated to the LMR phenomenon in PICs. The results of the Thesis have been published in four original research papers indexed in Scopus. The Doctoral Thesis contains 23 figures. The papers included in the Thesis have a cumulative CiteScore of 16.4 (data taken from the Scopus database). The results have been presented at three international conferences.

Publications of the Thesis

Original papers in which Thesis results are published

1. **E. Letko**, A. Bundulis, G. Mozolevskis, V. Vibornijs. Integrated Lossy Mode Resonance Sensor Based on SU-8 Waveguides. *Proceedings of SPIE – The International Society for Optical Engineering*. **2022**, 11998B, 1–6 (*Q4, Scopus CiteScore(2022) = 0.7*).
2. **E. Letko**, A. Bundulis, G. Mozolevskis. Theoretical Development of Polymer-Based Integrated Lossy-Mode Resonance Sensor for Photonic Integrated Circuits. *Photonics*, **2022**, 9(10), 764–773 (*Q3, Scopus CiteScore(2022) = 2.3*).
3. **E. Letko**, A. Bundulis, G. Mozolevskis. Lossy Mode Resonance Sensors Based on Planar Waveguides: Theoretical and Experimental Comparison. *IEEE Photonics Journal*, **2024**, 16(1), 1–7 (*Q2, Scopus CiteScore(2023) = 4.5*).
4. **E. Letko**, A. Bundulis, E. Vanags, G. Mozolevskis. Lossy Mode Resonance in Photonic Integrated Circuits. *Optics and Lasers in Engineering*, **2024**, 181, 1–11 (*Q1, Scopus CiteScore(2023) = 8.9*).

Other papers published during the development of the Thesis

1. A. Ozols, **E. Letko**, P. Augustovs, D. Saharovs, E. Zarins, V. Kokars. Photoinduced anisotropy of IWK-2D azobenzene molecular glassy films. *Key Engineering Materials*, **2018**, 762, 233–238. (*Q4, Scopus CiteScore(2018) = 0.7*).

2. A. Medvids, S. Varnagiris, **E. Letko**, D. Milcius, L. Grase, S. Gaidukovs, A. Mychko, A. Pludons, P. Onufrijevs, H. Mimura. Phase transformation from rutile to anatase with oxygen ion dose in the TiO_2 layer formed on a Ti substrate. *Materials Science and Semiconductor Processing*, **2020**, 106, 104776, 1–6. (*Q1, Scopus CiteScore(2020) = 5.9*).
3. A. Ozols, G. Mozolevskis, **E. Letko**, M. Rutkis, R. Zabels, E. Linina, I. Osmanis. Sputtered SiOxNy thin films – improving optical efficiency of liquid crystal diffuser elements in multi-focal near-to-eye display architecture. *Proceedings of SPIE – The International Society for Optical Engineering*, **2021**, 118720I, 1–5. (*Q4, Scopus CiteScore(2021) = 0.9*).

Participation in conferences

1. Oral presentation at the international conference "Proceeding of SPIE – The International Society for Optical Engineering", **E. Letko**, A. Bundulis, G. Mozolevskis, V. Vibornijs. Integrated Lossy Mode Resonance Sensor Based on SU-8 Waveguides. San Francisco, USA, 22–27 January 2022.
2. Poster presentation at the international conference "Nordic Nanolab User Meeting 2022", **E. Letko**, A. Bundulis, V. Vibornijs, G. Mozolevskis. Fabrication of Lossy Mode Resonance Sensor Based on SU-8 Waveguides. Gothenburg, Sweden, 5–6 May 2022.
3. Poster presentation at the international conference "Deep Tech Atelier 2023", **E. Letko**, A. Bundulis, I. Del Villar, G. Mozolevskis. Development of Integrated Lossy Mode Resonance Sensor Based on Polymer Photonics. Riga, Latvia, 20–21 April 2023.

MAIN RESULTS OF THE THESIS

Integrated LMR sensor based on SU-8 waveguides (Paper I)

Paper I represents the initial attempt to realize the LMR phenomenon within PICs. While this paper provided the first insights into the LMR phenomenon, it was challenging to estimate device performance due to the wideness of resonance lines. Nevertheless, this research significantly contributed to understanding the key challenges in LMR chip design and discussed potential future applications.

The primary objective outlined in Paper I was to measure transmittance in an integrated LMR device for the first time. Accordingly, the established tasks were:

- To develop fabrication workflow for integrated devices based on SU-8 waveguides.
- To evaluate the coverage of the SU-8 waveguide with lossy coating.
- To measure transmittance in LMR waveguides for various lossy coating materials.

The main results of Paper I are demonstrated in Fig. 8–10.

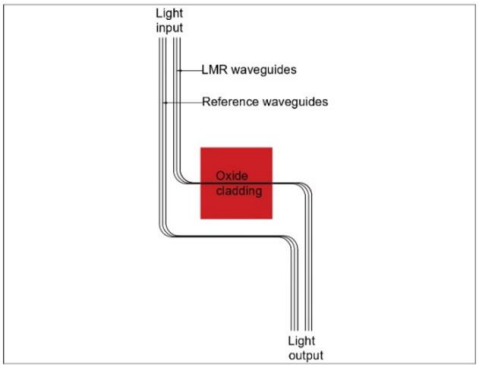

Fig. 8. LMR-based sensor design.[25]

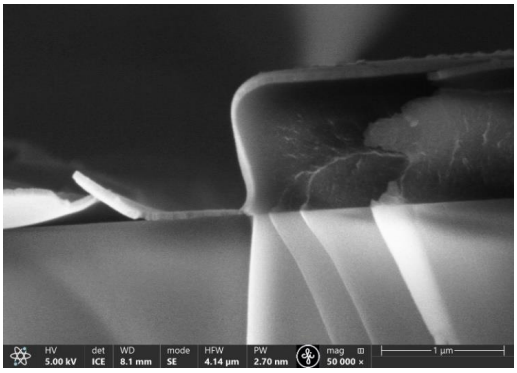

Fig. 9. Cross-section view of the waveguide with 65 nm thick ZnO cladding.[25]

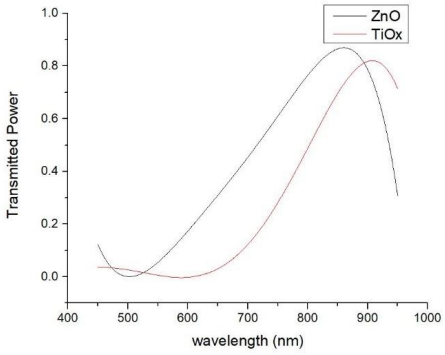

Fig. 10. Transmitted power of SU-8 waveguides with ZnO and TiO_x claddings.[25]

The main results and conclusions of Paper I:

- The chip design involved two batches of waveguides: reference waveguides for measuring the light source spectrum and LMR waveguides for observing the phenomenon. Optimal efficiency was achieved through a curved waveguide design to mitigate background illumination (see Fig. 8).
- Magnetron sputtering of oxides resulted in complete coverage of the SU-8 waveguide (see Fig. 9).
- Wide LMR lines were detected for ZnO and TiO_x materials. The observed LMRs occurred at wavelengths predicted by theory (see Fig. 10).

Theoretical development of polymer-based integrated LMR sensor for photonic integrated circuits (Paper II)

Given the challenges in fabricating an integrated LMR device with sensitivity comparable to LMR sensors using alternative configurations as highlighted in Paper I, Paper II was initiated to explore theoretical design solutions for integrated LMR devices and investigate the dimensional dependencies of the LMR phenomenon. The observation of LMR in PICs has not been accomplished before. Therefore, to streamline the transfer of LMR technology from optical fibers and planar waveguides to integrated photonics, it was essential to conduct theoretical research. Consequently, the objective of Paper II was to theoretically demonstrate the potential for achieving the LMR effect at the integrated chip level and determine the optimal geometry of the SU-8 waveguide and thickness of the lossy coating to enhance sensor sensitivity.

The goals set in Paper II :

- To investigate LMR dependency on SU-8 waveguides' cross-sectional dimensions.
- To investigate LMR dependency on lossy coating thickness.
- To investigate guided modes in LMR waveguides.
- To evaluate the sensing performance of the designed device.
- To observe multiple possible resonances in the designed LMR chip.

The main results of Paper II are demonstrated in Fig. 11–Fig. 13.

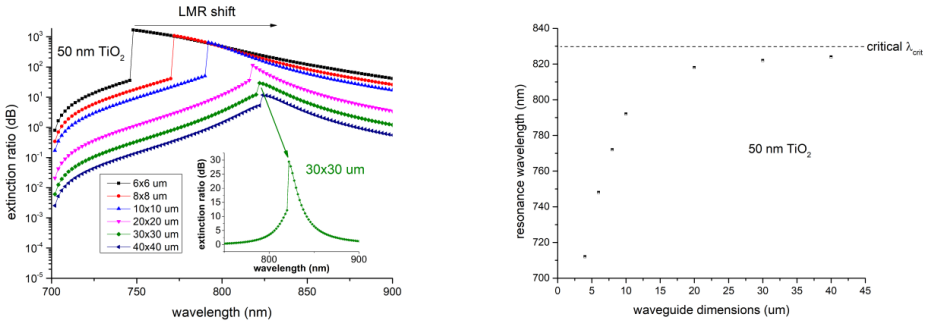

(a) (b)

Fig. 11. Effect of waveguide dimensions on the LMR effect: (a) normalized transmittance spectra for different waveguide dimensions, and (b) dependence of LMR wavelength on waveguide dimensions.[26]

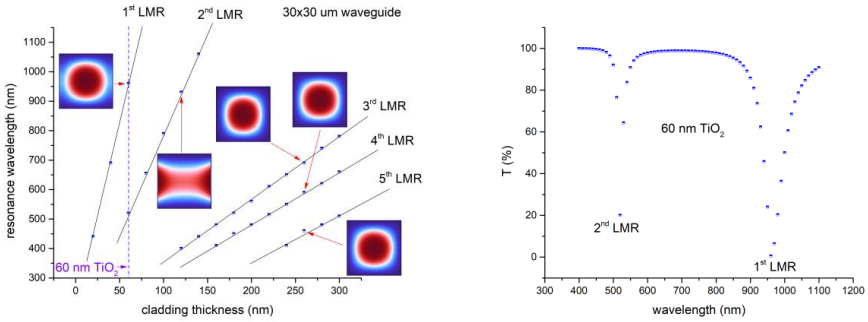

(a) (b)

Fig. 12. LMR in dependence of lossy cladding thickness: (a) LMR wavelength as a function of cladding thickness, and (b) transmittance spectrum for a device with a 60 nm TiO_2 coating thickness.[26]

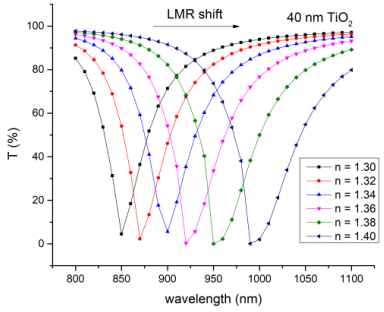

Fig. 13. LMR shift with a change in the refractive index of the medium.[26]

The main results and conclusions of Paper II:

- Theoretical simulations revealed the feasibility of observing the LMR phenomenon in integrated SU-8 waveguides coated with TiO_2 lossy coating.
- It was discovered that LMR tuning is achievable by adjusting the waveguide geometry, as the LMR wavelength exhibits high sensitivity to the waveguide dimensions (see Fig. 11). Additionally, it has been demonstrated that this sensitivity is higher for smaller waveguides, and once the waveguide reaches certain dimensions, the LMR wavelength stabilizes and exhibits minimal shift (see Fig. 11b).
- It was shown that multiple LMRs could theoretically be observed in the integrated SU-8 waveguides coated with TiO_2 lossy coating (see Fig. 12).

- Both TE and TM polarizations were shown to induce LMR in the designed integrated device at slightly disparate wavelengths.
- The maximum sensitivity of 1400 nm/RIU can be attained with a 40 nm thick TiO_2 coating, suitable for measuring environments with refractive indices ranging from 1.30 to 1.40 (see Fig. 13).

LMR sensors based on planar waveguides: theoretical and experimental comparison (Paper III)

The prevailing scientific literature on LMR primarily emphasizes engineering aspects, leading to a noticeable deficiency in the theoretical foundation and understanding of the fundamental processes inherent in the LMR phenomenon. Hence, Paper III delved into the LMR phenomenon in planar waveguides, specifically those with commonly used coatings in the LMR field, such as TiO_2, SnO_2, and ITO. Additionally, the experimental results obtained were compared with simulations conducted through the FEM in COMSOL Multiphysics. The distinctive novelty of this research lies in the integration of both experimental findings and theoretical calculations. Moreover, from the perspective of developing an integrated LMR sensor, this study was pivotal as it aimed to identify the optimal lossy coating material for subsequent research.

The goals set in Paper III:

- To experimentally observe the LMR phenomenon in sensing devices coated with various materials such as TiO_2, SnO_2, and ITO.
- To investigate the dependency of the LMR phenomenon on various thicknesses of lossy coatings.
- To ascertain the electro-optical properties of deposited thin films, including refractive indices and extinction coefficients, to enhance the accuracy of simulation results.
- To compare the measured transmittance spectra of all fabricated samples with theoretically calculated spectra using simulation tools based on the FEM.
- To observe LMRs induced by both TE and TM polarizations.
- To identify the most suitable lossy coating based on the shape of the LMR peak.
- To assess the sensing capabilities of the devices by applying liquid analytes onto the sensing area.
- To determine the Q-factors of the fabricated devices to gauge their performance.

The main results of Paper III are demonstrated in Fig. 14–Fig. 17.

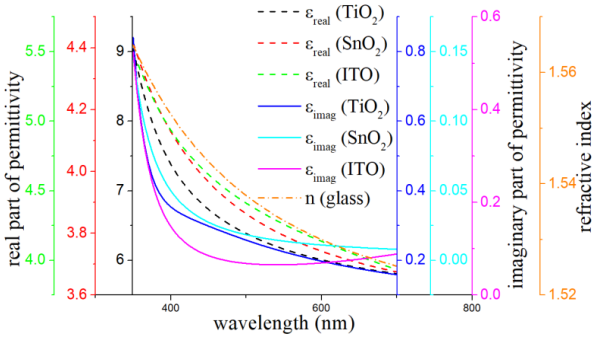

Fig. 14. Dispersion curves of glass waveguide, TiO_2, SnO_2 and ITO thin films.[27]

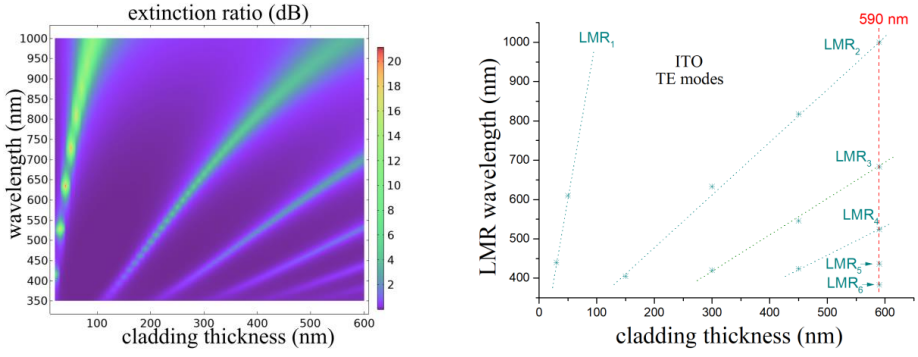

(a) (b)

Fig. 15. TE-polarized LMRs in dependence of wavelength and ITO thickness: (a) theoretical, and (b) experimental.[27]

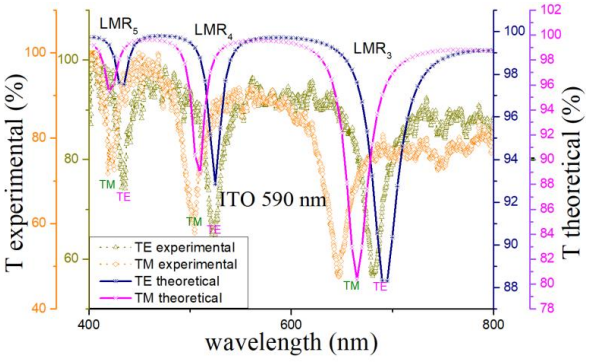

Fig. 16. Transmittance spectra for device with 590 nm thick ITO coating.[27]

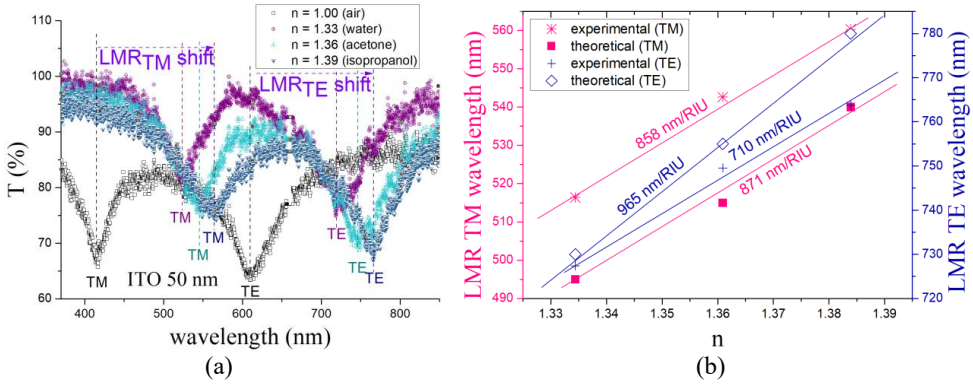

Fig. 17. Sensing performance of a 50 nm coated ITO sample: (a) experimental response in various liquids, and (b) LMR as a function of the refractive index of the surrounding medium for both TE and TM polarizations.[27]

The main results and conclusions of Paper III:

- ITO coating demonstrated the best suitability for LMR-based sensor applications – only this coating produced pronounced LMRs across the entire visible light spectrum (see Fig. 16). This was likely attributable to the deposition technique employed, wherein ITO was deposited using non-reactive magnetron sputtering, while the other oxides underwent deposition via a reactive process, leading to the formation of crystalline grains that exhibited limited interaction with long-wavelength light. An alternative explanation for this observation was attributed to the differences in the dispersion of extinction coefficients for ITO and other oxide coatings.
- Comprehensive comparison between theoretical simulations and experimental observations showed that the FEM, in combination with mode analysis, effectively captures the underlying physics of the LMR phenomenon within planar waveguides. The theoretical color plots demonstrated a sufficient level of agreement with the experimentally derived results across the entire range of coating thicknesses (see Fig. 15). However, it is important to note certain distinctions in Q-factors obtained theoretically and experimentally, which can be attributed to inhomogeneity of thin films and the possibility of less precise theoretical input data regarding the optical properties of the analyzed medium and coating thickness.
- Utilizing a linear polarizer during measurements confirmed the anticipated polarization dependency of the LMR phenomenon (see Fig. 16 and Fig. 17).

LMR in PICs (Paper IV)

Article IV was the final study of the Thesis. All three previous papers (Paper I, Paper II, and Paper III) were intended to provide insight into the LMR phenomenon and answer specific questions regarding the creation of the first fully integrated LMR-based sensor. Paper I gave us an

understanding of what direction to move in to create a working prototype. Paper II gave us insight into the sizing limitations of polymer waveguides. Paper III gave us the first real experimental experience of successful LMR generation. Paper IV demonstrated for the first time the observation of LMR in PICs with sensitivity and FOM comparable to those of optical fibers and planar waveguides. Additionally, Paper IV offered a comparison of different polymer materials such as OrmoClear, OrmoCore and SU-8 for fabricating integrated waveguides. In addition, Paper IV introduced a novel process for producing thick polymer waveguides. Finally, this study compared the experimental results with simulation results performed using the FEM in COMSOL Multiphysics.

The goals set in Paper IV:

- To develop an innovative workflow for fabricating thick waveguides.
- To establish an experimental measurement setup for testing integrated chips.
- To minimize light losses during the coupling of light into waveguides.
- To investigate the dependence of the LMR phenomenon on the geometry of straight and curved waveguides.
- To observe multiple LMRs in integrated chips.
- To compare the transmittance capabilities of waveguides made from various polymers.
- To compare experimentally obtained spectra with spectra expected theoretically by simulations.
- To contrast LMR behavior in integrated chip configurations with well-established configurations such as planar waveguides.
- To evaluate the sensing capabilities of the integrated devices by applying liquid analytes onto the sensing area.
- To determine the FOM of the fabricated devices to assess their performance.

The main results of Paper IV are demonstrated in Fig. 18–Fig. 23.

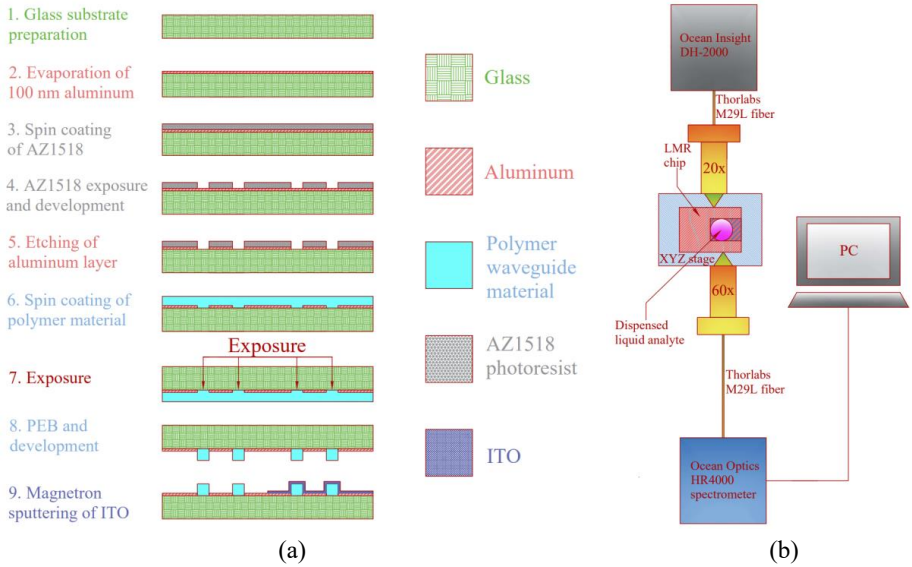

Fig. 18. LMR chip: (a) its fabrication workflow, and (b) its testing.[28]

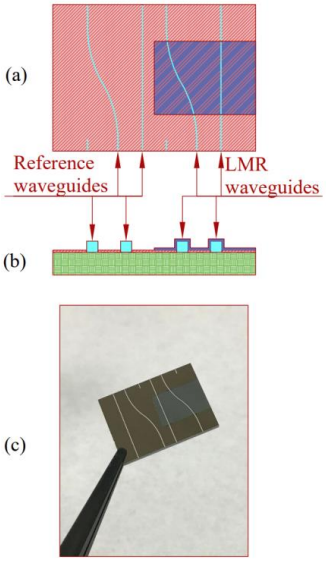

Fig. 19. The final design of the LMR chip: (a) top view, (b) cross-sectional view, (c) a photo of the actual device.[28]

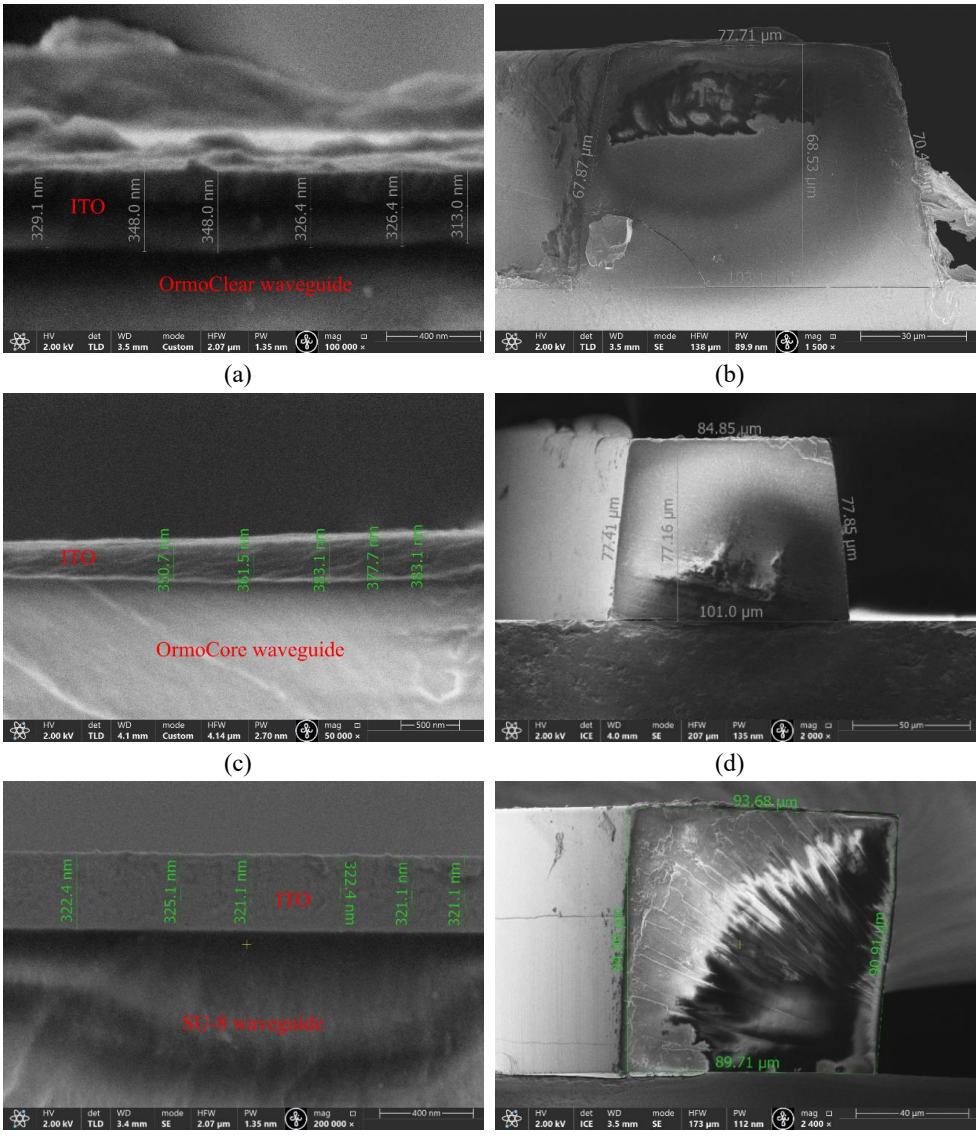

Fig. 20. SEM analysis: (a) ITO on an OrmoClear waveguide, (b) cross-section of an OrmoClear waveguide, (c) ITO on an OrmoCore waveguide, (d) cross-section of an OrmoCore waveguide, (e) ITO on a SU-8 waveguide, and (f) cross-section of a SU-8 waveguide.[28]

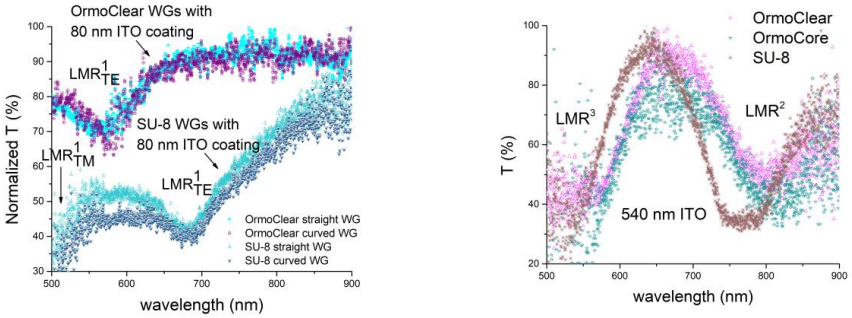

(a) (b)

Fig. 21. Comparison of LMR in different types of waveguides: (a) in straight and curved waveguides, and (b) in waveguides of different polymers.[28]

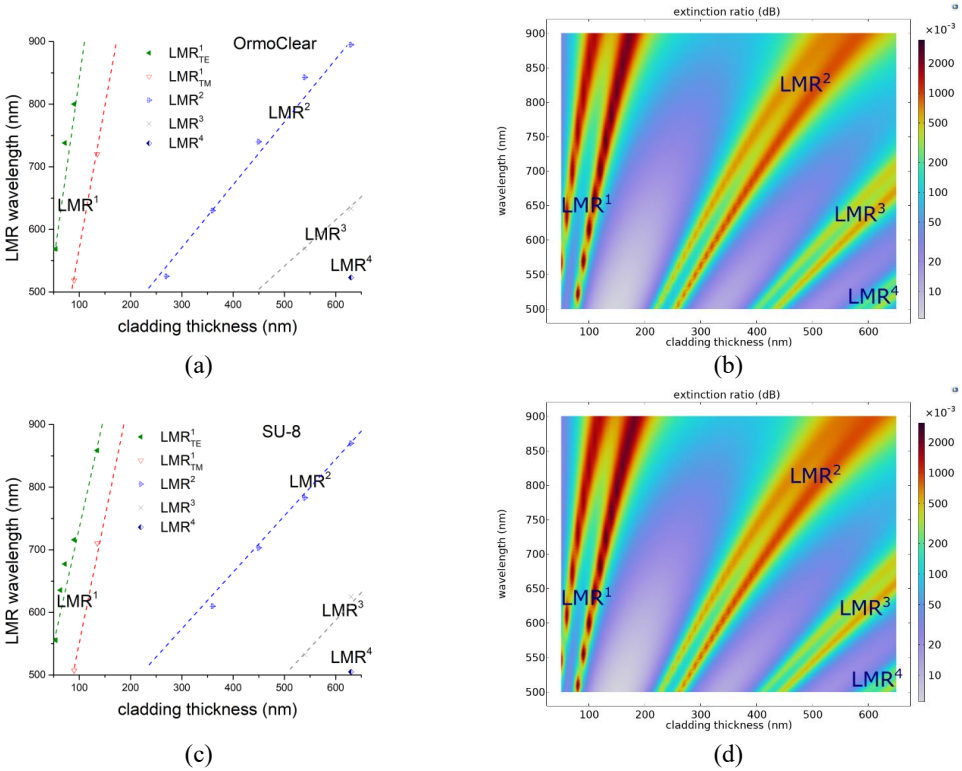

(a) (b)

(c) (d)

Fig. 22. LMRs in dependence of wavelength and ITO thickness: (a) experimental results for OrmoClear waveguides, (b) theoretical results for OrmoClear waveguides, (c) experimental results for SU-8 waveguides, and (d) theoretical results for SU-8 waveguides.[28]

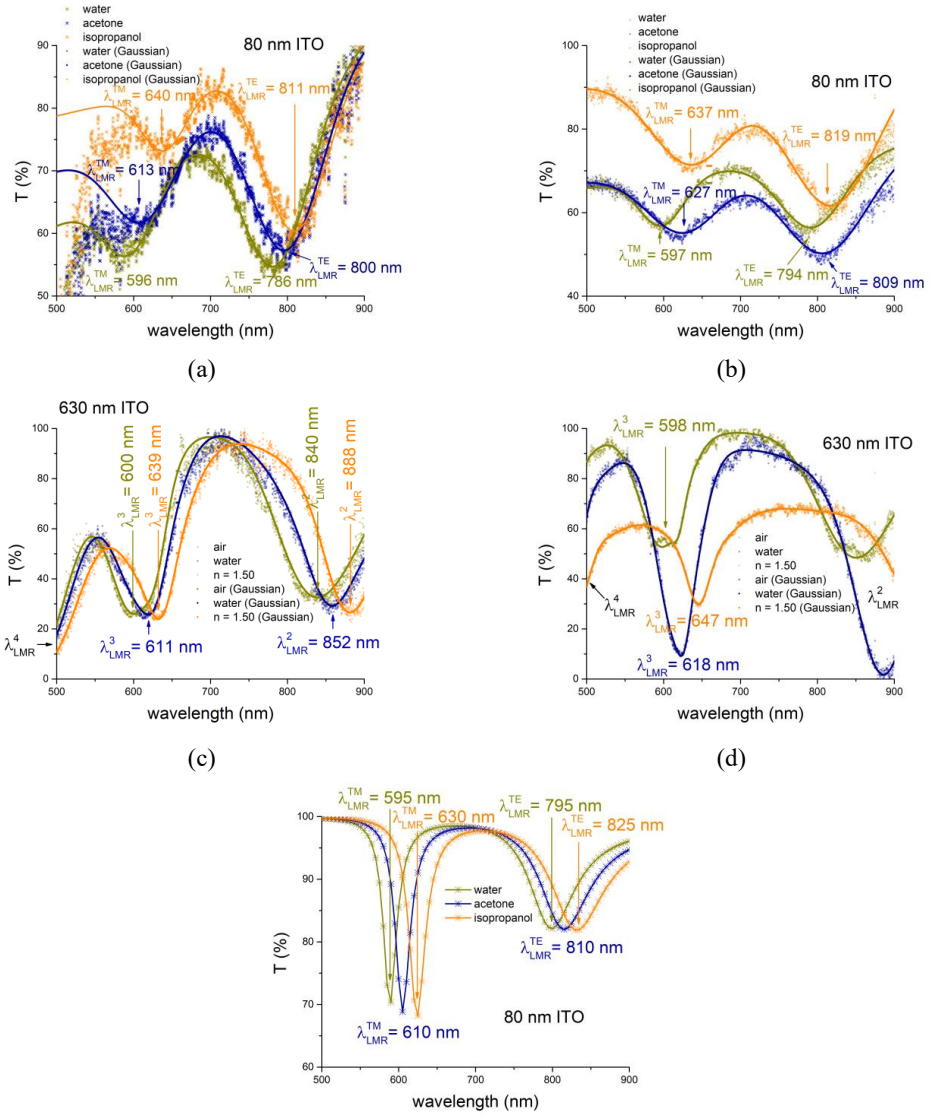

Fig. 23. Experimental sensing response in various liquids: (a) first-order LMRs in an integrated device based on SU-8 waveguides, (b) first-order LMRs in a planar glass waveguide, (c) higher-order LMRs in an integrated device based on SU-8 waveguides, (d) higher-order LMRs in a planar glass waveguide, and (e) theoretically calculated first-order LMRs in an integrated device based on SU-8 waveguides.[28]

The main results and conclusions of Paper IV:

- To test the LMR phenomenon in integrated chips, a custom-built measurement setup, depicted in Fig. 18b, was designed.
- Saw dicing outsourcing services were utilized to minimize light losses during light coupling into waveguides, ensuring smooth, flat waveguide edges. Light was coupled onto waveguide facets using an objective to focus light on the edge of the waveguide (see Fig. 18b).
- Multiple LMRs were observed in integrated chips for waveguides made of all tested polymers (see Fig. 21b).
- This research successfully demonstrated the observation of the LMR phenomenon in integrated waveguides of various geometries (see Fig. 21a).
- Among the polymer materials tested for waveguide fabrication, SU-8 emerged as the superior polymer for guiding the entire visible light spectrum, leading to more pronounced LMRs compared to other polymer materials.
- It was demonstrated that waveguide geometry has minimal impact on LMR, except for a reduction in light intensity observed in curved waveguides due to bend losses (see Fig. 21a).
- This paper introduces a novel fabrication method for thick waveguides, involving exposure through the glass substrate and an aluminum mask positioned directly on the chip (see Fig. 18a). This technique produces waveguides with a more rectangular cross-sectional profile, and in the case of SU-8 waveguides, it even resulted in a slightly negative trapezoidal shape (see Fig. 20). This approach enables the production of high-quality waveguides capable of propagating light to observe LMR, a capability not achievable with other fabrication techniques.
- The FOM and sensitivity of integrated polymer-based devices and planar waveguides were similar in both setups, highlighting the potential of integrated systems in LMR (see Fig. 23). The relative error between experimental (Fig. 23a) and simulated (Fig. 23e) LMR peak wavelengths was only 1 %.
- With the exception of OrmoCore, every tested polymer material exhibited LMR dependence on cladding thickness and resonance wavelength consistent with predictions from theoretical simulations conducted via COMSOL Multiphysics (see Fig. 22). The primary differences arose from the measurement setup, which did not utilize a linear polarizer. Consequently, it was not feasible to observe TM and TE modes separately for higher-order LMRs, as predicted by theoretical calculations. Additionally, experimentally obtained FOM closely aligned with simulated predictions.

CONCLUSIONS

1. For the first time, the LMR phenomenon has been observed in integrated waveguides made from various polymers, including OrmoClear, OrmoCore, and SU-8 photoresists.
2. Integrated LMR sensors can attain a sensing performance of 905 nm/RIU, which is comparable to alternative well-established configurations of LMR sensors. To achieve this, the integrated LMR chip should comprise SU-8 waveguides with dimensions of 100 × 100 μm in cross-section, coated with an 80 nm thick ITO lossy cladding.
3. For the first time, FEM simulation methodology was completely developed to model the LMR phenomenon in integrated polymer waveguides, demonstrating a 1 % relative error in matching experimental LMR peak wavelengths. This method can also optimize actual device designs to achieve maximum sensing performance.

REFERENCES

(1) Del Villar, I.; Arregui, F. J.; Zamarreño, C. R.; Corres, J. M.; Bariain, C.; Goicoechea, J.; Elosua, C.; Hernaez, M.; Rivero, P. J.; Socorro, A. B.; Urrutia, A.; Sanchez, P.; Zubiate, P.; Lopez, D.; De Acha, N.; Ascorbe, J.; Matias, I. R. Optical Sensors Based on Lossy-Mode Resonances. *Sensors Actuators, B Chem.* **2017**, *240*, 174–185. https://doi.org/10.1016/j.snb.2016.08.126.

(2) Wang, Q.; Zhao, W. M. A Comprehensive Review of Lossy Mode Resonance-Based Fiber Optic Sensors. *Opt. Lasers Eng.* **2018**, *100* (July 2017), 47–60. https://doi.org/10.1016/j.optlaseng.2017.07.009.

(3) Zamarreño, C. R.; Hernáez, M.; Del Villar, I.; Matías, I. R.; Arregui, F. J. Optical Fiber PH Sensor Based on Lossy-Mode Resonances by Means of Thin Polymeric Coatings. *Sensors Actuators, B Chem.* **2011**, *155* (1), 290–297. https://doi.org/10.1016/j.snb.2010.12.037.

(4) Zamarreño, C. R.; Hernaez, M.; Del Villar, I.; Matias, I. R.; Arregui, F. J. Tunable Humidity Sensor Based on ITO-Coated Optical Fiber. *Sensors Actuators, B Chem.* **2010**, *146*(1), 414–417. https://doi.org/10.1016/j.snb.2010.02.029.

(5) Fuentes, O.; Goicoechea, J.; Corres, J. M.; Villar, I. Del; Ozcariz, A.; Matias, I. R. Generation of Lossy Mode Resonances with Different Nanocoatings Deposited on Coverslips. *Opt. Express* **2020**, *28*(1), 288. https://doi.org/10.1364/oe.28.000288.

(6) Arregui, F. J.; Villar, I. Del; Corres, J. M.; Goicoechea, J.; Carlos, R.; Elosua, C.; Hernaez, M.; Rivero, P. J.; Socorro, A. B.; Sanchez, P.; Zubiate, P.; Lopez, D.; Acha, N. De; Matias, I. R. Fiber-Optic Lossy Mode Resonance Sensors. *Procedia Eng.* **2014**, *87*, 3–8. https://doi.org/10.1016/j.proeng.2014.11.253.

(7) Refractometer, F.; Sudas, D. P.; Zakharov, L. Y.; Jitov, V. A.; Golant, K. M. Silicon Oxynitride Thin Film Coating to Lossy Mode Resonance. **2022**, 1–12.

(8) Zhao, W. M.; Wang, Q. Analytical Solutions to Fundamental Questions for Lossy Mode Resonance. *Laser Photonics Rev.* **2023**, *17*(1), 1–18. https://doi.org/10.1002/lpor.202200554.

(9) Razquin, L.; Zamarreno, C. R.; Munoz, F. J.; Matias, I. R.; Arregui, F. J. Thrombin Detection by Means of an Aptamer Based Sensitive Coating Fabricated onto LMR-Based Optical Fiber Refractometer. *Proc. IEEE Sensors* **2012**, 3–6. https://doi.org/10.1109/ICSENS.2012.6411186.

(10) Zamarreño, C. R.; Hernaez, M.; Sanchez, P.; Del Villar, I.; Matias, I. R.; Arregui, F. J. Optical Fiber Humidity Sensor Based on Lossy Mode Resonances Supported by TiO2/PSS Coatings. *Procedia Eng.* **2011**, *25*, 1385–1388. https://doi.org/10.1016/j.proeng.2011.12.342.

(11) Ascorbe, J.; Corres, J. M.; Arregui, F. J.; Matias, I. R. Low voltage transducer based on the changes in the wavelength of the attenuation band. *SENSORS, 2014 IEEE*, **2014**, 1–4. https://doi.org/10.1109/ICSENS.2014.6985404

(12) Sánchez, P.; Zamarreño, C. R.; Arregui, F. J.; Matías, I. R. LMR-Based Optical Fiber Refractometers for Oil Degradation Sensing Applications in Synthetic Lubricant Oils. *J. Light. Technol.* **2016**, *34*(19), 4537–4542. https://doi.org/10.1109/JLT.2016.2562701.

(13) Zubiate, P.; Zamarreno, C. R.; Del Villar, I.; Matias, I. R.; Arregui, F. J. D-Shape Optical Fiber PH Sensor Based on Lossy Mode Resonances (LMRs). *2015 IEEE SENSORS* –

Proc. **2015**, 1–4. https://doi.org/10.1109/ICSENS.2015.7370421.
(14) Elosúa, C.; Vidondo, I.; Arregui, F. J.; Bariain, C.; Luquin, A.; Laguna, M.; Matías, I. R. Lossy Mode Resonance Optical Fiber Sensor to Detect Organic Vapors. *Sensors Actuators, B Chem.* **2013**, *187*, 65–71. https://doi.org/10.1016/j.snb.2012.09.046.
(15) Zamarreño, C. R.; Ardaiz, I.; Ruete, L.; Muñoz, F. J.; Matias, I. R.; Arregui, F. J. C-Reactive Protein Aptasensor for Early Sepsis Diagnosis by Means of an Optical Fiber Device. *Proc. IEEE Sensors* **2013**, 4–7. https://doi.org/10.1109/ICSENS.2013.6688222.
(16) Paliwal, N.; John, J. Lossy Mode Resonance Based Fiber Optic Sensors. *Smart Sensors, Meas. Instrum.* **2017**, *21*(10), 31–50. https://doi.org/10.1007/978-3-319-42625-9_2.
(17) Corres, J. M.; Ascorbe, J.; Arregui, F. J.; Matias, I. R. Tunable Electro-Optic Wavelength Filter Based on Lossy-Guided Mode Resonances. *Opt. Express* **2013**, *21*(25), 31668. https://doi.org/10.1364/oe.21.031668.
(18) Chiavaioli, F.; Gouveia, C. A. J.; Jorge, P. A. S.; Baldini, F. Towards a Uniform Metrological Assessment of Grating-Based Optical Fiber Sensors: From Refractometers to Biosensors. *Biosensors* **2017**, *7*(2). https://doi.org/10.3390/bios7020023.
(19) Paquet, C.; Kumacheva, E. Polymers for Photonics. **2008**, *11*(4), 48–56.
(20) Sciences, O. Hybrid Organic-Inorganic for Low-Cost Photonics Integration. **2007**, *00*, 234–235.
(21) Sherman, S.; Zappe, H. Printable Bragg Gratings for Polymer-Based Temperature Sensors. *Procedia Technol.* **2014**, *15*, 702–709. https://doi.org/10.1016/j.protcy.2014.09.041.
(22) Jiang, L.; Wu, J.; Chen, K.; Zheng, Y.; Deng, G.; Zhang, X.; Li, Z.; Chiang, K. S. Polymer Waveguide Mach-Zehnder Interferometer Coated with Dipolar Polycarbonate for on-Chip Nitroaromatics Detection. *Sensors Actuators, B Chem.* **2020**, *305* (September 2019), 127406. https://doi.org/10.1016/j.snb.2019.127406.
(23) Wei, H.; Krishnaswamy, S. Polymer Micro-Ring Resonator Integrated with a Fiber Ring Laser for Ultrasound Detection. *Opt. Lett.* **2017**, *42*(13), 2655. https://doi.org/10.1364/ol.42.002655.
(24) Benítez, M.; Zubiate, P.; Del Villar, I.; Socorro-Leránoz, A. B.; Matías, I. R. Lossy Mode Resonance Based Microfluidic Platform Developed on Planar Waveguide for Biosensing Applications. *Biosensors* **2022**, *12*(6), 403. https://doi.org/10.3390/bios12060403.
(25) Letko, E.; Bundulis, A.; Mozolevskis, G.; Vibornijs, V. Integrated Lossy Mode Resonance Sensor Based on SU-8 Waveguides. **2022**, No. March 2022, 26. https://doi.org/10.1117/12.2607716.
(26) Letko, E.; Bundulis, A.; Mozolevskis, G. Theoretical Development of Polymer-Based Integrated Lossy-Mode Resonance Sensor for Photonic Integrated Circuits. *Photonics* **2022**, *9*(10). https://doi.org/10.3390/photonics9100764.
(27) Letko, E.; Bundulis, A.; Mozolevskis, G. Lossy Mode Resonance Sensors Based on Planar Waveguides: Theoretical and Experimental Comparison. *IEEE Photonics J.* **2024**, *16*(1), 1–7. https://doi.org/10.1109/JPHOT.2023.3348993.
(28) Letko, E.; Bundulis, A.; Vanags, E.; Mozolevskis, G. Lossy Mode Resonance in Photonic Integrated Circuits. *Opt. Lasers Eng.* **2024**, *181* (May). https://doi.org/10.1016/j.optlaseng.2024.108387.

PIELIKUMI / APPENDICES

Integrated lossy mode resonance sensor based on SU-8 waveguides

Edvins Letko, Arturs Bundulis, Gatis Mozolevskis, Viktors Vibornijs

Edvins Letko, Arturs Bundulis, Gatis Mozolevskis, Viktors Vibornijs, "Integrated lossy mode resonance sensor based on SU-8 waveguides," Proc. SPIE 11998, Organic Photonic Materials and Devices XXIV, 119980B (7 March 2022); doi: 10.1117/12.2607716

SPIE.

Event: SPIE OPTO, 2022, San Francisco, California, United States

Integrated Lossy Mode Resonance Sensor Based on SU-8 Waveguides

Edvins Letko[1,2], Arturs Bundulis[1,2], Gatis Mozolevskis[1,2], Viktors Vibornijs[2]

[1]Cellboxlab SIA, Vienibas gatve 186A, Riga, Latvia
[2]Institute of Solid State Physics, University of Latvia, Kengaraga iela 8, Riga, Latvia,

ABSTRACT

In recent years, lossy mode resonance (LMR) biosensors have proven to be promising devices for the analysis of biological entities. In this work, for the first time, the possibility of observing the LMR effect in photonic integrated sensor based on SU-8 waveguides for biosensing applications is presented. SU-8 is a polymer that is ideally suited for optical waveguide applications due to its very high optical transparency, chemical stability and simple fabrication process. The LMR effect is achieved by using ZnO and TiO_x claddings over the waveguides. The influence of different cladding thicknesses and materials on the LMR effect is demonstrated. Different design waveguides are tested. Potential future applications and development steps of integrated LMR sensor will be discussed.

Keywords: Lossy mode resonance, SU-8 waveguides, magnetron sputtering, photolithography

1. INTRODUCTION

Today it is impossible to imagine life without a wide variety of biosensors. In last years, sensors implementing optical resonance structures (ring resonators, photonic crystals etc.) are becoming more popular due to their high sensitivity to any external changes[1,2]. Among devices of this type, sensors based on optical waveguides with a cladding that generates surface plasmon resonance (SPR) or lossy mode resonance (LMR) have received great interest due to their simple design and fabrication, while providing high sensitivity as well as immunity to external electromagnetic fields[3].

Nowadays, polymers are becoming an increasingly popular material for waveguides fabrication[4]. Compared to inorganic counterparts polymers are relatively inexpensive, they are flexible and can be functionalized to achieve required optical, electronic or mechanical properties for specific photonic applications[5]. One of the most commonly used polymers in the field of integrated optics is the SU-8 photoresist. SU-8 is chemically stable and resistant to most acids and other solvents and can be patterned using direct write laser lithography. It has very high optical transparency in the visible and near-infrared regions of the spectrum, making the SU-8 ideal for optical waveguide applications in visible range[6].

The most popular fiber-optic and waveguide biosensors are based on the SPR effect[7]. To achieve this effect, it is necessary to synthesize or deposit a thin film or nanoparticles on the surface of an optical fiber or waveguides. SPR occurs when the real part of the thin film permittivity is negative and higher in magnitude than both its own imaginary part and the permittivity of the material surrounding the thin film[8]. This imposes rather severe restrictions on the possible choice of coating material, which, in fact, narrows down to a number of metals[9]. Another disadvantage of SPR-based sensors is the ability to observe SPR effect exclusively with TM polarized light. Nowadays LMR sensors are becoming a popular alternative to SPR sensors as it is sensitive to both TM and TE modes. To realize LMR effect a material with a positive real part of permittivity is used as coating for an optical waveguide, while observing all other conditions necessary for the implementation of SPR, all the above disadvantages can be eliminated. In addition, a wide range of materials, such as polymers, semiconductors, dielectrics and their various combinations, meet these conditions [3]. Another

Organic Photonic Materials and Devices XXIV, edited by William M. Shensky III, Ileana Rau, Okihiro Sugihara,
Proc. of SPIE Vol. 11998, 119980B · © 2022 SPIE · 0277-786X · doi: 10.1117/12.2607716

significant LMR advantage is the possibility to generate multiple resonances in the same optical fiber or waveguide geometry[10].

Up to date most of researches focuses on LMR effect sensors based on fiber-optics and planar waveguides. The aim of the research presented in this paper is to step towards integrated LMR sensors and demonstrate that LMR effect can be well achieved using on-chip polymer waveguides. In this work, the LMR effect is shown for the first time in SU-8 waveguides with a cladding of various oxides. This research will be the first step in the development of a photonic integrated sensor based on LMR for the analysis of biological entities such as extracellular vesicles, which are promising biomarkers in diagnostic applications[11].

2. EXPERIMENTAL

2.1. Sample preparation

SU-8 photoresist (Gersteltec GM1040) was spin coated 30 seconds with 3000 rpm on glass substrates with Laurell WS650 system which resulted in 1 µm thick photoresist layer. SU-8 waveguides were fabricated by selectively exposing the spin coated photoresist with laser writer Heidelberg µPG system (375 nm UV light source) and developing in mr-Dev 600. Before waveguides fabrication glass substrates were scribed with diamond scriber ATV RV-129. This was necessary in order to break the substrate together with the waveguide for efficient light input. Each fabricated sample consisted of 6 waveguides, 3 of which have a width of 5 µm, 10 µm and 15 µm, respectively, and pass through the oxide cladding layer. The remaining 3 waveguides play a reference role for measuring the actual spectra of the light source, they have the same width as the first 3 waveguides and do not pass through the oxide cladding layer Figure 1. Waveguides has such a design due to the fact that when using straight waveguides, part of the scattered light from waveguide input facet will enter the detector not through the waveguides, but propagating through the air or the substrate creating unwanted background illumination.

Sidrabe G500M reactive DC magnetron sputtering system was used for oxide claddings (ZnO, TiO_x and WO_x) deposition. Cladding deposition on each sample was done through a shadow mask to ensure the presence of also the waveguides without oxide coating Figure 1. Sputtering process was done in Ar/O_2 plasma using Zn, Ti and W 100x200x9mm targets.

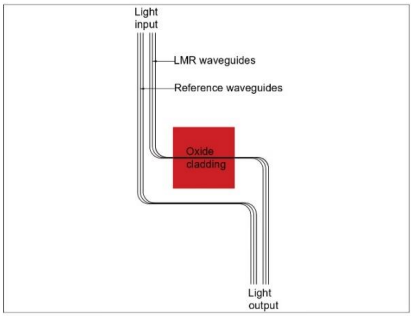

Figure 1. LMR-based sensor design.

2.2. Sample characterization

Oxide cladding layer thickness was measured using spectral ellipsometer Woollam RC2-XI. Sputtered oxide layer coverage of waveguides was characterized using Thermo Fisher Scientific Helios 5 UX SEM.

To measure the transmitted power of produced waveguide structures was used an experimental setup shown in Figure 2. As a light source was used Ocean Insight DH-2000 UV-VIS-NIR lightsource that was coupled into waveguide using objective. Output light was collected using another objective and analysed using a spectrometer Ocean Optics HR4000 and spectra was measured in spectral range of 450 - 900 nm . The sample was placed on XYZ stage to position the waveguide facet in the focal point of input objective. Output objective was also placed on a XYZ stage to align it with waveguide output facet.

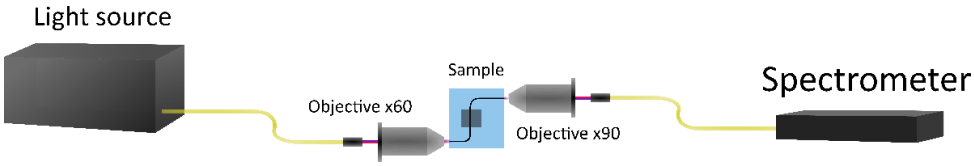

Figure 2. Experimental setup for transmission measurements.

3. RESULTS AND DISCUSSION

Different oxide cladding materials and thicknesses were tested for observing LMR effect in SU-8 waveguides (Table 1). It was found that if the thickness of the oxide cladding exceeds the critical value (≈60 nm), then there was not output signal observed in the fabricated device. Apparently due to the fact that the waveguides are relatively thin, the evanescent field of the guided mode penetrates deeply into the oxide cladding, which leads to significant losses when layer thickness reaches threshold value. Samples without output signal were not further analyzed.

Table 1. Influence of different cladding materials and thicknesses on LMR effect.

Cladding material	Cladding thickness, nm	Results
ZnO	100	No output signal due to losses.
ZnO	65	No output signal due to losses.
ZnO	50	Spectrum measured
WO_x	100	No output signal due to losses.
TiO_x	50	Spectrum measured

SEM cross section picture of the waveguide with 65 nm thick ZnO cladding is shown in Figure 3. It is well seen that cladding coverage was sufficient to ensure guided mode interaction with cladding.

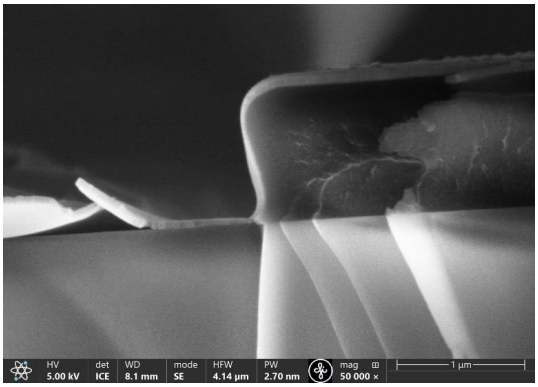

Figure 3. Cross section view of the waveguide with 65 nm thick ZnO cladding.

An example of an output signal for a waveguide with and without ZnO cladding is shown in Figure 4. The signal of SU-8 waveguide without cladding was observed in the spectral range of 450 – 900 nm.

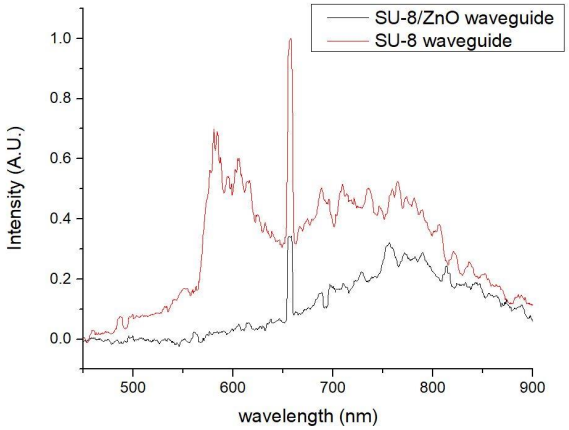

Figure 4. Output signal of SU-8 waveguide and SU-8 waveguide with ZnO.

By dividing both signals the transmittance spectra was acquired. Results for ZnO and TiO_x are shown in Figure 5. According to literature[12,13] LMR effect for ZnO is observed at lower wavelengths in comparison with TiO_x. It agrees with results in our experiments – for ZnO LMR appears at ≈500 nm, but for TiO_x LMR appears at ≈600 nm. It is also known that for thin waveguides losses in the lossy mode resonance region are higher[14]. This explains why obtained resonances are so wide for 1 µm thin waveguides. In near-infrared region for both claddings the decrease in transmittance could be related to another lossy mode resonance which is related to TM polarization according to literature[12].

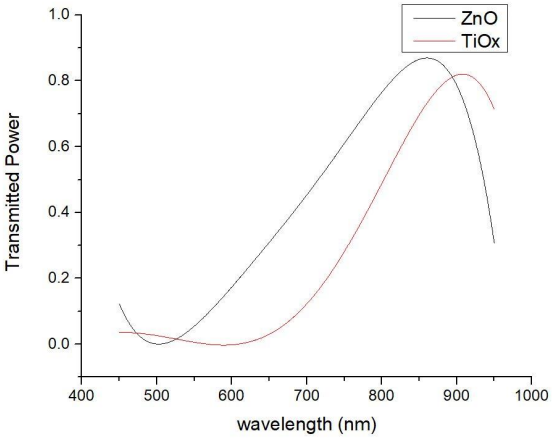

Figure 5. Transmitted power of SU-8 waveguides with ZnO and TiO_x claddings.

4. CONCLUSIONS

First steps in the development of photonic integrated sensors based on LMR effect in SU-8 waveguides are done. LMR effect in SU-8 waveguides with different oxide claddings and thicknesses was tested. LMR effect was observed in 1 μm thick waveguides with 50 nm thick ZnO and TiO_x claddings.

The next tasks would be to fabricate devices with thicker waveguides. This will increase the spectral range that can be introduced into the waveguide and reduce losses. In turn, with less losses it will be possible to use thicker oxide claddings that will make possible to observe multiple lossy mode resonances.

In the distant future is planned to fabricate photonic integrated circuit consisting of light source, detector and SU-8 waveguides with oxide cladding for biological entities analysis. Considering that the device will be used to detect various extracellular vesicles, another important task will be the functionalization of LMR oxide claddings for efficient catching of these entities.

5. REFERENCES

[1] Ali, L., Mohammed, M. U., Khan, M., Yousuf, A. H. B. and Chowdhury, M. H., "High-Quality Optical Ring Resonator based Biosensor for Cancer Detection," IEEE Sens. J. **PP**(c), 1 (2019).
[2] Inan, H., Poyraz, M., Inci, F., Lifson, M. A., Baday, M., Cunningham, B. T. and Demirci, U., "Chem Soc Rev promise for point-of-care applications," Chem. Soc. Rev. (2016).
[3] Kuznetsov, P. I., Sudas, D. P., Yapaskurt, V. O. and Savelyev, E. A., "Lossy mode resonance fiber-optic sensors based on niobium pentoxide thin film," Opt. Mater. Express **11**(8), 2650 (2021).
[4] Eldada, L., Member, S. and Shacklette, L. W., "Advances in Polymer Integrated Optics," 54–68 (2000).
[5] Paquet, C. and Kumacheva, E., "polymers for photonics," 48–56 (2008).

[6] Search, H., Journals, C., Contact, A., Iopscience, M. and Address, I. P., "SU-8 : a low-cost negative resist for" (1997).
[7] Zhao, Y., Tong, R. jie, Xia, F. and Peng, Y., "Current status of optical fiber biosensor based on surface plasmon resonance," Biosens. Bioelectron. **142**, 111505 (2019).
[8] Yang, F. and Sambles, J. R., "Determination of the optical permittivity and thickness of absorbing films using long range modes," J. Mod. Opt. **44**(6), 1155–1163 (1997).
[9] Gupta, B. D., Pathak, A. and Semwal, V., "Carbon-based nanomaterials for plasmonic sensors: A review," Sensors (Switzerland) **19**(16) (2019).
[10] Del Villar, I., Zamarreño, C. R., Hernaez, M., Arregui, F. J. and Matias, I. R., "Lossy mode resonance generation with indium-tin-oxide-coated optical fibers for sensing applications," J. Light. Technol. **28**(1), 111–117 (2010).
[11] Gaillard, M., Thuaire, A., Nonglaton, G., Agache, V., Roupioz, Y. and Raillon, C., "Biosensing extracellular vesicles: Contribution of biomolecules in affinity-based methods for detection and isolation," Analyst **145**(6), 1997–2013 (2020).
[12] Usha, S. P. and Gupta, B. D., "Performance analysis of zinc oxide-implemented lossy mode resonance-based optical fiber refractive index sensor utilizing thin film/nanostructure," Appl. Opt. **56**(20), 5716 (2017).
[13] Burnat, D., Koba, M., Wachnicki, Ł., Gierałtowska, S., Godlewski, M. and Śmietana, M., " Refractive index sensitivity of optical fiber lossy-mode resonance sensors based on atomic layer deposited TiO x thin overlay ," Sixth Eur. Work. Opt. Fibre Sensors **9916**, 99161G (2016).
[14] Fuentes, O., Del Villar, I., Corres, J. M. and Matias, I. R., "Lossy mode resonance sensors based on lateral light incidence in nanocoated planar waveguides," Sci. Rep. **9**(1), 1–10 (2019).

photonics

MDPI

Communication

Theoretical Development of Polymer-Based Integrated Lossy-Mode Resonance Sensor for Photonic Integrated Circuits

Edvins Letko [1,2,3,*], Arturs Bundulis [2] and Gatis Mozolevskis [1,2]

[1] Cellboxlabs Ltd., LV-2164 Riga, Latvia
[2] Institute of Solid State Physics, LV-1063 Riga, Latvia
[3] Faculty of Materials Science and Applied Chemistry, Riga Technical University, LV-1048 Riga, Latvia
* Correspondence: edvins.letko@cfi.lu.lv

Abstract: A promising phenomenon such as lossy-mode resonance (LMR) is of great interest in sensor applications. Until now, this phenomenon has been shown only in fibers or planar waveguides; however, given the rapid development of such an important technological area as photonic integrated circuits (PICs), it is important to transfer LMR technology specifically to PICs. In this article, we propose the theoretical development of an integrated polymer-based LMR sensor that will also contribute to the development of hybrid organic–inorganic PICs. This work theoretically shows that LMR can be achieved using polymer SU-8 waveguides on a glass substrate, on top of which TiO_2 is deposited. In addition, the paper shows that multiple resonances can be achieved in the developed integrated sensor. The highest sensor sensitivity (about 1400 nm/RIU) was achieved with 40 nm of TiO_2. The effect of the waveguide and coating geometries, as well as the polarizations of propagating modes, is studied in this paper.

Keywords: lossy-mode resonance; photonic integrated circuits; COMSOL Multiphysics; SU-8; TiO_2

Citation: Letko, E.; Bundulis, A.; Mozolevskis, G. Theoretical Development of Polymer-Based Integrated Lossy-Mode Resonance Sensor for Photonic Integrated Circuits. *Photonics* **2022**, *9*, 764. https://doi.org/10.3390/photonics9100764

Received: 6 September 2022
Accepted: 11 October 2022
Published: 12 October 2022

1. Introduction

In last few decades, sensors implementing optical resonance structures, such as ring resonators, photonic crystals, etc., have been in high demand due to their high sensitivity to external changes [1,2]. In recent years, there has been great interest in the phenomenon of lossy-mode resonance (LMR) [3]. LMR can be observed when light is propagating through an optical fiber or waveguide, and it interacts with thin films that have positive real parts of permittivity higher in magnitude than both their own imaginary parts and the permittivity of the fiber or waveguide materials [4]. Lossy coatings that are deposited on optical fibers or waveguides induce attenuation bands in the transmission spectra, which can be explained as a coupling between core and lossy modes of dielectric-cladding thin film [5]. These attenuation bands are sensitive to a huge number of external parameters (pH [6], humidity [7], etc.); therefore they can be used as sensors in various applications [5].

LMR has several advantages over other optical-fiber- and waveguide-based sensing techniques. Compared to similar and more commonly used sensing methods, such as surface plasmon resonance (SPR), LMR can generate multiple resonances. At the same time, in comparison with SPR, LMR is observed using both TE- and TM-polarized light [8]. In addition, LMR is a more practical method due to the fact that this effect can be observed for various cladding materials, such as polymer [6], semiconductor [9] and dielectric coatings [10], providing flexibility and low-cost sensing-device fabrication.

Recently, polymers have become popular materials for waveguides fabrication [11]. Compared with inorganic materials, polymers are inexpensive, flexible, and can be functionalized to achieve desired properties for specific photonic applications [12]. Photoresist SU-8 is one of the most commonly used polymers in the field of integrated photonics due its chemical stability and simple patterning with direct laser lithography. SU-8 is ideal for

waveguide applications in visible and near-infrared ranges due to its high transparency [13]. In the literature, LMR is observed mostly in the visible and near-infrared regions, making polymers a perfect candidate for the core material of LMR sensors [9]. However, it should be noted that LMR is observed in the UV range for some materials, which can cause certain difficulties when it is combined with polymer waveguides [14]. Among all materials, TiO_2 was chosen as a coating for two reasons. First, there are many ways to deposit it over potential waveguides (magnetron sputtering [15], atomic-layer deposition [16], etc.). Secondly, SU-8 does not guide UV radiation very well, while TiO_2 provides LMR in the red and near-infrared ranges, unlike some other dielectric coatings [14].

So far, the LMR effect has been shown in the literature only in fibers [9] or planar waveguides [17]. The transfer of LMR sensor technology to photonic integrated circuits (PICs) will gain huge interest from industry due to fabrication cheapness and scalability potential. This would be essential for Point-of-Care (POC) applications and Lab-on-Chip development where integrated sensors play a huge role. In addition to the above, the development of an integrated polymer-based LMR could also be extended to hybrid organic–inorganic PICs due to the simple integration of polymer with other photonic materials.

The aim of this work is to theoretically demonstrate for the first time the possibility of achieving the LMR effect in a level of integrated chip. At the same time, we consider it important to provide the simplest design so there will be no difficulties in the experimental implementation. Considering the above, the paper will evaluate the influence of the geometry of the SU-8 waveguide and lossy TiO_2 coating thickness on the LMR signal, and will also propose the optimal solution with the highest sensor sensitivity.

2. Materials and Methods

2.1. Materials Fabrication and Characterization

This section will describe the fabrication of SU-8 and TiO_2 thin films for the subsequent measurement of their optical properties, which will be necessary for simulations. We spin-coated SU-8 on glass slides (75 × 25 × 1 mm) using Laurell WS650 system. We prepared these glass slides before photoresist spin coating using acetone, detergent, deionized water, and isopropanol in ultrasonic bath. We also performed photoresist oxygen plasma ashing using GIGAbatch 360 M for better adhesion of SU-8. All critical photolithography parameters are given in Table 1.

We sputtered TiO_2 lossy thin film on glass slides (75 × 25 × 1 mm) using Sidrabe G500M reactive DC magnetron sputtering system. We performed sputtering process in Ar/O_2 (Ar and O_2 flow ratio was 3:1) plasma using Ti 100 × 200 × 9 mm target at 5 mTorr pressure and 300 W power.

We determined SU-8 photoresist, TiO_2 thin film, and SiO_2 glass slide optical properties using a Woollam RC2-XL spectral ellipsometer and CompleteEASE software. We carried out measurements at angles of incidence from 45° to 80° in the visible and near-infrared ranges. We found dispersion curves for SU-8 photoresist and SiO_2 glass slide using Sellmeier equation from CompleteEASE software manual:

$$n = \sqrt{\varepsilon_\infty + \frac{A\lambda^2}{\lambda^2 - B^2} - E\lambda^2}, \quad (1)$$

where A, B and E are fitted coefficients and λ is given in μm.

TiO_2 is an absorbing thin film; therefore, we used Lorentz oscillator model to determine optical properties. We determined TiO_2 permittivity using equation from CompleteEASE software manual:

$$\varepsilon = \varepsilon_\infty + \frac{Amp}{En^2 - E^2} + \sum \frac{Amp_n Br_n En_n}{En_n^2 - E^2 - iEBr_n}, \quad (2)$$

where all parameters except photon energy E are fitted parameters.

Table 1. SU-8 thin film fabrication.

Process Steps	Equipment and Materials Used	Critical Parameters
Spin coating	Laurell WS650, Gersteltec GM1060 photoresist	1. Acceleration for 30 s: 100 rpm/s 2. Constant rotation speed for 30 s: 1000 rpm 3. Acceleration for 30 s: −100 rpm/s
Soft bake	Unitemp high-precision hot plates	1. Temperature ramp rate for 500 s: 6 °C/min 2. Holding temperature for 300 s: 95 °C
Exposure	Mask aligner Suss MA6	1. Light source wavelength: 365 nm 2. Flood exposure dose: 300 mJ/cm^2
Post bake	Unitemp high-precision hot plates	1. Temperature rate for 270 s: 6 °C/min 2. Holding temperature for 300 s: 95 °C
Development	mr-Dev 600	1. Development time: 120 s
Hard bake	Unitemp high-precision hot plates	1. Temperature ramp rate for 1200 s: 6 °C/min 2. Holding temperature for 1800 s: 165 °C

2.2. LMR Device Simulations

The design of the developed LMR sensor is shown in Figure 1. We used COMSOL Multiphysics and the finite element method (FEM) to simulate this problem. First, we defined geometry. We used two-dimensional cross-sectional geometry to determine the electromagnetic distribution of the guided mode. This approach characterizes the behavior of the guided mode in an infinite homogeneous waveguide and ignores many parameters that are unnecessary at this stage (e.g., the light input), which also increases the performance of calculations. This geometry is shown in Figure 1b. The next step was materials definition. At this stage, we defined four different environments (SiO_2, SU-8, TiO_2, and sensing media) with experimentally determined optical properties. To solve posed problems, we used "Electromagnetic Waves, Frequency Domain" physics. After choosing the physics, we also chose the mesh. We meshed thin-film domain with physics-controlled element size (element size of 200 nm). We meshed other domains with element sizes comparable to wavelength. The last step was to find solutions. We performed a parametric sweep to test various waveguide and coating geometries. WE carried out a mode analysis to determine the distribution of the electromagnetic field in the waveguide for various wavelengths from 400 to 1100 nm. From this, we evaluated electromagnetic field distribution effective refractive index value n_{eff}, which can be used to simulate transmittance spectra from equation in Ref. [18]:

$$T = exp\left(-\frac{4\pi}{\lambda} imag\left(n_{eff}\right) L\right), \quad (3)$$

where T is transmittance, λ refers to light-source wavelength, and L corresponds to the sensing region length of 1 cm, which is the same as in other literature sources [14].

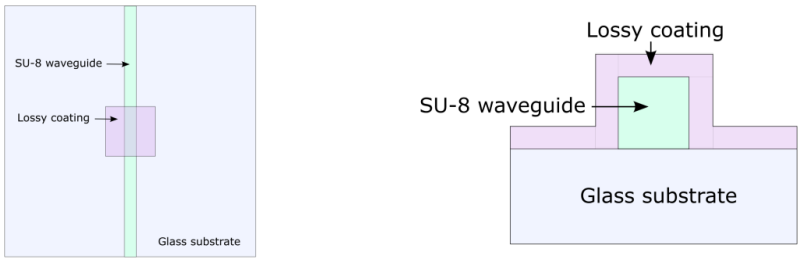

(**a**) (**b**)

Figure 1. Integrated LMR sensor design: (**a**) top view, (**b**) cross-sectional view.

2.3. LMR Device Fabrication Guidelines

This section will describe the theoretical stages of fabrication for the developed LMR sensor, according to which we will later fabricate it ourselves. Before photolithography, glass slides should be scribed using diamond tool in order to cleave them with fabricated waveguides after photolithography procedure later for efficient fiber attachment.

SU-8 waveguide fabrication can be performed using the same photolithography procedure described in Section 2.1, excepting exposure step. Exposure should be performed using tool that provides possibility to selectively expose spin-coated photoresist.

After waveguide fabrication, TiO_2 thin film should be sputtered over it through a shadow mask for cladding patterning using magnetron sputtering procedure described in Section 2.1. This approach will provide sufficient waveguide coverage with lossy coating.

Glass slides then should be cleaved along scribed lines, thus creating access to waveguide ends from the substrate-edge sides for edge-coupling light into photonic chip. Substrate edges with SU-8-waveguide ends should be flattened and smoothened by using grinder–polisher machine. MM fiber should be positioned carefully and permanently bonded to chip using rigid UV adhesive.

3. Results

The dispersion curves experimentally obtained after ellipsometry measurements for SiO_2, SU-8, and TiO_2 are given in Figure 2. The dispersions curves gave possibility to fit parameters from Equations (1) and (2). These parameters are summarized in Table 2.

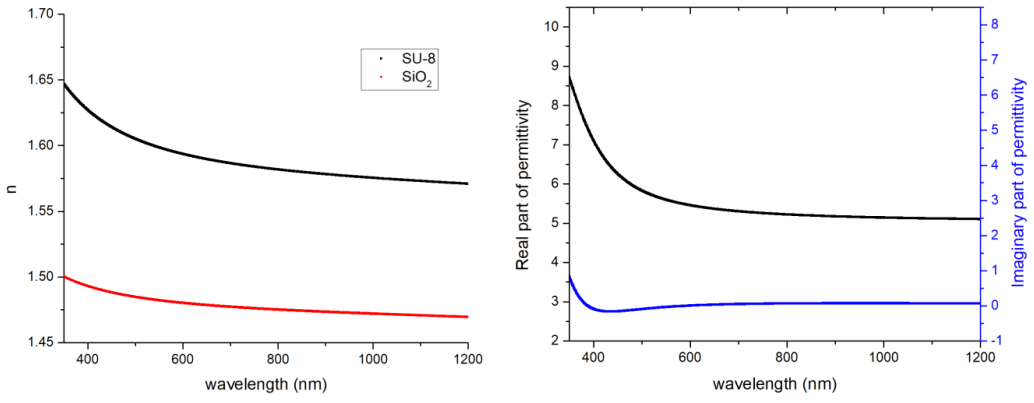

(**a**) (**b**)

Figure 2. Dispersion curves: (**a**) transparent SU-8 and SiO_2; (**b**) absorbing TiO_2.

Table 2. Materials' fitted parameters.

Material	Equation Used	Fitted Parameters
SU-8	(1)	$\varepsilon_\infty = 1,\ A = 1.389,\ B = 0.15083\ \mu m^2, E = 0.0184\ \mu m^{-2}$
SiO_2	(1)	$\varepsilon_\infty = 1,\ A = 1.168,\ B = 0.09091\ \mu m^2, E = 0.0100\ \mu m^{-2}$
TiO_2	(2)	$\varepsilon_\infty = 1,\ Amp = 106.9\ eV^2,\ En = 5.9\ eV,\ Amp_1 = 24.0,$ $Br_1 = 1.4\ eV,\ En_1 = 4.1\ eV,\ Amp_2 = -19.9,\ Br_2 = 1.4\ eV,\ En_2 = 4.0\ eV.$

Various square-type waveguides with side lengths from 4 to 40 µm were tested. To compare optical properties of these waveguides, extinction ratio spectra was used. First of all, it is clearly seen from Figure 3a that a higher extinction ratio is achieved for smaller waveguides, which is explained by the stronger interaction of the guided modes with the waveguide facets. In addition, from Figure 3a, it is clearly seen that the LMR absorbance depends on these dimensions—it shifts to near-infrared range with increasing waveguide dimensions. In this case, it is clearly seen that the resonance line tends to a critical value ($\lambda_{crit} = 830$ nm) and, upon reaching certain dimensions of the waveguide, it almost does not shift (see Figure 3b). The effect of the optical fiber size on the LMR effect has been previously studied in the literature [14]; however, no shift has been observed there. Most likely, in this work, the authors have already reached a critical value at the smallest fiber diameter because the dependence of the LMR signal on the diameter was studied in the range from 50 to 800 µm. This critical wavelength corresponds to the LMR that should be observed when using multimode fiber. The dependence of the optical fiber diameter on the value of the effective refractive index has been studied in the literature [19]. This can explain the shift of the resonance line with a change in the dimensions of the waveguide due to changes in the resonance conditions. Another interesting effect worth noting is the relative change in transmittance when resonance is reached—it decreases with increasing waveguide dimensions.

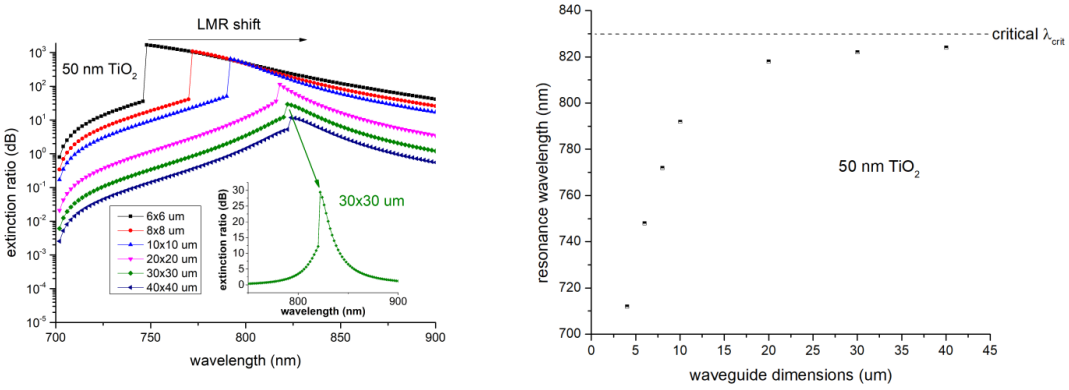

(**a**) (**b**)

Figure 3. Effect of waveguide dimensions on the LMR effect: (**a**) extinction ratio spectra for different waveguide dimensions; (**b**) LMR wavelength depending on the dimensions of the waveguide.

In addition to the waveguide geometry, the thickness of the lossy coating also significantly affects the behavior of the LMR (see Figure 4). The resonance line shifts towards the near-infrared region when the lossy coating thickness increases. In addition, it is clearly seen that multiple resonances appear at a certain thickness of a thin film. Figure 4a is visually similar to the graph given in Ref. [20], where the optical fiber is coated with TiO_2; however, some differences are also observed. First, in our particular case, LMR began to appear at thinner coatings, which is explained by a rather large difference in the refractive

indices of the polymer waveguide and optical fiber silica. Secondly, it can be noted that in our case the difference in wavelength between the second and third LMR is much greater than between other LMRs.

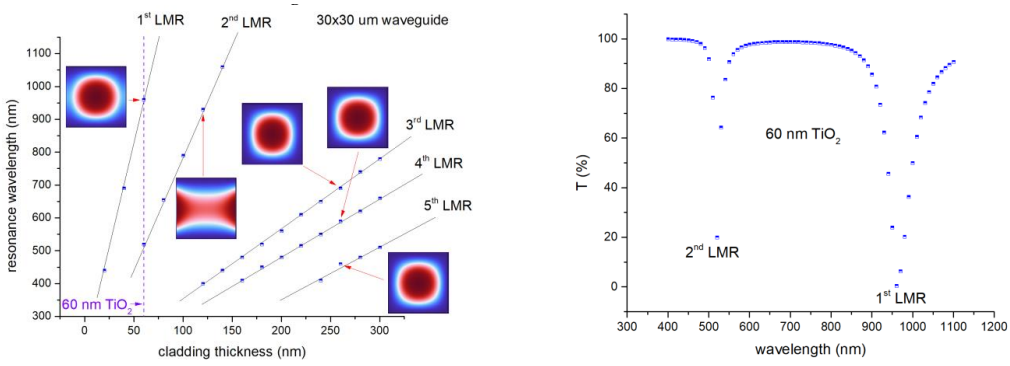

(**a**) (**b**)

Figure 4. LMR in dependence of lossy cladding thickness: (**a**) resonance wavelength vs. cladding thickness; (**b**) transmittance spectrum at TiO_2 thickness of 60 nm.

As mentioned earlier, the LMR effect is used for sensing applications, so in addition to the simulations shown above, the sensitivity of the developed sensor was evaluated (see Figure 5). The sensitivity S of the LMR sensor is defined as the following formula [21]:

$$S = \frac{\Delta\lambda}{\Delta n}, \tag{4}$$

where $\Delta\lambda$ is the resonance wavelength shift and Δn is the variation in the analyte refractive index.

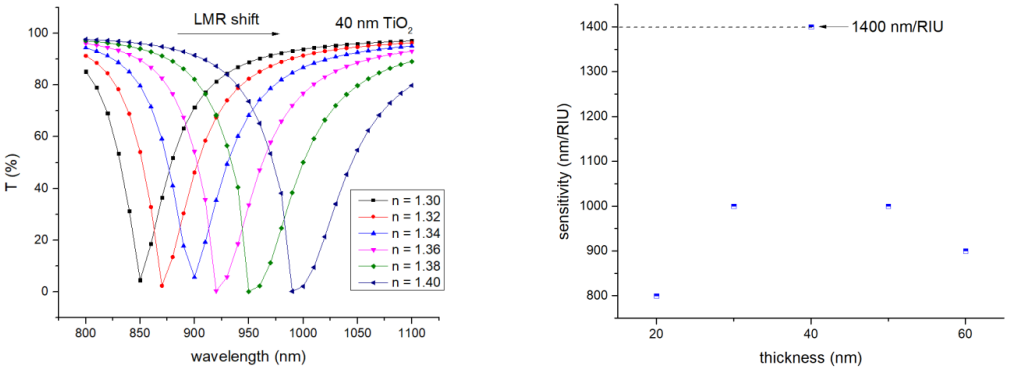

(**a**) (**b**)

Figure 5. LMR sensor sensitivity: (**a**) LMR shift with a change in the refractive index of the medium; (**b**) influence of lossy coating thickness on sensitivity.

Waveguide-based sensors are mainly used to detect analytical biomarkers in aqueous solutions; therefore, the sensor must provide high sensitivity in the refractive index range of 1.3–1.4 [21]. In this range for 40 nm, TiO_2 lossy cladding simulations showed the highest sensitivity around 1400 nm/RIU. This sensitivity is significantly higher than that reported in the literature for a TiO_2-coated LMR sensor (634 nm/RIU) [22]. Comparing the obtained

results with other coatings (e.g., ZnO), the results are also encouraging. It was shown in the literature that in the considered range of refractive indices, the authors achieved a sensitivity of 500 nm/RIU [14].

The detection accuracy is related to the FWHM, which depends on the width of the LMR resonance dip. Q-factor is a parameter that characterizes the overall performance of the LMR sensor, which is defined as the following formula [23]:

$$Q = \frac{S}{FWHM}. \quad (5)$$

The Q-factor in the dependence of TiO_2 thickness is shown in Figure 6. The highest Q-factor was achieved with a TiO_2 coating thickness of 40 nm (28 RIU^{-1}). This value is lower than for the LMR sensor mentioned in Ref. [23]; however, it is worth noting that this sensor is not based on fibers or waveguides. It is possible that the use of waveguides significantly reduces the quality factor.

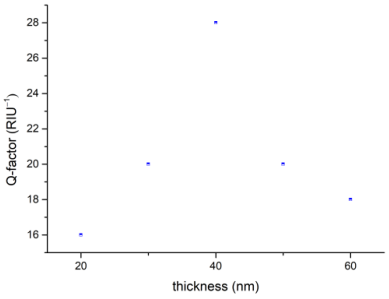

Figure 6. Q-factor in dependence of TiO_2 thickness.

The effect of light polarization on the behavior of the LMR was also studied. It can be seen from Figure 7 that the TE and TM modes have a small shift in the resonance line relative to each other. This is very important from the point of view that when unpolarized light is introduced, the resulting resonance line will be wider than in simulations. It is also worth noting that the FWHM is larger for TE-polarized light, which is most likely due to the fact that the guided mode interacts with the side facets of the waveguide, while TM-polarized light interacts with only one top facet.

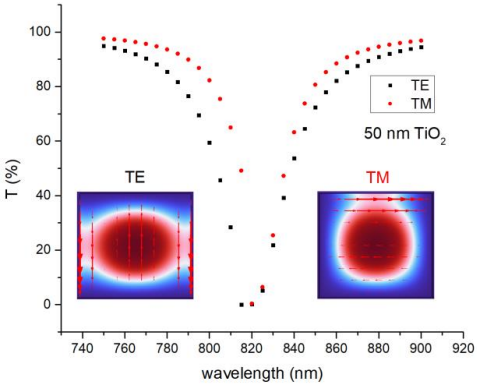

Figure 7. Differences in LMR depending on the polarization of light.

4. Discussion

In this paper, we studied the LMR effect in the SU-8 waveguide with TiO_2 cladding and the influence of the waveguide and coating geometries on the LMR effect. In cases where it is necessary to adjust the LMR wavelength, smaller waveguides can be used because this wavelength is sensitive to small waveguide dimensions. If this wavelength is not so important, then from a practical point of view, it is advisable to use larger waveguides—it is easier to introduce light into such waveguides.

We have shown that multiple resonances can also be observed in coated polymer waveguides; however, some differences have also been observed compared with inorganic silica optical fibers [20]. In the SU-8 waveguide, in order to achieve a similar LMR as in optical fiber [4], it is necessary to use thinner TiO_2 coating, which is explained by a rather large difference in the refractive indices of the polymer waveguide and optical fiber silica.

The highest sensitivity of the developed sensor was 1400 nm/RIU, which is higher than that indicated in the literature for a similar coating [22]. This sensitivity was achieved at 40 nm TiO_2 for a square-type waveguide with a side length of 30 μm. However, it is worth noting that some applications may require additional resonance lines, in which case a thicker lossy coating will be required.

The highest Q-factor of the developed sensor was 28 RIU^{-1}. This Q-factor was achieved at 40 nm TiO_2 for a square-type waveguide with a side length of 30 μm. This Q-factor is lower than for the Kretschmann configuration-based LMR sensor mentioned in Ref. [23] and for the waveguide-based ring resonator sensors mentioned in Refs. [24–26].

The effect of polarization on the LMR was also considered. TE and TM polarizations give different FWHMs in the LMR peak. In addition, TE and TM polarizations generate LMR at slightly different wavelengths; however, this shift is less than those found in the literature [3].

The next step in this study will be the actual fabrication of the sensor, as well as its testing. In the future, this developed sensor will be used to analyze such biological entities as the extracellular vesicles of cancer cells. So far, the literature has not shown the possibility of analyzing EVs using the LMR technique; therefore, it makes sense to compare the sensitivity of the designed sensor with other optical waveguide-based sensors for EVs analysis. For example, the sensitivity of a refractive index sensor based on polymer Bragg grating for EVs detection is only 408–861 nm/RIU, which is almost twice worse compared with our suggested solution [27].

Author Contributions: Conceptualization, E.L. and A.B.; methodology, E.L. and A.B.; software, E.L.; validation, G.M. and A.B.; formal analysis, E.L. and A.B.; writing—original draft preparation, E.L.; writing—review and editing, E.L.; visualization, E.L.; supervision, G.M.; project administration, G.M.; funding acquisition, G.M. All authors have read and agreed to the published version of the manuscript.

Funding: This research was funded by the European Regional Development Fund project "Development of a Novel Microfluidic Device for Label-Free Quantification of Prostate Cancer-Derived Extracellular Vesicles and Analysis of their RNA Content" (PROCEX) (1.1.1.1/20/A/045) and the European Union's Horizon 2020 Framework Program H2020-WIDESPREAD-01-2016-2017-TeamingPhase2 under grant agreement No. 739508, project CAMART2.

Acknowledgments: The authors acknowledge Riga Technical University, the Institute of Solid State Physics, Cellboxlab Ltd., and the European Regional Development Fund for the opportunity to publish this research.

Conflicts of Interest: The authors declare no conflict of interest.

References

1. Ali, L.; Mohammed, M.U.; Khan, M.; Yousuf, A.H.B.; Chowdhury, M.H. High-Quality Optical Ring Resonator Based Biosensor for Cancer Detection. *IEEE Sens. J.* **2019**, *20*, 1867–1875. [CrossRef]
2. Inan, H.; Poyraz, M.; Inci, F.; Lifson, M.A.; Baday, M.; Cunningham, B.T.; Demirci, U. Photonic crystals: Emerging biosensors and them Soc irev promise for point-of-care applications. *Chem. Soc. Rev.* **2016**, *46*, 366–388. [CrossRef] [PubMed]

3. Fuentes, O.; Del Villar, I.; Corres, J.M.; Matias, I.R. Lossy Mode Resonance Sensors Based on Lateral Light Incidence in Nanocoated Planar Waveguides. *Sci. Rep.* **2019**, *9*, 8882. [CrossRef]
4. Del Villar, I.; Arregui, F.J.; Zamarreño, C.R.; Corres, J.M.; Bariain, C.; Goicoechea, J.; Elosua, C.; Hernaez, M.; Rivero, P.J.; Socorro, A.B.; et al. Optical Sensors Based on Lossy-Mode Resonances. *Sens. Actuators B Chem.* **2017**, *240*, 174–185. [CrossRef]
5. Wang, Q.; Zhao, W.M. A Comprehensive Review of Lossy Mode Resonance-Based Fiber Optic Sensors. *Opt. Lasers Eng.* **2018**, *100*, 47–60. [CrossRef]
6. Zamarreño, C.R.; Hernáez, M.; Del Villar, I.; Matías, I.R.; Arregui, F.J. Optical Fiber PH Sensor Based on Lossy-Mode Resonances by Means of Thin Polymeric Coatings. *Sensors Actuators B Chem.* **2011**, *155*, 290–297. [CrossRef]
7. Zamarreño, C.R.; Hernaez, M.; Del Villar, I.; Matias, I.R.; Arregui, F.J. Tunable Humidity Sensor Based on ITO-Coated Optical Fiber. *Sens. Actuators B Chem.* **2010**, *146*, 414–417. [CrossRef]
8. Fuentes, O.; Goicoechea, J.; Corres, J.M.; Del Villar, I.; Ozcariz, A.; Matias, I.R. Generation of Lossy Mode Resonances with Different Nanocoatings Deposited on Coverslips. *Opt. Express* **2020**, *28*, 288. [CrossRef]
9. Arregui, F.J.; Del Villar, I.; Corres, J.M.; Goicoechea, J.; Carlos, R.; Elosua, C.; Hernaez, M.; Rivero, P.J.; Socorro, A.B.; Sanchez, P.; et al. Fiber-Optic Lossy Mode Resonance Sensors. *Procedia Eng.* **2014**, *87*, 3–8. [CrossRef]
10. Sudas, D.P.; Zakharov, L.Y.; Jitov, V.A.; Golant, K.M. Silicon Oxynitride Thin Film Coating to Lossy Mode Resonance Fiber-Optic Refractometer. *Sensors* **2022**, *22*, 3665. [CrossRef]
11. Eldada, L.; Shacklette, L. Advances in polymer integrated optics. *IEEE J. Sel. Top. Quantum Electron.* **2000**, *6*, 54–68. [CrossRef]
12. Paquet, C.; Kumacheva, E. Nano Structured Polymers for Photonics. *Mater. Today* **2008**, *11*, 48–56. [CrossRef]
13. Lorenz, H.; Despont, M.; Fahrni, N.; LaBianca, N.; Renaud, P.; Vettiger, P. SU-8: A Low-Cost Negative Resist For MEMS. *J. Micormech. Microeng.* **1997**, *7*, 121. [CrossRef]
14. Usha, S.P.; Gupta, B.D. Performance Analysis of Zinc Oxide-Implemented Lossy Mode Resonance-Based Optical Fiber Refractive Index Sensor Utilizing Thin Film/Nanostructure. *Appl. Opt.* **2017**, *56*, 5716. [CrossRef] [PubMed]
15. Nezar, S.; Saoula, N.; Sali, S.; Faiz, M.; Mekki, M.; Laoufi, N.A.; Tabet, N. Properties of TiO 2 Thin Films Deposited by Rf Reactive Magnetron Sputtering on Biased Substrates. *Appl. Surf. Sci.* **2017**, *395*, 172–179. [CrossRef]
16. Chung, H.K.; Won, S.O.; Park, Y.; Kim, J.S.; Park, T.J.; Kim, S.K. Atomic-Layer Deposition of TiO2 Thin Films with a Thermally Stable (CpMe5)Ti(OMe)3 Precursor. *Appl. Surf. Sci.* **2021**, *550*, 149381. [CrossRef]
17. Benítez, M.; Zubiate, P.; Del Villar, I.; Socorro-Leránoz, A.B.; Matías, I.R. Lossy Mode Resonance Based Microfluidic Platform Developed on Planar Waveguide for Biosensing Applications. *Biosensors* **2022**, *12*, 403. [CrossRef] [PubMed]
18. Kadhim, R.A.; Yuan, L.; Xu, H.; Wu, J.; Wang, Z. Highly Sensitive D-Shaped Optical Fiber Surface Plasmon Resonance Refractive Index Sensor Based on Ag-α-Fe_2O_3 Grating. *IEEE Sens. J.* **2020**, *20*, 9816–9824. [CrossRef]
19. Shahzadi, R.; Shahzad, A.; Qamar, F.; Shahzadi, R.; Ali, M. Effective Refractive Index and V-Parameter Characterization for Guided Modes in Multilmode. Nano and Three Layer Optical Fibers. *Int. J. Inf. Technol. Electr. Eng.* **2018**, *7*, 20–27.
20. Del Villar, I.; Hernaez, M.; Zamarreño, C.R.; Sánchez, P.; Fernández-valdivielso, C.; Arregui, F.J.; Matias, I.R. Design Rules for Lossy Mode Resonance Based Sensors. *Appl. Opt.* **2012**, *51*, 4298–4307. [CrossRef]
21. Tien, C.-L.; Mao, T.-L.; Li, C.-Y. Lossy Mode Resonance Sensors Fabricated by RF Magnetron Sputtering GZO Thin Film and D-Shaped Fibers. *Coatings* **2020**, *10*, 29. [CrossRef]
22. Burnat, D.; Koba, M.; Wachnicki, Ł.; Gierałtowska, S.; Godlewski, M.; Śmietana, M. Refractive Index Sensitivity of Optical Fiber Lossy-Mode Resonance Sensors Based on Atomic Layer Deposited TiO x Thin Overlay. In Proceedings of the Sixth European Workshop on Optical Fibre Sensors (EWOFS'2016), Limerick, Ireland, 30 May 2016; Volume 9916, p. 99161G. [CrossRef]
23. Zhang, Y.; Zhang, P.; Zhao, M.; Xu, D.; Wang, J.; Li, Z.; Tang, T.; Shen, J.; Li, C. A High Sensitivity Lossy Mode Resonance Refractive Index Sensor Based on SBS Structure. *Results Phys.* **2022**, *36*, 105454. [CrossRef]
24. Ciminelli, C.; Innone, F.; Brunetti, G.; Conteduca, D.; Dell'Olio, F.; Tatoli, T.; Armenise, M.N. Rigorous model for the design of ultra-high Q-factor resonant cavities. In Proceedings of the 18th International Conference on Transparent Optical Networks 2016, Trento, Italy, 10–14 July 2016; pp. 1–4. [CrossRef]
25. Madani, A.; Kleinert, M.; Stolarek, D.; Zimmermann, L.; Ma, L.; Schmidt, O.G. Vertical Optical Ring Resonators Fully Integrated with Nanophotonic Waveguides on Silicon-on-Insulator Substrates. *Opt. Lett.* **2015**, *40*, 3826. [CrossRef] [PubMed]
26. Madani, A.; Harazim, S.M.; Quiñones, V.A.B.; Kleinert, M.; Finn, A.; Naz, E.S.G.; Ma, L.; Schmidt, O.G. Optical microtube cavities monolithically integrated on photonic chips for optofluidic sensing. *Opt. Lett.* **2017**, *42*, 486–489. [CrossRef]
27. Saha, N.; Brunetti, G.; Kumar, A.; Armenise, M.N.; Ciminelli, C. Highly Sensitive Refractive Index Sensor Based on Polymer Bragg Grating: A Case Study on Extracellular Vesicles Detection. *Biosensors* **2022**, *12*, 415. [CrossRef] [PubMed]

PJ-014368-2023

Lossy Mode Resonance Sensors Based on Planar Waveguides: Theoretical and Experimental Comparison

Edvins Letko*, Arturs Bundulis, Gatis Mozolevskis

***Abstract*—Lossy mode resonance (LMR) has garnered significant attention in sensor applications. LMR was primarily explored in fiber-based systems, however, there has been a recent upsurge in its application within planar waveguides. This article compares the LMR phenomenon in planar waveguides with the most employed coatings in the field, specifically SnO_2, TiO_2, and ITO. Additionally, the experimental findings are compared with simulations conducted using the finite element method (FEM) within the COMSOL Multiphysics environment. The novelty of this research lies in the integration of both experimental results and theoretical calculations, utilizing strong FEM simulation tools, in a single study.**

***Index Terms*—lossy mode resonance, planar waveguide, titanium dioxide, tin oxide, indium tin oxide, finite element method.**

I. INTRODUCTION

OVER the past few decades, there has been a significant demand for sensors utilizing optical resonance structures (e.g., microcavity-based resonators [1], photonic crystal [2], plasmonic-based resonators [3], etc.) due to their sensitivity to external changes. In more recent years, particular attention has been given to the phenomenon known as lossy mode resonance (LMR). LMR occurs when light propagates through an optical fiber or waveguide and interacts with thin film possessing positive real part of permittivity that exceed both their own imaginary part and the permittivity of the fiber or waveguide materials. When LMR coating is applied to optical fiber or waveguides, it induces attenuation bands in the transmission spectra. This can be attributed to the coupling between core and lossy modes of dielectric-cladding film [4]. These attenuation bands exhibit sensitivity to a wide array of external parameters such as pH [5], humidity [6], voltage [7], temperature [8], magnetic field [9], volatile organic compounds concentration [10] and various biomolecules concentration [4], making them highly suitable as sensors for various [4] applications.

LMR presents several advantages of other fiber and waveguide-based sensing techniques. Unlike widely used methods such as surface plasmon resonance (SPR), LMR has the ability to generate multiple resonances. Moreover, LMR can be observed using both TE and TM polarized light, whereas SPR is limited to TM polarization [11]. Furthermore, LMR proves to be a more versatile approach as it can be observed with various cladding materials, including polymer [5], semiconductor [12] and dielectric [13] materials. This characteristic offers flexibility and cost-effectiveness in the fabrication of sensing devices.

More recently, generation of LMR through lateral light incidence in nanocoated planar waveguides has been demonstrated [14]. There are several advantages in using a planar structure as opposed to an optical fiber. Firstly, planar waveguide offers a more robust platform than optical fibers, eliminating the need for splices and making the setup easier to handle. Another important benefit of the planar waveguide is its ability to operate in a wide spectrum with either the TE or the TM resonance separately. Moreover, thin films can be deposited on both sides, enabling the creation of a two-parameter sensor. Lastly, the diverse range of available coverslip geometries enables seamless integration of LMR sensors of this configuration into more complex systems [11]. Considering its simplicity, robustness, and other advantages, the transfer of planar waveguide technology to the industry appears more straightforward than its fiber optic counterpart.

Subsequent to the demonstration of LMR generation in planar waveguides [14], this scientific discipline has undergone significant advancement. Over the recent years, applications such as measuring voltage [15], monitoring breath [16], biosensing [17], gas detection [18], and temperature measurements [19] have been conducted utilizing the LMR phenomenon within planar waveguides. Nevertheless, it is crucial to underscore that the existing literature in this field predominantly focuses on engineering aspects, resulting in a notable lack of theoretical background and comprehension of the fundamental processes intrinsic to the LMR phenomenon.

This research was funded by the European Regional Development Fund project "Development of a Novel Microfluidic Device for Label-Free Quantification of Prostate Cancer-Derived Extracellular Vesicles and Analysis of their RNA Content" (PROCEX) (1.1.1.1/20/A/045) and the European Union's Horizon 2020 Framework Program H2020-WIDESPREAD-01-2016-2017-TeamingPhase2 under grant agreement No. 739508, project CAMART2.

Edvins Letko is with Cellboxlabs Ltd., LV-2164, Riga, Latvia, Institute of Solid State Physics, LV-1063, Riga, Latvia, and Faculty of Materials Science and Applied Chemistry, Riga Technical University, LV-1048, Riga, Latvia (e-mail: edvins.letko@cfi.lu.lv).

Arturs Bundulis is with Institute of Solid State Physics, LV-1063, Riga, Latvia (e-mail: arturs.bundulis@cfi.lu.lv).

Gatis Mozolevskis is with Cellboxlabs Ltd., LV-2164, Riga, Latvia, and Institute of Solid State Physics, LV-1063, Riga, Latvia (e-mail: gatis.mozolevskis@cfi.lu.lv).

This paper conducts a comparison of the LMR phenomenon in planar waveguides with the most common coatings used in the LMR field, including SnO_2 [20], TiO_2 [21], and ITO [22]. Furthermore, the experimental results obtained will be compared with simulations performed using the finite element method (FEM) in COMSOL Multiphysics. The solid novelty of this research lies in the integration of both experimental results and theoretical calculations, utilizing strong FEM simulation tools, in a single study.

II. Methods

A. Sample fabrication

The deposition of SnO_2, TiO_2, and ITO coatings on microscope coverslips (12 x 12 x 0.15 mm) was carried out using the Sidrabe G500M DC magnetron sputtering system. For the SnO_2 coating, a reactive sputtering process was employed in an Ar/O_2 plasma with a flow ratio of 1:1. The process utilized a Sn 100 x 200 x 9 mm target and operated at a pressure of 4.5 mTorr and a power of 200 W. Similarly, the TiO_2 coating was produced through a reactive sputtering process in an Ar/O_2 plasma with a flow ratio of 10:1 due to the intensive oxidation of the target during the process. The TiO_2 coating process employed a Ti 100 x 200 x 9 mm target at a pressure of 4.5 mTorr and a power of 500 W. The ITO coating process employed an ITO (In_2O/SnO_2 with a weight ratio 9:1) 100 x 200 x 9 mm target at a pressure of 5 mTorr and a power of 200 W. Compared to TiO_2 and SnO_2 deposition, ITO deposition involved a non-reactive sputtering process that exclusively used Ar plasma. Prior to deposition, the microscope coverslips underwent a cleaning process using acetone and isopropanol. To achieve selective area deposition, the coverslip was masked with Kapton tape, resulting in the fabrication of the device illustrated in Fig. 1.

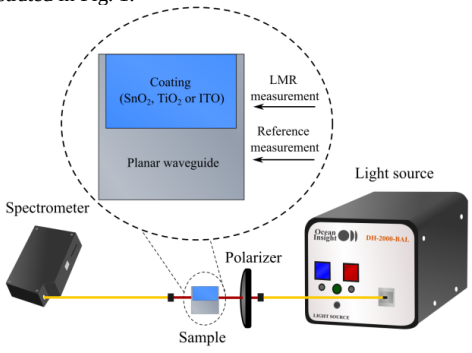

Fig. 1. Experimental setup.

B. Sample characterization

Spectral ellipsometry was employed, using the Woollam RC2-XL equipment and CompleteEASE software, to assess the optical properties of both the microscope coverslip and the deposited thin films. The measurements were conducted within the visible and near-infrared ranges, covering angles of incidence from 45° to 80°. The dispersion of the microscope coverslip was characterized using the Cauchy equation [23]:

$$n = A + \frac{B}{\lambda^2}, \tag{1}$$

where λ represents the wavelength in µm, while A and B are coefficients obtained through fitting. Since the deposited thin films are absorbing layers, the optical properties were determined using the Lorentz oscillator model. The permittivities of SnO_2, TiO_2, and ITO were calculated using the equation provided in the CompleteEASE software manual:

$$\varepsilon = \varepsilon_\infty + \frac{Amp}{En^2\text{-}E^2} + \sum \frac{Amp_n\, Br_n En_n}{En^2\text{-}E^2\text{-}iEBr_n}, \tag{2}$$

where all parameters except photon energy E are fitted parameters.

To investigate the LMR phenomenon in fabricated samples, a specific experimental setup was utilized (see Fig. 1). The light source used was an Ocean Insight DH-2000, which was coupled into an optical fiber (Thorlabs M29L) and directed into the rectangular edge of the sample, which had dimensions of 15 x 0.15 mm, transforming it into a planar waveguide with a thickness of 150 µm. The outgoing light from the sample was collected using another optical fiber (Thorlabs M29L) and then subjected to analysis using an Ocean Optics HR4000 spectrometer. To establish a reference spectrum, an initial measurement was conducted through the uncoated sector of the sample. This reference spectrum served as a baseline for subsequent measurements. A linear polarizer was employed between the sample and the input fiber to investigate LMR shifts related to various light polarizations. Additionally, LMR shifts induced by solvents by dispensing it on the covered part of the sample were investigated.

C. Sample simulations

The behavior of the designed device was simulated using COMSOL Multiphysics based on FEM. Initially, a two-dimensional cross-sectional geometry was defined to analyze electromagnetic distribution of the guided modes (see Fig. 2). This simplified approach characterizes the behavior of the guided mode in an infinite homogeneous planar waveguide, disregarding certain parameters that are relevant at this stage. Next, materials were defined for five different environments, including glass coverslip, SnO_2 TiO_2, ITO, and the sensing media. The optical parameters of these materials were determined experimentally through spectral ellipsometry. To establish an infinite planar waveguide, materials were assigned not only within domains but also at boundaries. The “Electromagnetic Waves, Frequency Domain” physics module was employed to solve the posed problems. The geometry was meshed with physics-controlled element size less than the coating thickness in its domain, while other domains were meshed with element sizes comparable to the wavelength. The grid comprised 88000 triangular elements with maximum element size of 100 nm, covering an overall area of $4 \cdot 10^{-8}$ m^2, with the majority of elements situated in the thin film structure. A parametric sweep was conducted to explore various coating thicknesses and materials. To analyze the distribution of the electromagnetic field in the planar waveguide, mode analysis was performed, allowing for the evaluation of the effective refractive index n_{eff}. This parameter was subsequently utilized to simulate transmittance spectra using equation [24]:

$$T = exp\left(-\frac{4\pi}{\lambda} imag(n_{eff})L\right), \quad (3)$$

where T represents the transmittance, λ denotes the wavelength, and L corresponds to the length of the sensing region of 1 cm.

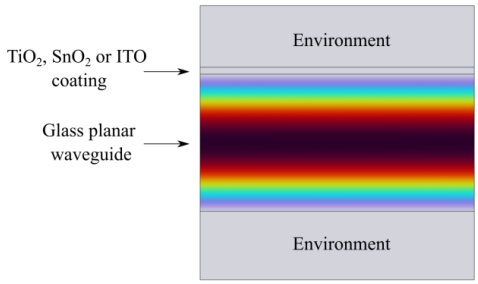

Fig. 2. Two-dimensional cross-sectional geometry of the simulated problem and an example of the resulting electromagnetic distribution in the waveguide.

III. Results and Discussions

Fig. 3 displays dispersion curves obtained from ellipsometry measurements for both the glass coverslip and the thin films that were deposited. These curves have been generated using the fitted parameters extracted from equations (1) and (2), which are outlined in Table I. The curves depicted in Fig. 3 and the parameters fitted from Table I are then utilized to characterize the optical properties of materials in simulations conducted through the finite element method.

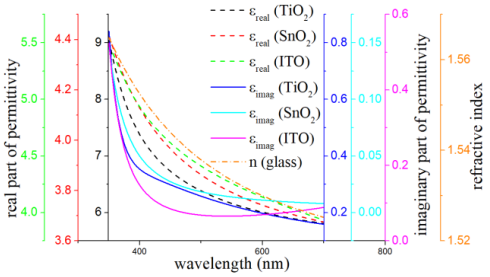

Fig. 3. Dispersion curves of glass waveguide, TiO_2, SnO_2 and ITO thin films.

TABLE I
Materials Fitted Parameters

Material	Equation used	Fitted parameters
Glass	(1)	$A = 1.5$, $B = 0.0065\ m^2$
TiO_2	(2)	$\varepsilon_\infty = 1.0$, $Amp = 106.9\ eV^2$, $En = 5.9\ eV$, $Amp_1 = 24.0$, $Br_1 = 1.4\ eV$, $En_1 = 4.1\ eV$, $Amp_2 = -19.9$, $Br_2 = 1.4\ eV$, $En_2 = 4.0\ eV$
SnO_2	(2)	$\varepsilon_\infty = 1.0$, $Amp = 132.3\ eV^2$, $En = 7.4\ eV$, $Amp_1 = 0.5$, $Br_1 = 0.6\ eV$, $En_1 = 4.0\ eV$
ITO	(2)	$\varepsilon_\infty = 1.9$, $Amp = 74.9\ eV^2$, $En = 6.1\ eV$, $Amp_1 = 1.1$, $Br_1 = 0.5\ eV$, $En_1 = 3.8\ eV$, $Amp_2 = 23.4$, $Br_2 = 0.3\ eV$, $En_2 = 0.2\ eV$

The most effective method for comparing simulations and experimental outcomes involves employing color plots that cover a range of cladding thicknesses. This strategy will offer a comprehensive overview of whether the theoretical model effectively explains the physics of LMR phenomenon in fabricated devices. Theoretical calculations of extinction ratios corresponding to various TiO_2 thicknesses are presented as a function of wavelength in Fig. 4, while the experimentally obtained LMRs are displayed in Fig. 5. A comparison was made between the theoretical and experimental results specifically for TE-polarized light.

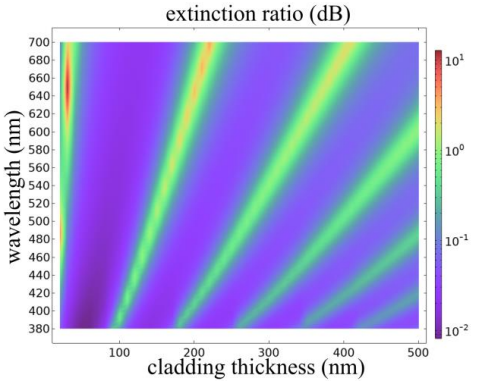

Fig. 4. Theoretical TE-polarized LMRs in dependence of wavelength and TiO_2 thickness.

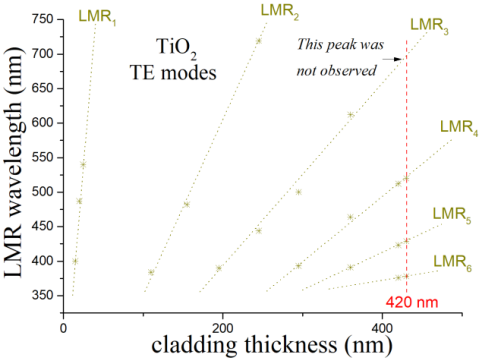

Fig. 5. Experimental TE-polarized LMRs in dependence of wavelength and TiO_2 thickness.

A similar assessment between theoretical predictions and experimental data was conducted for SnO_2 (Fig. 6 and Fig. 7) and ITO coatings (Fig. 8 and Fig. 9).

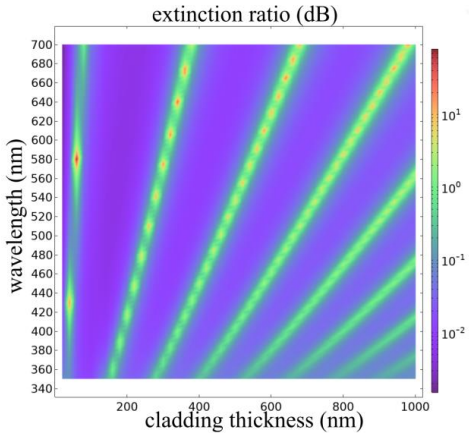

Fig. 6. Theoretical TE-polarized LMRs in dependence of wavelength and SnO_2 thickness.

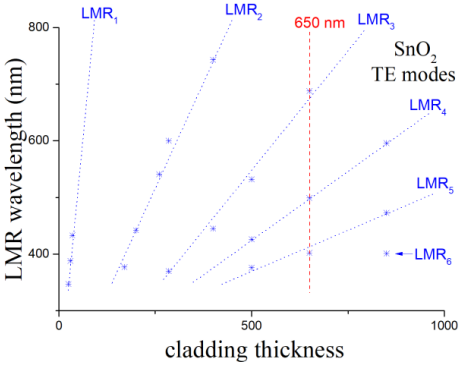

Fig. 7. Experimental TE-polarized LMRs in dependence of wavelength and SnO_2 thickness.

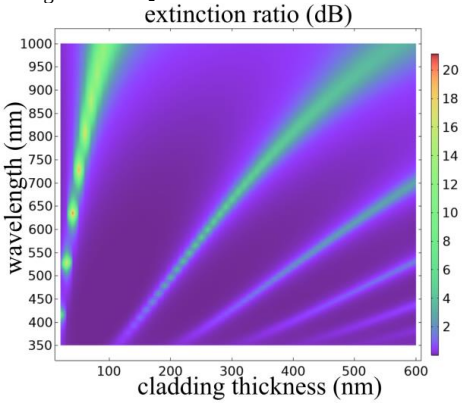

Fig. 8. Theoretical TE-polarized LMRs in dependence of wavelength and ITO thickness.

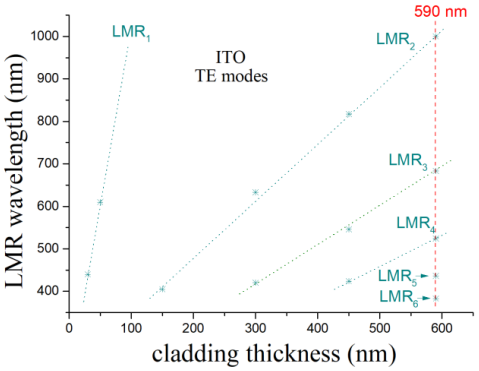

Fig. 9. Experimental TE-polarized LMRs in dependence of wavelength and ITO thickness.

For every cladding material a specific thickness was chosen as an example in order to display the spectra across different polarizations and enable a direct comparison with theoretical predictions. These example thicknesses for TiO_2, SnO_2, and ITO are indicated in Fig. 5, Fig. 7, and Fig. 9, respectively. We chose these thicknesses as an example because they allow us to observe the largest number of LMRs simultaneously, making it easier to compare with theoretical calculations. Fig. 10, Fig. 11, and Fig. 12 depict the transmittance spectra that have been theoretically calculated and experimentally measured for TiO_2, SnO_2 and ITO coatings at selected thicknesses, respectively. The resonance wavelength of the theoretical and experimental spectra exhibits a minor inconsistency, which can be attributed to slight variations in coating thickness between the experimental and theoretical outcomes. Even a variance of a few nanometers in the film thickness can result in a noticeable divergence in the LMR wavelength. This is further supported by the observation that lower order LMRs exhibit a greater degree of sensitivity to changes in coating thickness, resulting in a more pronounced resonance wavelength divergence compared to higher order LMRs. It is worth observing that there are variations in the shapes of the LMR peaks between theoretical and experimental spectra, which can be attributed to the inhomogeneity of the deposited coating. Nonetheless, the differences in FWHM are relatively minor. It is important to note that in devices coated with TiO_2 and SnO_2, the LMR effect became less noticeable with increasing wavelength. This effect was so significant that some peaks simply ceased to be observed at wavelengths over 600 nm, although theoretical calculations predicted their presence. In Fig. 5, within the wavelength range of approximately 700 nm, for a TiO_2 coating with a thickness of 420 nm, theoretical calculations indicated the possibility of an additional peak, but this peak was not observed in the actual experiments. This behavior aligns with what was observed in [14] study for similar coverslips.

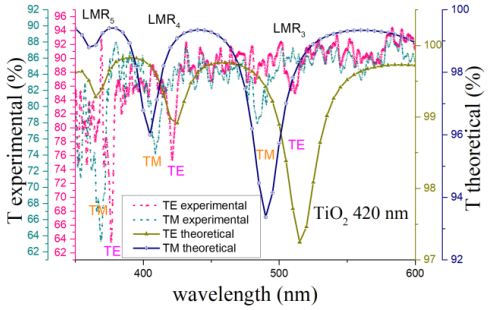

Fig. 10. Transmittance spectra for device with 420 nm thick TiO_2 coating.

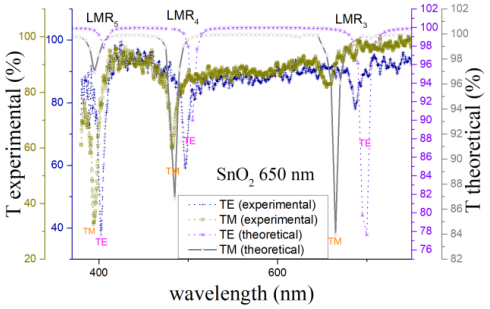

Fig. 11. Transmittance spectra for device with 650 nm thick SnO_2 coating.

In the case of ITO, the LMR effect did not disappear with increasing wavelength. In [19] was shown that increased O_2 flow during the reactive magnetron sputtering results in increased surface roughness and the formation of crystalline grains. This phenomenon provides an explanation of the LMR behavior observed in coatings produced through both reactive and non-reactive magnetron sputtering. The weakening of the LMR effect at longer wavelengths in TiO_2 and SnO_2 coatings can be attributed to the creation of crystalline grains whose sizes are comparable to the operational wavelength. An alternative explanation for the observed phenomenon may be associated with the dispersion of the extinction coefficient. It is widely known that having a non-zero extinction coefficient is a fundamental requirement for observing the LMR phenomenon [4]. As depicted in Fig. 3, the extinction coefficient shows a decreasing trend with increasing wavelength for TiO_2 and SnO_2 coatings. In contrast, when considering ITO coating, extinction coefficient rises at wavelengths above 500 nm, leading to more pronounced LMRs at longer wavelengths.

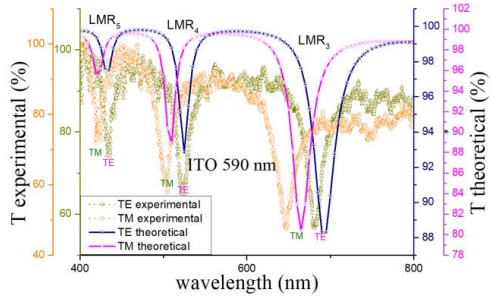

Fig. 12. Transmittance spectra for device with 590 nm thick ITO coating.

Sensing performance assessment, involving both theoretical simulations and experimental measurements (Fig. 13 and Fig. 14, respectively), was exclusively conducted for the ITO coated sample. This was explained by the fact that the first order LMR shift could not be observed due to the disappearance of the LMR effect at longer wavelengths described above for TiO_2 and SnO_2 coatings. Fig. 13 and Fig. 14 clearly illustrate that the LMR wavelengths and sensitivities obtained from both theoretical simulations and experimental data closely align with each other. Small variations in LMR wavelengths can be attributed to the potential inhomogeneity of the applied coating and minor discrepancies of a few nanometers in thickness between the theoretical and actual measurements. This fact is further supported by ellipsometry mapping, wherein the thickness of the ITO coating on one of the fabricated samples was assessed at different points to determine the approximate thickness variation in the samples. Results from ellipsometry mapping revealed variations in thickness of around 2 % in the designated area. As depicted in Fig. 15, subsequent simulations illustrated that considering this 2 % thickness variability situates the experimental LMR peaks between the theoretical LMR peaks in the boundary cases.

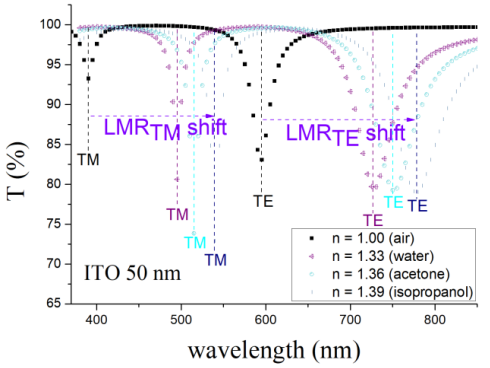

Fig. 13. Theoretical sensing response in various solvents.

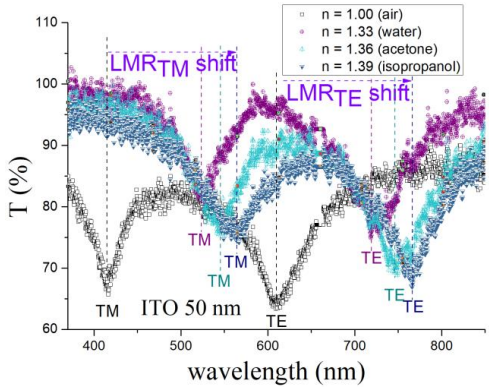

Fig. 14. Experimental sensing response in various solvents.

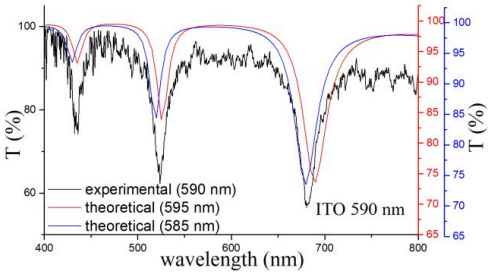

Fig. 15. Comparison between theoretical and experimental TE-polarized LMRs considering thickness variations.

The spectra given in Fig. 13 and Fig. 14 can be utilized to assess the sensing capabilities of the fabricated device. The relationship between LMR wavelength and the refractive index of the surrounding environment is depicted in Fig. 16. The sensitivity characteristics obtained experimentally and calculated theoretically have some differences. The sensitivity characteristics obtained experimentally and calculated theoretically have some differences: for TM polarized light experimentally obtained sensitivity is 98.5 % of calculated theoretically, for TE polarized light experimentally obtained sensitivity is 73.6 % of calculated theoretically. The disparities, again, can be attributed to a slight variation of a few nanometers in thickness between the theoretical and experimental values.

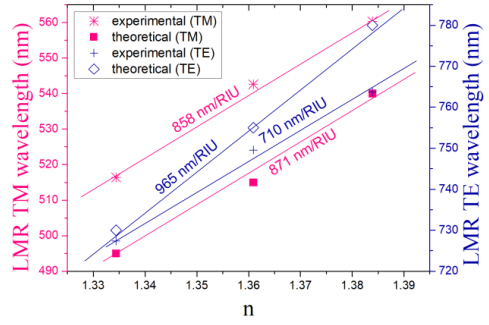

Fig. 16. Sensing performance of a 50 nm coated ITO sample.

The shape of the LMR peak and its associated sensitivity can be employed to compute the Q-factor [9] for an ITO coated device and subsequently compare it with theoretical values:

$$Q = \frac{S}{FWHM_{LMR}}, \tag{4}$$

where S represents the sensitivity, and $FWHM_{LMR}$ is the full width at half minimum of the LMR peak. These calculated Q-factor values are summarized in Table II and calculated from spectra given in Fig. 13 and Fig. 14. The results clearly demonstrate that there is a discrepancy between theoretical and experimental results, which is explained by the wider FWHM expected due to the fact that this parameter is very sensitive to the quality and homogeneity of thin film. It is worth noting that both theoretical and experimental data indicate a superior Q-factor for TM-polarized light in comparison to TE-polarized light, corroborating findings from prior literature [25]. The Q-factor and sensitivity values achieved are lower compared to those obtained with silica optical fibers using the same coating [22], as can be straightforwardly accounted for by the higher refractive index of the planar waveguide, as detailed in reference [26].

TABLE II
THEORETICAL AND EXPERIMENTAL Q-FACTOR CALCULATIONS

$Q^{TE}_{theoretical}$	$Q^{TE}_{experimental}$	$Q^{TM}_{theoretical}$	$Q^{TM}_{experimental}$
32 RIU^{-1}	18 RIU^{-1}	44 RIU^{-1}	29 RIU^{-1}

IV. CONCLUSION

In this study, the LMR effect was studied on planar waveguides with TiO_2, SnO_2, and ITO coatings. Comparing the experimental data obtained with each other, a noteworthy finding emerged: the ITO coating demonstrated the best suitability for LMR-based sensor applications. This is likely attributable to the deposition technique employed, wherein ITO was deposited using non-reactive magnetron sputtering, while the other oxides underwent deposition via a reactive process, leading to the formation of crystalline grains that exhibited limited interaction with long-wavelength light. An alternative explanation for this observation may be attributed to the differences in the dispersion of extinction coefficients for ITO and other oxide coatings.

Through a comprehensive comparison between theoretical simulations and experimental observations, it was deduced that the finite element method's mode analysis effectively captures the underlying physics of the LMR phenomenon within planar waveguides. The theoretical color plots demonstrated a sufficient level of agreement with the experimentally derived results across the entire range of coating thicknesses. However, it is important to note certain distinctions in Q-factors obtained theoretically and experimentally, which can be attributed to inhomogeneity of thin films and the possibility of less precise theoretical input data regarding the optical properties of the analyzed medium and coating thickness.

The sensitivities and Q-factors obtained do not reach a level where they can rivel fiber-based LMR sensors. However, it is important to note that this study did not aim to achieve that goal, primarily because planar waveguides come with their inherent

drawbacks, such as significant light losses and a high refractive index. It is worth emprasizing that despite these limitations, planar waveguides offer unique advantages over optical fibers, including ease of handling, the ability to deposit thin films on both sides, and straightforward integration into more complex systems.

ACKNOWLEDGMENT

The authors would like to thank Ignacio Del Villar from the Public University of Navarre for his kind support and useful comments. The authors would like to acknowledge the Riga Technical University, the Institute of Solid State Physics, Cellboxlabs Ltd., and the European Regional Development Fund for the opportunity to publish this research.

REFERENCES

[1] L. Ali, M. U. Mohammed, M. Khan, A. H. B. Yousuf, and M. H. Chowdhury, "High-Quality Optical Ring Resonator based Biosensor for Cancer Detection," *IEEE Sens. J.*, vol. PP, no. c, p. 1, 2019, doi: 10.1109/JSEN.2019.2950664.

[2] H. Inan *et al.*, "Chem Soc Rev promise for point-of-care applications," *Chem. Soc. Rev.*, 2016, doi: 10.1039/C6CS00206D.

[3] J. C. Ramirez, D. Grajales García, J. Maldonado, and A. Fernández-Gavela, "Current Trends in Photonic Biosensors: Advances towards Multiplexed Integration," *Chemosensors*, vol. 10, no. 10, 2022, doi: 10.3390/chemosensors10100398.

[4] Q. Wang and W. M. Zhao, "A comprehensive review of lossy mode resonance-based fiber optic sensors," *Opt. Lasers Eng.*, vol. 100, no. July 2017, pp. 47–60, 2018, doi: 10.1016/j.optlaseng.2017.07.009.

[5] C. R. Zamarreño, M. Hernáez, I. Del Villar, I. R. Matías, and F. J. Arregui, "Optical fiber pH sensor based on lossy-mode resonances by means of thin polymeric coatings," *Sensors Actuators, B Chem.*, vol. 155, no. 1, pp. 290–297, 2011, doi: 10.1016/j.snb.2010.12.037.

[6] C. R. Zamarreño, M. Hernaez, I. Del Villar, I. R. Matias, and F. J. Arregui, "Tunable humidity sensor based on ITO-coated optical fiber," *Sensors Actuators, B Chem.*, vol. 146, no. 1, pp. 414–417, 2010, doi: 10.1016/j.snb.2010.02.029.

[7] J. Ascorbe, J. M. Corres, F. J. Arregui, and I. R. Matias, "LOW VOLTAGE TRANSDUCER BASED ON THE ATTENUATION BAND," pp. 1–4, 2014.

[8] P. Sánchez, C. R. Zamarreño, F. J. Arregui, and I. R. Matías, "LMR-based optical fiber refractometers for oil degradation sensing applications in synthetic lubricant oils," *J. Light. Technol.*, vol. 34, no. 19, pp. 4537–4542, 2016, doi: 10.1109/JLT.2016.2562701.

[9] Y. Fan *et al.*, "Bilaterally Polished Photonic Crystal Fiber Magnetic Field Sensor Based on Lossy Mode Resonance," *IEEE Sensors Journal*, vol. 22, no. 24, pp. 23786-23792, 2022, doi: 10.1109/JSEN.2022.3217506.

[10] C. Elosúa *et al.*, "Lossy mode resonance optical fiber sensor to detect organic vapors," *Sensors Actuators, B Chem.*, vol. 187, pp. 65–71, 2013, doi: 10.1016/j.snb.2012.09.046.

[11] O. Fuentes, J. Goicoechea, J. M. Corres, I. Del Villar, A. Ozcariz, and I. R. Matias, "Generation of lossy mode resonances with different nanocoatings deposited on coverslips," *Opt. Express*, vol. 28, no. 1, p. 288, 2020, doi: 10.1364/oe.28.000288.

[12] F. J. Arregui *et al.*, "Fiber-Optic Lossy Mode Resonance Sensors," *Procedia Eng.*, vol. 87, pp. 3–8, 2014, doi: 10.1016/j.proeng.2014.11.253.

[13] F. Refractometer, D. P. Sudas, L. Y. Zakharov, V. A. Jitov, and K. M. Golant, "Silicon Oxynitride Thin Film Coating to Lossy Mode Resonance," pp. 1–12, 2022.

[14] O. Fuentes, I. Del Villar, J. M. Corres, and I. R. Matias, "Lossy mode resonance sensors based on lateral light incidence in nanocoated planar waveguides," *Sci. Rep.*, vol. 9, no. 1, pp. 1–10, 2019, doi: 10.1038/s41598-019-45285-x.

[15] Y. C. Lin and L. Y. Chen, "Subtle application of electrical field-induced lossy mode resonance to enhance performance of optical planar waveguide biosensor," *Biosensors*, vol. 11, no. 3, 2021, doi: 10.3390/bios11030086.

[16] D. Bohorquez, I. Del Villar, J. M. Corres, and I. R. Matias, "Wavelength and intensity based lossy mode resonance breathing sensor," *Opt. Laser Technol.*, vol. 140, no. February, p. 107063, 2021, doi: 10.1016/j.optlastec.2021.107063.

[17] M. Benítez, P. Zubiate, I. Del Villar, A. B. Socorro-Leránoz, and I. R. Matías, "Lossy Mode Resonance Based Microfluidic Platform Developed on Planar Waveguide for Biosensing Applications," *Biosensors*, vol. 12, no. 6, p. 403, 2022, doi: 10.3390/bios12060403.

[18] I. Vitoria, E. E. Gallego, S. Melendi-Espina, M. Hernaez, C. Ruiz Zamarreño, and I. R. Matías, "Gas Sensor Based on Lossy Mode Resonances by Means of Thin Graphene Oxide Films Fabricated onto Planar Coverslips," *Sensors*, vol. 23, no. 3, pp. 1–9, 2023, doi: 10.3390/s23031459.

[19] J. Txintxurreta, E. G-berasategui, and O. Hern, "Indium Tin Oxide Thin Film Deposition by Magnetron," 2021.

[20] Q. Wang, X. Li, W. M. Zhao, and S. Jin, "Lossy mode resonance-based fiber optic sensor using layer-by-layer SnO2 thin film and SnO2 nanoparticles," *Appl. Surf. Sci.*, vol. 492, pp. 374–381, 2019, doi: 10.1016/j.apsusc.2019.06.168.

[21] M. Hernaez, C. R. Zamarreño, I. Del Villar, I. R. Matias, and F. J. Arregui, "Lossy mode resonances supported by TiO2-coated optical fibers," *Procedia Eng.*, vol. 5, pp. 1099–1102, 2010, doi: 10.1016/j.proeng.2010.09.302.

[22] I. Del Villar, C. R. Zamarreño, M. Hernaez, F. J. Arregui, and I. R. Matias, "Lossy mode resonance generation with indium-tin-oxide-coated optical fibers for sensing applications," *J. Light. Technol.*, vol. 28, no. 1, pp. 111–117, 2010, doi: 10.1109/JLT.2009.2036580.

[23] W. C. Tan, K. Koughia, J. Singh, and S. O. Kasap, "Fundamental Optical Properties of Materials I," *Opt. Prop. Condens. Matter Appl.*, pp. 1–25, 2006, doi: 10.1002/0470021942.ch1.

[24] R. A. Kadhim, L. Yuan, H. Xu, J. Wu, S. Member, and Z. Wang, "Highly sensitive D-shaped optical fibre surface plasmon resonance refractive index sensor based on Ag- α -Fe2O3 grating," vol. 1748, no. c, 2020, doi: 10.1109/JSEN.2020.2992854.

[25] Y. Zhang *et al.*, "A high sensitivity lossy mode resonance refractive index sensor based on SBS structure," *Results Phys.*, vol. 36, no. January, p. 105454, 2022, doi: 10.1016/j.rinp.2022.105454.

[26] W. M. Zhao and Q. Wang, "Analytical Solutions to Fundamental Questions for Lossy Mode Resonance," *Laser Photonics Rev.*, vol. 17, no. 1, pp. 1–18, 2023, doi: 10.1002/lpor.202200554.

Edvins Letko received his MSc degree in the field of Materials Nanotechnology and is presently working on his PhD in Materials Science at Riga Technical University. His primary research focus lies in integrated polymer photonics at the Institute of Solid State Physics, University of Latvia. Alongside his research, he co-founded the startup "OG Sense" dedicated to developing optical-based ammonia sensors.

Arturs Bundulis received his PhD degree in Physics from University of Latvia in 2020. Currently he is a leading researcher at the Laboratory of Organic Materials, Institute of Solid State Physics. His main research areas are connected to nonlinear optics and integrated photonics.

Gatis Mozolevskis leads the Micro and Nanodevices Laboratory at the Institute of Solid State Physics, University of Latvia. He earned his PhD in Material Science from Riga Technical University. A significant part of his career has been dedicated to the development of photonic and optical devices within both academic and industrial environments.

Optics and Lasers in Engineering 181 (2024) 108387

Contents lists available at ScienceDirect

Optics and Lasers in Engineering

journal homepage: www.elsevier.com/locate/optlaseng

Lossy mode resonance in photonic integrated circuits

Edvins Letko [a,b,*], Arturs Bundulis [a], Edgars Vanags [a], Gatis Mozolevskis [a]

[a] Institute of Solid State Physics, University of Latvia, Riga, LV-1063, Latvia
[b] Faculty of Natural Sciences and Technology, Riga Technical University, Riga, LV-1063, Latvia

ARTICLE INFO

Keywords:
Lossy mode resonance
Photonic integrated circuits
Polymer waveguides
Indium tin oxide
Finite element method

ABSTRACT

In recent years, the promising phenomenon known as lossy mode resonance (LMR) has garnered significant attention in sensing applications. While existing literature in the field of LMR focuses on optical fiber systems and planar waveguides due to their simplicity, there is an absence of research on systems based on photonic integrated circuits (PICs). This article aims to demonstrate, for the first time, the generation of LMR in PICs with sensitivity and a figure of merit (FOM) comparable to that of optical fibers and planar waveguides. Additionally, the article offers a comparison of various polymer materials such as OrmoClear, OrmoCore and SU-8 for integrated waveguides fabrication. To summarize, the main novelty of the article is the demonstration of the LMR phenomenon in integrated chips and the comparison of different polymers commonly used in photonics to fabricate these chips. Moreover, the authors present a novel fabrication workflow for thick polymer waveguides. Finally, the study compares the experimental results obtained with simulations conducted using the finite element method (FEM) in COMSOL Multiphysics environment.

1. Introduction

In recent decades, there has been a growing demand for sensors that utilize optical resonance structures like microcavity-based resonators [1], photonic crystals [2], and plasmonic-based resonators [3], primarily due to their high sensitivity to external influences. A particular attention has been drawn to a phenomenon known as lossy mode resonance (LMR). LMR manifests when light propagates through an optical fiber or waveguide and interacts with a thin film cladding that exhibits a positive real part of permittivity exceeding both its own imaginary part and the permittivity of the light guiding media. When an LMR coating is applied to optical fibers or waveguides, it leads to the creation of attenuation bands in the transmission spectra, which can be attributed to the interaction between the core and lossy modes of the dielectric-cladding film [4]. These attenuation bands exhibit sensitivity to various external factors such as temperature [5], pH [6], humidity [7], concentrations of volatile organic compounds [8], and diverse biomolecules [4], making them highly suitable for numerous sensor applications [4].

LMR offers several advantages over other fiber and waveguide-based sensing techniques. From a design perspective, surface plasmon resonance (SPR) is the technique most similar to LMR. As a result, these methods are typically compared to each other. In certain specific configurations, it is even feasible to generate both phenomena simultaneously [9]. One of the main differences between SPR and LMR phenomena lies in their polarization dependency. Both transverse magnetic (TM) and transverse electric (TE) polarizations can generate LMR, unlike SPR, which is restricted specifically to TM polarization [10]. Furthermore, LMR exhibits the capability to produce multiple resonances [11] and demonstrates greater versatility, being observable with various cladding materials such as polymers [6], semiconductors [12], and dielectrics [13]. This flexibility enhances cost-effectiveness in the manufacturing of sensing devices.

As of today, two primary configurations persist for LMR devices: those utilizing optical fibers [4] and those employing planar waveguides [11]. Initially, LMR was shown in optical fiber setups, benefiting from the ability of multimode fibers to effectively transmit the entire visible and IR spectrum with minimal losses, enabling seamless light propagation between the source, fiber, and spectrometer [4]. Several years ago, the LMR phenomenon was first demonstrated in planar waveguides, offering several advantages. Firstly, planar waveguides provide a more robust platform compared to optical fibers, eliminating the need for splices and simplifying setup handling. Another notable advantage of planar waveguides is their ability to operate across a wide spectrum using either the TE or TM resonance independently. Additionally, planar waveguides allow for thin films to be deposited on both sides, enabling

* Corresponding author at: Institute of Solid State Physics, University of Latvia, Riga, LV-1063, Latvia.
E-mail address: edvins.letko@cfi.lu.lv (E. Letko).

https://doi.org/10.1016/j.optlaseng.2024.108387
Received 24 April 2024; Received in revised form 17 May 2024; Accepted 9 June 2024
Available online 13 June 2024

the development of a two-parameter sensor [11]. Despite all the above advantages of fiber optic and planar waveguide systems, their potential has been nearly maximized, since they do not allow the device to be integrated with other photonic elements on a single chip, a direction toward which the optics and photonics industry is steadily progressing. The transition from the mentioned configurations to integrated photonic circuits is not only logical but also holds great promise. However, successful implementation in this direction has yet to be achieved. This transition poses significant challenges for the fabrication of LMR devices, particularly concerning the requirement for integrated waveguides to transmit the entire visible spectrum simultaneously. This constraint imposes limitations on the minimum size of the waveguide for LMR sensor, thus further necessitate the development of novel fabrication methods for thick waveguides and the materials themselves. Our theoretical research into the LMR phenomenon in integrated waveguides [14] indicates that waveguides with dimensions on the order of tens of micrometers are necessary to observe this effect. Notably, the challenge lies in efficiently coupling light across the entire visible spectrum into the waveguide and collecting the emerging light from the chip. Despite the fabrication and operational challenges associated with LMR devices based on integrated waveguides, this approach offers a distinct advantage - the potential for integration with other photonic elements. For instance, existing literature has demonstrated the feasibility of fabricating an integrated spectrometer [15]. Additionally, successful advancements are being made in the field of on-chip integrated light sources [16]. In the future, this could be integrated on a single chip with an LMR device, marking a significant breakthrough in terms of commercial application. Since the spectrometer and light source typically constitute the most expensive components of a measurement setup, such integration can lead to significant cost savings and increase the practicality of LMR-based devices for a various applications. Furthermore, the shift of LMR sensor technology to PICs is anticipated to garner considerable attention from the industry due to its potential for scalability. This holds particular importance for Point-of-Care (POC) applications and Lab-on-Chip development, where integrated sensors serve as key components [14].

Recently, polymers have risen as promising materials for waveguides fabrication [17]. Unlike their inorganic counterparts, polymers provide cost-effectiveness, flexibility, and the potential for functionalization to attain specific properties tailored for various photonic applications [18]. Among the commercially available polymer materials extensively utilized in integrated photonic applications and amenable to lithographic patterning, negative photoresist SU-8 and the Ormo series of inorganic-organic hybrid polymers are particularly sought after. SU-8 photoresist is prominently used in integrated photonics due to its chemical stability and its ease of patterning through photolithography. Its high transparency makes SU-8 an optimal selection for waveguide applications, particularly in the visible and near-infrared ranges, where LMR is predominantly observable [19]. Integrated SU-8 waveguides find applications in various areas such as microdisk resonators [20], photonic crystals [21], surface plasmon resonance [22], Mach-Zehnder interferometers [23], and more. The Ormo series of photoresists, on the other hand, consists of negative photoresists that come in solvent-free, UV-curable formulations ready for immediate use. They are compatible with UV lithography or UV molding processes. OrmoCore photoresist is known for its low optical losses at data communication wavelengths, high-resolution capabilities down to sub-50 nm pattern dimensions, and high chemical and physical stability [24]. In contrast, OrmoClear photoresist provides superior transparency in the near UV and visible wavelength range when compared to OrmoCore [25]. Ormo series integrated waveguides are utilized across a spectrum of photonic applications, including Bragg gratings [26], ring resonators [27], and bimodal interferometers [28]. It is noteworthy to highlight the advantages of polymer photonics over waveguides composed of inorganic materials, particularly in the context of LMR. Firstly, as mentioned earlier, the dimensions of waveguides needed to generate LMR extend beyond the typical dimensions of silicon-based waveguides. Consequently, fabricating inorganic waveguides with similar dimensions would either be prohibitively expensive or technically infeasible. Moreover, the refractive index of inorganic waveguides tends to be significantly higher than that of polymers. This is crucial, as the sensitivity decreases proportionally with the increasing refractive index of the waveguide [29]. Finally, the increased refractive index of the waveguide prohibits the use of substantial amounts of lossy coating materials.

Table 1
Polymer waveguides photolithography parameters.

Process step	Polymer	Parameters
Spin coating	OrmoClear	2200 rpm for 45 s
	OrmoCore	800 rpm for 45 s
	SU-8	900 rpm for 45 s
Soft bake	OrmoClear	80 °C for 3 min
	OrmoCore	80 °C for 3 min
	SU-8	95 °C for 30 min
Exposure	OrmoClear	i-line filter, 500 mJ/cm^2
	OrmoCore	i-line filter, 500 mJ/cm^2
	SU-8	i-line filter, 300 mJ/cm^2
Post bake	OrmoClear	130 °C for 5 min
	OrmoCore	130 °C for 5 min
	SU-8	95 °C for 10 min
Development	OrmoClear	3 min in OrmoDev
	OrmoCore	3 min in OrmoDev
	SU-8	3 min in mr-Dev 600
Hard bake	OrmoClear	150 °C for 3 h
	OrmoCore	150 °C for 3 h
	SU-8	185 °C for 2 h

This article aims to present a novel integrated LMR device onto a chip, marking a substantial progression not only within the LMR field but also in the broader realm of integrated photonics. Additionally, the study evaluates various polymers for producing integrated waveguides tailored for LMR applications and introduces their innovative fabrication method. Moreover, this research will compare experimental findings with simulations conducted using the finite element method (FEM) in COMSOL Multiphysics, emphasizing the importance of combining experimental data with theoretical analysis, especially considering the novelty of the LMR topic.

2. Materials and methods

Initially, 4'' glass wafers with a thickness of 1.1 μm underwent wet cleaning using detergent, acetone, and isopropanol in an ultrasonic bath operating at 37 kHz frequency for 10 min for each solvent. Subsequently, the cleaned wafers were subjected to oxygen plasma ashing in a GIGAbatch 360 M tool at 800 W and 1000 sccm of O_2 flow for 10 min. Following this, a 100 nm thick aluminum layer was thermally evaporated onto the wafers. To enhance the adhesion of the AZ1518 photoresist, HMDS priming was applied to the aluminum surface, followed by spin coating of the photoresist at a speed of 4000 rpm for 30 seconds using Laurell WS650 spin coater. A soft bake at 100 °C for 2 min was then conducted. The next step involved selective direct laser exposure with a dose of 60 mJ/cm^2 using a μPG Heidelberg laser writer, resulting in the pattern of future polymer waveguides. After exposure, the AZ1518 photoresist was developed in AZ 726 MIF developer for 1 minute. Subsequently, samples with AZ1518 structures underwent a hard bake at 130 °C for 10 min. Following the hard bake of AZ1518, wet etching of the aluminum was performed in AZ 726 MIF at 70 °C for 1 minute. These etched aluminum structures will serve as photolithography mask on the wafer itself. The next step involved stripping the photoresist in acetone for 1 minute. At this stage, the wafers consisted only of aluminum structures and were ready for the polymer waveguide fabrication sequence. Oxygen plasma ashing was conducted once more prior to the photolithography procedure. For each wafer, specific polymer (OrmoClear, OrmoCore, and SU-8) underwent spin coating, soft bake,

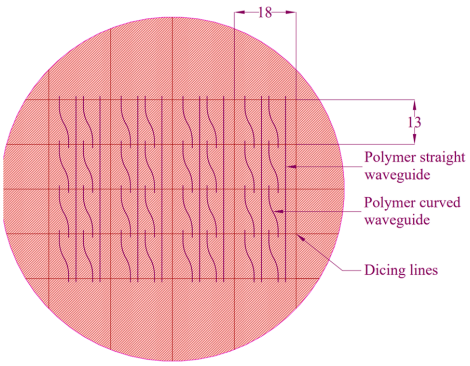

Fig. 1. Schematic top view of the fabricated wafer with polymer waveguide structures.

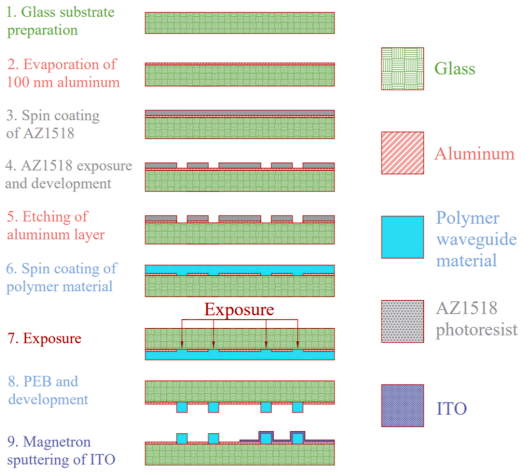

Fig. 2. LMR chip fabrication workflow.

exposure, post bake, development, and hard bake steps, with specific parameters indicated in the accompanying Table 1. A notable aspect of this photolithography procedure was the exposure step, where exposure was conducted using the Mask Aligner Suss MA6 tool from the bottom of the substrate - exposure was carried out through the glass substrate and etched aluminum openings. This approach proved advantageous for several reasons. Firstly, Ormo series photoresists are solvent-free and remain liquid even after the soft bake, making only proximity exposure possible. Secondly, the standard photolithography masking approach would result in a pronounced trapezoid shape of the waveguide cross-section for thick structures, whereas exposure from the bottom resulted in a slightly negative trapezoid shape. This negative trapezoid shape compensates the temperature gradient during the post bake and the slightly different development rates on the waveguide top and bottom, resulting in a more rectangular cross-section compared to standard proximity exposure. As a result, three wafers were produced, each containing waveguide structures made of OrmoClear, OrmoCore, and SU-8, respectively. The next stage involved outsourcing the wafer saw dicing services to DISCO HI-TEC EUROPE GmbH to divide each wafer into 16 chips measuring 13 × 18 mm. A schematic representation showing the fabricated wafer with polymer structures and the saw

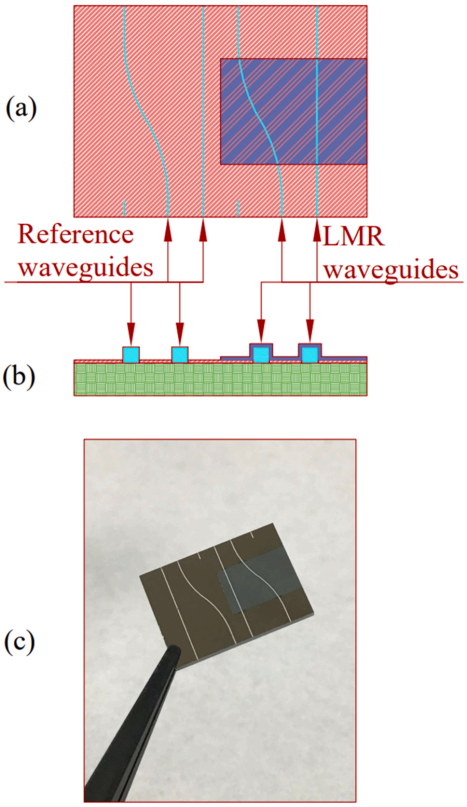

Fig. 3. The final design of the LMR chip: (a) top view, (b) cross-sectional view, (c) a photo of the actual device.

dicing pattern is provided in the Fig. 1. Each chip on the wafer contains both straight and curved waveguides to explore the dependency of the LMR phenomenon on waveguide geometry.

Our recent research [30] about LMR in planar waveguides highlighted indium tin oxide (ITO) as the most suitable material among the commonly used options due to its ability to produce profound LMRs across the entire visible spectrum. Consequently, for our integrated LMR chips, we opted for ITO as the lossy coating. Upon receipt of the diced wafer, the deposition of ITO coating over each fabricated chip was performed using the Sidrabe G500M DC magnetron sputtering system. The ITO coating process utilized an ITO (In_2O/SnO_2 with a weight ratio of 9:1) target measuring 100 × 200 × 9 mm, at a pressure of 5 mTorr and a power of 200 W using Ar plasma. To enable selective area deposition, the chip was masked with Kapton tape, facilitating the provision of both reference and LMR waveguides on the same sample. Fig. 2 illustrates the entire fabrication workflow of the LMR chip. This fabrication process yields the device depicted in Fig. 3.

Spectral ellipsometry was employed using the Woollam RC2-XL instrument and CompleteEASE software manual to assess the optical properties of the deposited ITO coating. Moreover, ellipsometry analysis was conducted to ascertain the thickness of the ITO coating over the waveguides following each deposition procedure. Measurements were conducted across the visible and near-infrared regions, covering angles of incidence ranging from 50° to 70°. This data was subsequently used to fit Lorentz oscillator [31] parameters, facilitating the calculation of the dielectric permittivity of ITO [32]:

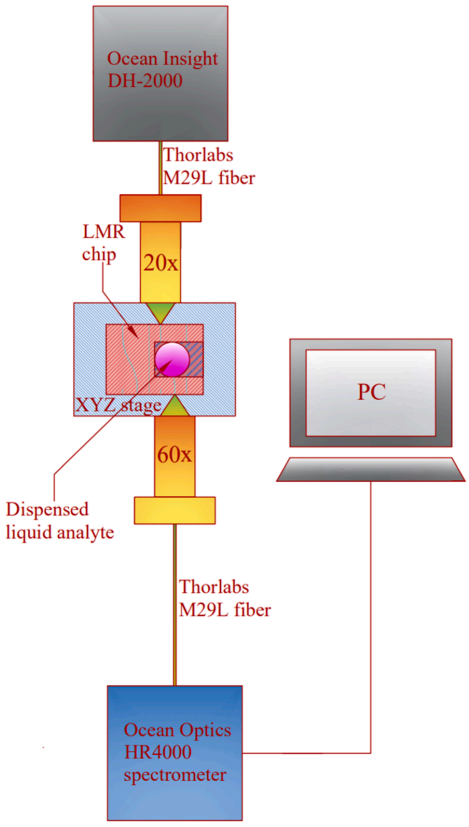

Fig. 4. Experimental setup.

$$\varepsilon = \varepsilon_\infty + \frac{Amp}{En^2 - E^2} + \sum \frac{Amp_n Br_n En_n}{En_n^2 - E^2 - iEBr_n}, \quad (1)$$

where all parameters except E are fitted parameters. The dispersion characteristics of the glass substrate were determined utilizing the Sellmeier equation [33] from CompleteEASE:

$$n = \sqrt{\varepsilon_\infty + \frac{A\lambda^2}{\lambda^2 - B^2} - E\lambda^2}, \quad (2)$$

where λ denotes the wavelength in micrometers, while A, B and E are coefficients derived through fitting. Highly precise optical properties of polymers are furnished by photoresist manufacturers ($n_{\text{Ormo}} = 1.5414 + 0.0019/\lambda^2 + 0.0013/\lambda^4$ and $n_{\text{SU-8}} = 1.5690 + 0.0088/\lambda^2 + 0.0004/\lambda^4$ for Ormo series [34] and SU-8 [35], respectively), yet information regarding the optical properties of the glass substrate and ITO was unavailable. Consequently, ellipsometry was exclusively employed for analyzing the ITO coating and glass substrate.

The Thermo Scientific™ Helios™ 5 UX high-resolution field emission scanning electron microscope (SEM) was employed to examine the cross-section of the waveguide and evaluate the homogeneity of the deposited lossy coating. Imaging procedures were carried out using an electron acceleration voltage of 2 kV and a beam current of 25 pA, with secondary electrons detected using both a through-the-lens detector (TLD) and an ion conversion and electron (ICE) detector. To counteract charging effects during imaging, scan interlacing and integration

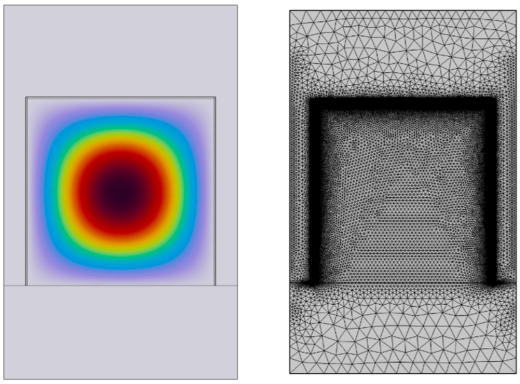

(a) (b)

Fig. 5. 2D cross-section geometry in COMSOL simulation: (a) example of electromagnetic field distribution in a polymer waveguide, and (b) user-controlled mesh.

methods were applied. To explore the waveguide cross-section within the region of the lossy coating via SEM analysis, samples were initially scribed from the underside of the substrate using a diamond scriber RV-129 and then fractured using a cleaving tool. Although this method poses the risk of causing localized damage to the polymer waveguides and introducing contamination, it was deemed appropriate for the cross-sectional analysis of the devices.

To characterize the LMR spectrum of the produced devices, a custom-built experimental setup was utilized. Light emanating from an Ocean Insight DH-2000 source was directed through an optical fiber (Thorlabs M29L) and then coupled into the sample. The resulting signal was collected via an optical fiber and analyzed using the Ocean Optics HR4000 spectrometer. Measurements were conducted for both the fabricated devices and planar waveguides to compare the behavior of the PICs with a well-established configuration. In the case of planar waveguides, light was directly coupled from the fiber into the glass substrate from the side, and the outgoing light was similarly collected through the fiber. This method has previously proven effective in our previous work on LMR in planar waveguides [30]. Typically, LMR measurement setups include polarizers to separate TE and TM modes. However, for this study, it was decided not to employ such optical elements to avoid signal reduction, which is crucial for integrated waveguides. In the case of devices based on waveguides, the light was focused onto the waveguide facet using a 20x microscope objective, and the output light was subsequently coupled back into the fiber using a 60x microscope objective (refer to Fig. 4). The LMR chip was positioned on XYZ stage to ensure precise light coupling.

The performance of the designed device was simulated using COMSOL Multiphysics. Initially, a two-dimensional cross-sectional geometry was established to analyze the electromagnetic distribution of guided modes within 100 × 100 μm polymer waveguides (refer to Fig. 5a). Following this, various materials were defined, including glass substrate, ITO, SU-8, OrmoClear, OrmoCore, and the sensing mediums. The optical properties of ITO and the glass substrate were established via spectral ellipsometry, whereas the optical properties of the other materials were sourced from provided data sheets. The "Electromagnetic Waves, Frequency Domain" physics module was employed to address the defined issues. Meshing of the geometry was performed with user-controlled element sizes: the lossy coating domain, being the most tiny structure, was meshed with element sizes less than 50 nm; the waveguide domain was meshed with element sizes less than 1 μm, and the remaining domains were meshed with element sizes less than 10 μm.

Table 2
Materials fitted parameters.

Material	Fitted parameters
ITO	$\varepsilon_\infty = 2.32$, $Amp = 71.43\ eV^2$, $En = 7.33\ eV$, $Amp_1 = 3.71$, $Br_1 = 0.37\ eV$, $En_1 = 3.86\ eV$, $Amp_2 = 40.57$, $Br_2 = 0.06\ eV$, $En_2 = 0.52\ eV$.
Glass	$\varepsilon_\infty = 1.00$, $A = 1.17$, $B = 0.09\ \mu m^2$, $E = 0.01\ \mu m^{-2}$.

The mesh comprised 260,000 triangular elements and 10,000 edge elements, covering an area of $2{\cdot}10^{-8}$ m^2, with the majority of elements situated in the thin film structure (refer to Fig. 5b). A parametric sweep was conducted to explore various coating thicknesses and materials. Calculations were performed within a spectral range from 500 nm to 900 nm due to poor transmittance outside this range for polymer structures.

Mode analysis was conducted to examine the distribution of the electromagnetic field in the polymer waveguide, facilitating the assessment of the effective refractive index n_{eff}. This parameter was subsequently utilized to simulate transmittance spectra using equation [36]:

$$T = \exp\left(-\frac{4\pi}{\lambda}\,\text{imag}(n_{\text{eff}})L\right), \tag{3}$$

where T represents transmittance, λ stands for wavelength, and L represents the length of the sensing region, which is 1 cm.

3. Results and discussion

The optical properties acquired through spectral ellipsometry, which were subsequently utilized in simulations, are presented in the Table 2.

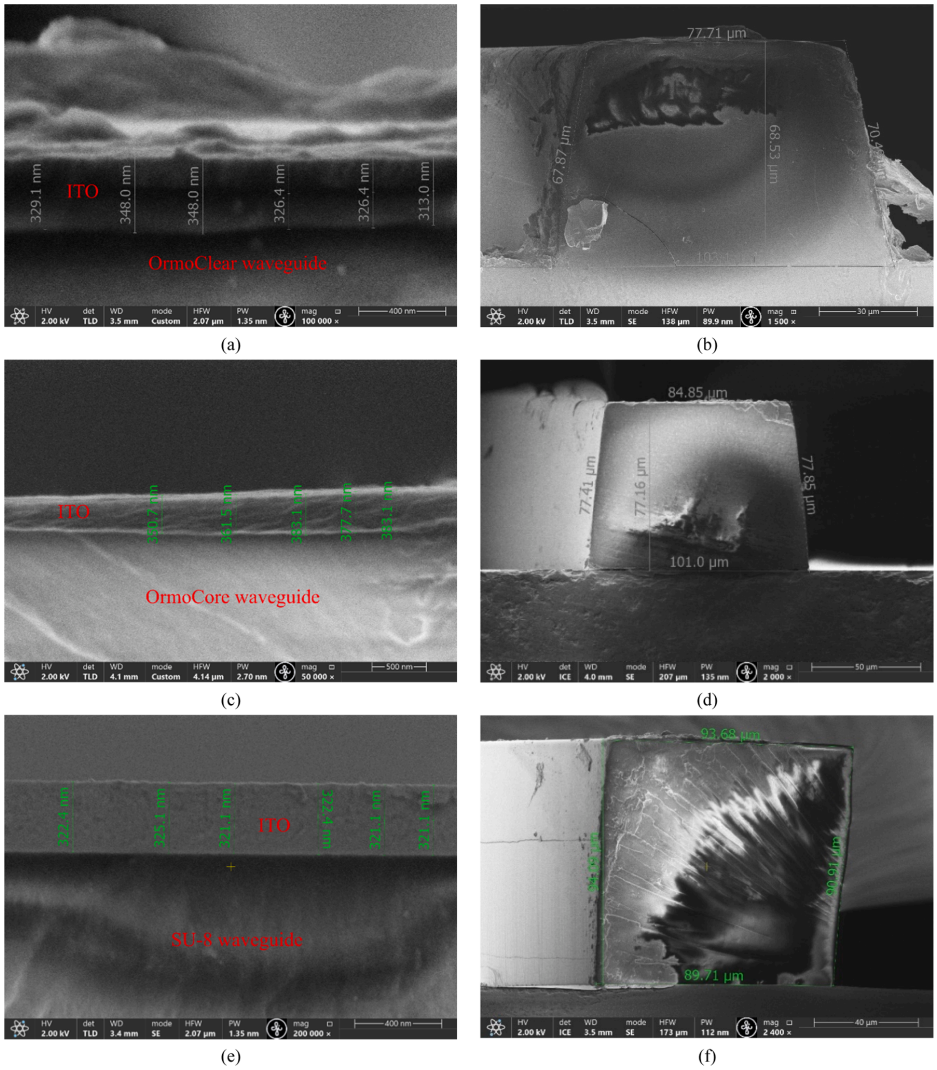

Fig. 6. SEM analysis: (a) ITO on an OrmoClear waveguide, (b) cross-section of an OrmoClear waveguide, (c) ITO on an OrmoCore waveguide, (d) cross-section of an OrmoCore waveguide, (e) ITO on a SU-8 waveguide, and (f) cross-section of a SU-8 waveguide.

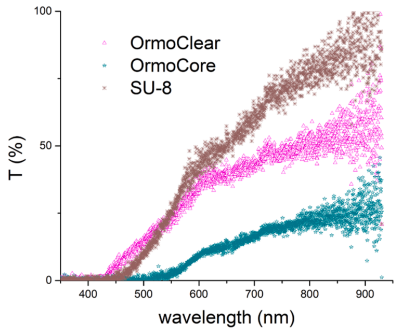

Fig. 7. Different polymer waveguide transmittance performance.

Scanning electron microscopy revealed that the cross-sectional shape of the waveguides closely resembled a square type (refer to Fig. 6), particularly evident in the SU-8 waveguide, thereby validating the success of proposed novel photolithography technique in fabricating thick waveguides. For OrmoClear and OrmoCore waveguides, the cross-sectional shape still retains a slight trapezoidal form, likely attributable to the liquid state of the photoresist following the soft bake process. Analysis of SEM images indicates slight dimensional variations among the OrmoClear, OrmoCore, and SU-8 waveguide structures, potentially impacting the output signal power. These dimensional and shape differences may partly account for the observed variations in transmittance power across different polymers. Additionally, SEM was employed to assess the uniformity of the ITO coating. Thickness variations in the ITO coating were approximately 4 % for OrmoClear and OrmoCore waveguides, while for SU-8, it was less than 1 %. As depicted in Fig. 6e, the edge of the SU-8 waveguide appears flatter and smoother compared to OrmoClear and OrmoCore waveguides (refer to Fig. 6a and Fig. 6c, respectively), which may contribute to the more homogeneous thin film growth on the surface of the SU-8 waveguide.

Fig. 7 demonstrates the ability of various polymer waveguides to effectively transmit the entire spectrum of the light source. All acquired spectra were normalized to the spectrum of the light source. It is evident that SU-8 and OrmoClear waveguides exhibit similar transmittance performance over a 100 ms integration time, while the OrmoCore waveguide shows significantly lower performance, as expected given its intended application. OrmoCore waveguides are designed for use in data communication wavelengths, hence higher losses were anticipated. Conversely, OrmoClear waveguides are optimized for efficiency in the visible and near-UV regions, resulting in superior transmission, particularly below 500 nm, even outperforming SU-8 waveguides. However, for wavelengths beyond 500 nm, SU-8 waveguides display slightly better performance. Furthermore, the working wavelength range spans from 500 nm to 900 nm, indicating that all subsequent spectra and theoretical calculations will be precisely conducted within this range. This can be attributed to the high optical losses for wavelengths below 500 nm and the low output light intensity of the source for wavelengths above 900 nm, evident from the significantly higher background noise compared to the rest of the spectrum. In fabricated devices, optical power losses occur from various sources, including light coupling from the optical fiber to the waveguide, scattering and absorption within the polymer waveguide, and bending losses. In the optimal wavelength range around 800 nm, optical power losses are 2.3 dB/cm, 4.6 dB/cm and 1.0 dB/cm for OrmoClear, OrmoCore and SU-8 waveguides, respectively. The wavelength thresholds are 440 nm, 470 nm, and 550 nm for the OrmoClear, SU-8, and OrmoCore waveguides, respectively.

The Fig. 8a provides a comparison of LMRs observed in both straight and curved waveguides for OrmoClear and SU-8 polymers. It is evident that, regardless of the waveguide geometry, the depth of LMR peaks and the full width at half minimum (FWHM) are similar for polymer both waveguides. In essence, the LMR behavior in waveguides with curved geometry does not differ from those with straight geometry, suggesting no requirement for additional testing of both configurations, leading to the decision to focus measurements exclusively on straight waveguides due to their lower optical losses. It is worth noting that comparison data for OrmoCore waveguides are not depicted in Fig. 8a due to their notably lower transmittance and the complexities associated with observing LMRs in curved waveguides. However, LMRs were observable for all explored straight polymer waveguides, including OrmoCore, when utilizing a 540 nm thick ITO coating. The transmittance spectra for these devices are provided in the Fig. 8b. It is worth noting that at an ITO coating thickness of 80 nm, only first-order LMR is observed. It is widely known that in this LMR order the resonance lines for TE and TM polarizations are separated even without the use of a linear polarizer (refer to Fig. 8a) [11]. However, for higher-order LMRs, the resonance lines of TE and TM polarizations become closer to each other with each subsequent order. As a result, observing TE and TM resonances separately

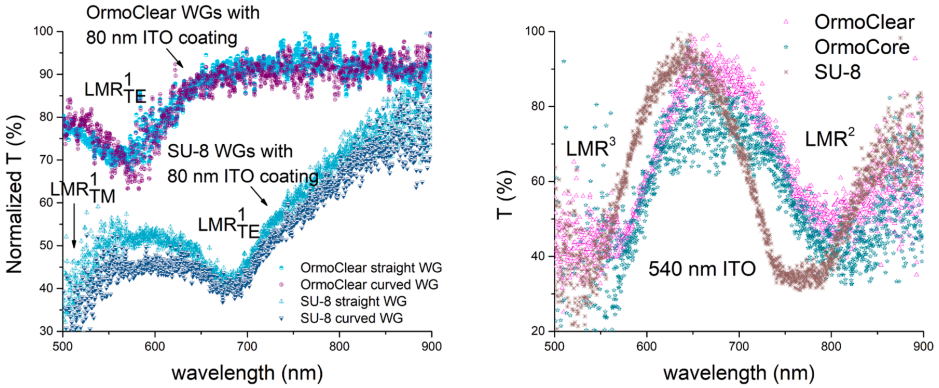

Fig. 8. Comparison of LMR in different types of waveguides: (a) comparison in straight and curved waveguide, and (b) comparison in waveguides of different polymers.

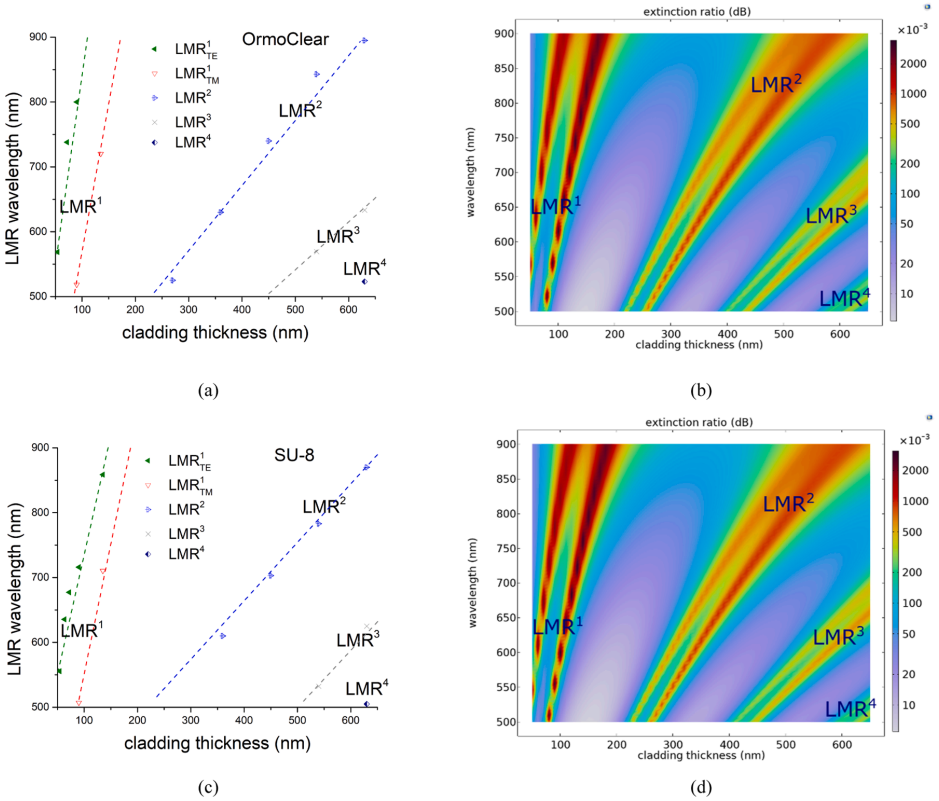

Fig. 9. LMRs in dependence of wavelength and ITO thickness: (a) experimental results for OrmoClear waveguides, (b) theoretical results for OrmoClear waveguides, (c) experimental results for SU-8 waveguides, and (d) theoretical results for SU-8 waveguides.

without using a linear polarizer becomes impossible. Therefore, in Fig. 8b, only the LMR order can be identified, but not the polarization in which the resonance was observed. In addition, Fig. 8 shows that the LMR wavelengths differs slightly between the SU-8 and Ormo series polymers, which is explained by slight differences in their refractive indices. Conversely, LMRs in the OrmoClear and OrmoCore waveguides occur at similar wavelengths, as expected theoretically due to their nearly identical refractive indices (refer to Fig. 8b).

Comparing experimental results with simulations commonly involves utilizing color plots spanning various cladding thicknesses. This method provides a comprehensive assessment of whether the theoretical model effectively matches the physics of the LMR phenomenon in fabricated devices. Theoretical calculations of extinction ratios corresponding to different ITO coating thicknesses are depicted as a function of wavelength in the Fig. 9. Again, for both SU-8 and OrmoClear polymer waveguides, experimentally obtained separated TM and TE polarizations were achieved only for the first-order LMR, whereas for higher-order LMRs, these modes overlap and manifest as a single peak. The experimental setup did not utilize a polarizer to differentiate between different guided modes. Conversely, mode analysis in COMSOL Multiphysics simulates each mode independently, hence theoretically, two resonances were expected for every LMR order. These disparities between theoretical predictions and experimental findings constitute the main differences. The minor deviations of the resonant wavelengths are due to the inhomogeneity and roughness of the ITO coating, which was theoretically demonstrated in our previous study [30]. For OrmoCore waveguides, such dependencies were challenging to ascertain due to the difficulties in observing LMRs for every cladding thickness - most cases encountered critical losses, impeding the generation of LMRs.

For sensitivity assessment, a device utilizing SU-8 waveguides was chosen for its lower optical losses, facilitating the evaluation of sensitivity characteristics. Various liquids were applied to the sensing area to monitor the shift in the LMR. The precise determination of LMR peak shapes and resonance wavelengths proved challenging due to signal noise, particularly in TM polarization (refer to Fig. 10a). Consequently, Gaussian approximations were employed to estimate the acquired spectra, streamlining the analysis process. Fig. 10a and Fig. 10b depict the first-order LMRs for SU-8 waveguides and planar waveguides, respectively. For the first-order LMRs, an 80 nm thick ITO coating was selected because at this thickness, both TE and TM mode resonances are observable within the operational wavelength range of 500 nm to 900 nm when measuring signals in a liquid environment. The sensitivity and FWHM for both configurations exhibit notable similarity, proving competitive performance between integrated waveguides and the well-established planar waveguide design. This trend extends to higher-order LMRs, as observed in Fig. 10c and d. For higher-order LMRs, a 630 nm thick ITO coating was selected because it enables the simultaneous observation of the largest number of LMRs (LMR [2], LMR [3], and LMR [4]) within the operational wavelength range. Thinner coatings allow only LMR [2] and LMR [3] to be observed simultaneously. Given the significantly higher sensitivity for first-order LMRs, sensitivity measurements were conducted using liquids with refractive indices ranging

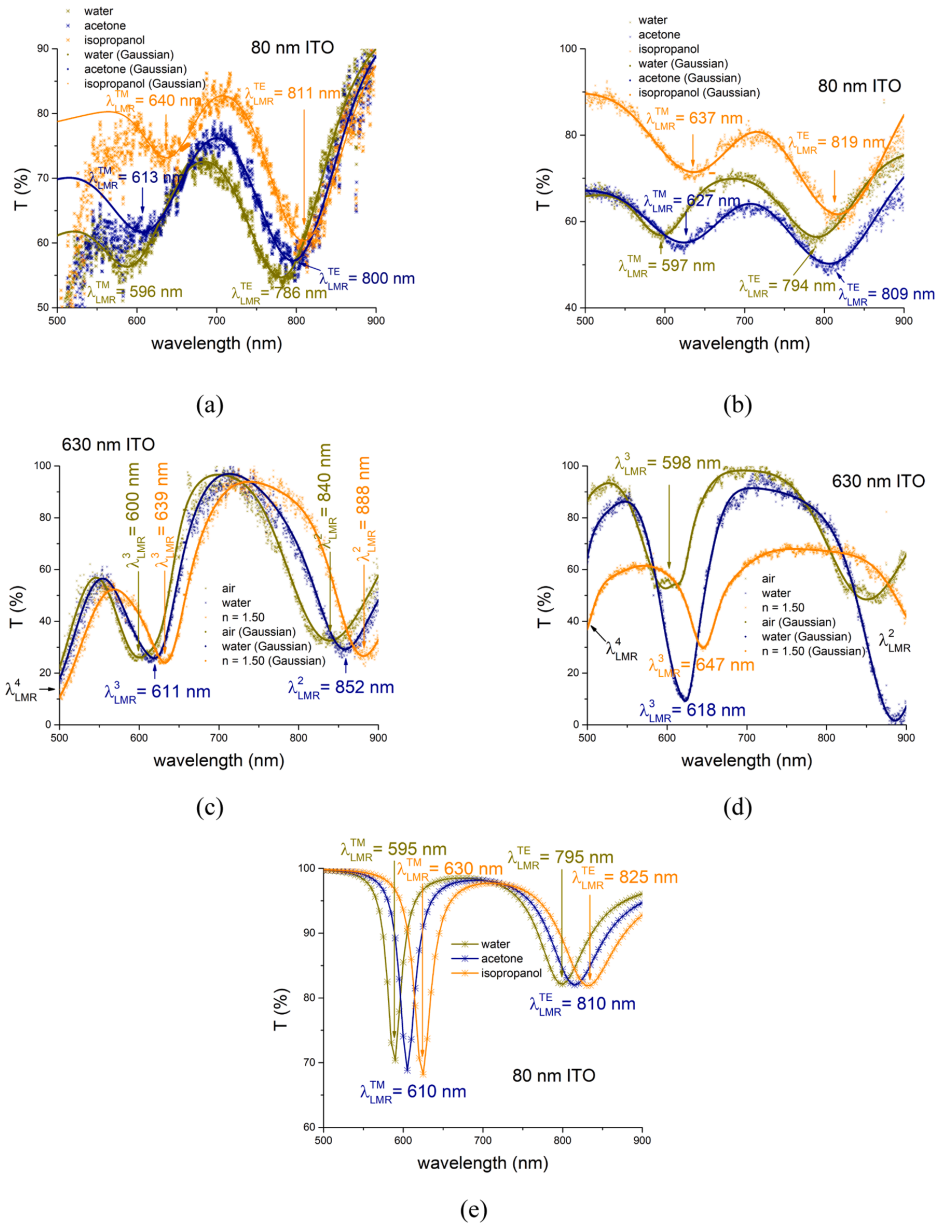

Fig. 10. Experimental sensing response in various liquids: (a) first-order LMRs in an integrated device based on SU-8 waveguides, (b) first-order LMRs in a planar glass waveguide, (c) higher-order LMRs in an integrated device based on SU-8 waveguides, (d) higher-order LMRs in a planar glass waveguide, and (e) theoretically calculated first-order LMRs in an integrated device based on SU-8 waveguides.

from 1.33 to 1.39, while for higher-order LMRs, sensitivity measurements encompassed environments with refractive indices ranging from 1.00 to 1.50. Simulations were also conducted for SU-8 waveguide coated with an 80 nm thick layer of ITO to compare the theoretical performance of the device with the experimental results (refer to Fig. 10e). While slightly different LMR wavelengths and peak shapes were anticipated theoretically compared to those obtained experimentally, these differences were minor. Surprisingly, the observed experimental sensitivity was higher than theoretically expected. This can be explained by small differences in the optical dispersion of the medium specified in the simulation compared to the real data. The first-order LMRs as a function of the refractive index of the medium for both TM and TE polarizations for the SU-8 waveguide and the planar waveguide are shown in the Fig. 11. As evident from the data, the

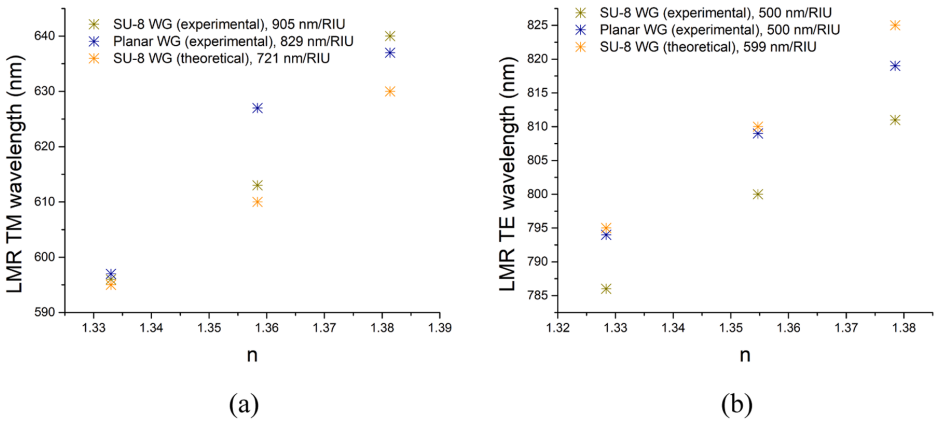

Fig. 11. First-order LMR sensing performance: (a) TM mode, and (b) TE mode.

Table 3
Sensor sensitivities and FOMs.

Analysis	Waveguide type	$S, \frac{\text{nm}}{\text{RIU}}$	FOM, RIU^{-1}
Experimental	SU-8, TM mode	905	23
	SU-8, TE mode	500	10
	Planar, TM mode	829	21
	Planar, TE mode	499	10
Theoretical	SU-8, TM mode	721	25
	SU-8, TE mode	599	12

sensitivity for TM mode considerably surpasses that of TE mode in both theoretical and experimental observations, consistent with expectations outlined in the literature [37].

The primary standardized parameter that characterizes the overall performance of a sensing device is the figure of merit (FOM) [38], defined by the equation:

$$\text{FOM} = \frac{S}{\text{FWHM}}, \tag{4}$$

where S represents the slope of the function $\lambda_{\text{LMR}} = f(n)$. The calculated FOMs and sensitivities for the fabricated device based on SU-8 waveguide, planar waveguide, and theoretically simulated device based on SU-8 waveguide are summarized in the Table 3. Given that first-order LMRs are known for higher sensitivity and FOM, it was decided to focus specifically on this order LMRs and not consider higher-order LMRs. It is evident that the sensitivities and FOMs for both integrated SU-8 waveguides and planar waveguides exhibit remarkable similarity, underscoring the competitiveness and promise of integrated waveguides in the field of LMR. In fact, the TM mode sensitivity achieved in the SU-8 waveguide surpasses that of the planar waveguide by 8 %, with values of 905 nm/RIU compared to 829 nm/RIU. The theoretically calculated and experimentally obtained FOMs for device based on SU-8 have very similar values. The experimental sensitivity in TM mode exceeded the theoretical prediction. However, the experimentally obtained FWHM was broader as a consequence of the thickness variations confirmed in our recent research [30], leading to nearly identical FOM values.

4. Conclusions

This study marks a significant advancement, showcasing the LMR effect for the first time within integrated on-chip hybrid organic-inorganic systems. This achievement represents substantial progress not only in the field of LMR but also in the broader field of photonics. The main novelty of this research is the successful observation of the LMR phenomenon in different types of integrated polymer waveguides covering different materials (OrmoClear, OrmoCore and SU-8) as well as geometries (straight and curved). Among the tested materials, SU-8 emerged as better polymer at guiding the entire visible light spectrum, thereby facilitating more pronounced LMRs compared to other polymer materials. Moreover, it was demonstrated that waveguide geometry has minimal impact on LMR, except for a decrease in light intensity observed in curved waveguides due to bend losses.

With the exception of OrmoCore, every tested polymer material exhibited LMR dependence on cladding thickness and resonance wavelength consistent with predictions from theoretical simulations conducted via COMSOL Multiphysics. The primary differences arose from the measurement setup, which did not employ a linear polarizer. Consequently, it was not feasible to observe TM and TE modes separately for higher-order LMRs, as predicted by theoretical calculations. Additionally, experimentally obtained FOM closely aligned with simulated predictions.

This article introduces a novel fabrication method for thick waveguides, involving exposure through the glass substrate and aluminum mask positioned directly on the chip. This technique yields waveguides with a more rectangular cross-sectional profile, and in the case of SU-8 waveguides, it even resulted in a slightly negative trapezoidal shape. This approach enables the production of high-quality waveguides capable of propagating light to observe LMR, a capability not achievable with other fabrication techniques.

The FOM and sensitivity performance of integrated polymer-based devices and planar waveguides showed similarity for both setups, highlighting the promising potential of integrated systems in the LMR field. Integrated waveguides, in contrast to planar counterparts, exhibit enhanced flexibility, indicating that continued development in this direction could position them as dominant alternatives to planar waveguides and fiber-based configurations.

A key advantage of photonic integrated circuits lies in their ability to integrate diverse elements on a single chip to deliver unique functionalities. The next stage in the development of integrated LMR sensors could involve integrating them with spectrometers and on-chip light sources, thereby significantly reducing device costs.

Author agreement statement

We the undersigned declare that this manuscript is original, has not been published before and is not currently being considered for

publication elsewhere.

We confirm that the manuscript has been read and approved by all named authors and that there are no other persons who satisfied the criteria for authorship but are not listed. We further confirm that the order of authors listed in the manuscript has been approved by all of us.

We understand that the Corresponding Author is the sole contact for the Editorial process. He/she is responsible for communicating with the other authors about progress, submissions of revisions and final approval of proofs

CRediT authorship contribution statement

Edvins Letko: Writing – original draft, Methodology, Investigation, Formal analysis, Conceptualization. **Arturs Bundulis:** Writing – review & editing, Methodology. **Edgars Vanags:** Visualization. **Gatis Mozolevskis:** Writing – review & editing, Supervision.

Declaration of competing interest

The authors declare the following financial interests/personal relationships which may be considered as potential competing interests: Edvins Letko reports financial support and article publishing charges were provided by University of Latvia Institute of Solid State Physics. If there are other authors, they declare that they have no known competing financial interests or personal relationships that could have appeared to influence the work reported in this paper.

Data availability

Data will be made available on request.

Acknowledgment

The authors would like to acknowledge the Institute of Solid State Physics, University of Latvia. This research was supported by the European Regional Development Fund project 1.1.1.1/20/A/045 and the European Union's Horizon 2020 Framework Program H2020-WIDESPREAD-01-2016-2017-TeamingPhase2 under grant agreement No. 739508, project CAMART2. This work was supported by National Research Program 'Smart Materials, Photonics, Technologies and Engineering Ecosystem' (project No. VPPEM-FOTONIKA-2022/1-0001).

References

[1] Ali L, Mohammed MU, Khan M, Yousuf AHB, Chowdhury MH. High-quality optical ring resonator based biosensor for cancer detection. IEEE Sens J 2019;1(C): 1867–75. https://doi.org/10.1109/JSEN.2019.2950664. *PP*.

[2] Inan H, Poyraz M, Inci F, Lifson MA, Baday M, Cunningham BT, Demirci U. Promise for point-of-care applications. Chem Soc Rev 2016:366–88. https://doi.org/10.1039/C6CS00206D.

[3] Ramirez JC, Grajales García D, Maldonado J. Fernández-Gavela, A. Current trends in photonic biosensors: advances towards multiplexed integration. Chemosensors 2022;10(10):398–420. https://doi.org/10.3390/chemosensors10100398.

[4] Wang Q, Zhao WM. A comprehensive review of lossy mode resonance-based fiber optic sensors. Opt Lasers Eng 2018;100(July 2017):47–60. https://doi.org/10.1016/j.optlaseng.2017.07.009.

[5] Sánchez P, Zamarreño CR, Arregui FJ, Matías IR. LMR-based optical fiber refractometers for oil degradation sensing applications in synthetic lubricant oils. J Light Technol 2016;34(19):4537–42. https://doi.org/10.1109/JLT.2016.2562701.

[6] Zamarreño CR, Hernáez M, Del Villar I, Matías IR, Arregui FJ. Optical fiber PH sensor based on lossy-mode resonances by means of thin polymeric coatings. Sens Actuators, B Chem 2011;155(1):290–7. https://doi.org/10.1016/j.snb.2010.12.037.

[7] Zamarreño CR, Hernaez M, Del Villar I, Matias IR, Arregui FJ. Tunable Humidity sensor based on ITO-coated optical fiber. Sens Actuators, B Chem. 2010;146(1): 414–7. https://doi.org/10.1016/j.snb.2010.02.029.

[8] Elosúa C, Vidondo I, Arregui FJ, Bariain C, Luquin A, Laguna M, Matías IR. Lossy mode resonance optical fiber sensor to detect organic vapors. Sens Actuators, B Chem 2013;187:65–71. https://doi.org/10.1016/j.snb.2012.09.046.

[9] Del Villar I, Zamarreño CR, Hernaez M, Arregui FJ, Matias IR. Lossy mode resonance generation with indium-tin-oxide-coated optical fibers for sensing applications. J Light Technol 2010;28(1):111–7. https://doi.org/10.1109/JLT.2009.2036580.

[10] Fuentes O, Goicoechea J, Corres JM, Villar IDel, Ozcariz A, Matias IR. Generation of lossy mode resonances with different nanocoatings deposited on coverslips. Opt Express 2020;28(1):288–301. https://doi.org/10.1364/oe.28.000288.

[11] Fuentes O, Del Villar I, Corres JM, Matias IR. Lossy mode resonance sensors based on lateral light incidence in nanocoated planar waveguides. Sci Rep 2019;9(1): 1–10. https://doi.org/10.1038/s41598-019-45285-x.

[12] Arregui FJ, Villar IDel, Corres JM, Goicoechea J, Carlos R, Elosua C, Hernaez M, Rivero PJ, Socorro AB, Sanchez P, Zubiate P, Lopez D, Acha NDe. Matias, I. R. Fiber-optic lossy mode resonance sensors. Procedia Eng 2014;87:3–8. https://doi.org/10.1016/j.proeng.2014.11.253.

[13] Refractometer, F.; Sudas, D. P.; Zakharov, L. Y.; Jitov, V. A.; Golant, K. M. Silicon oxynitride thin film coating to lossy mode resonance. 2022, 1–12.

[14] Letko E, Bundulis A, Mozolevskis G. Theoretical development of polymer-based integrated lossy-mode resonance sensor for photonic integrated circuits. Photonics 2022;9(10):764–73. https://doi.org/10.3390/photonics9100764.

[15] Li A, Yao C, Xia J, Wang H, Cheng Q, Penty R, Fainman Y, Pan S. Advances in cost-effective integrated spectrometers. Light Sci Appl 2022;11(1):1–18. https://doi.org/10.1038/s41377-022-00853-1.

[16] Zhou Z, Yin B, Michel J. On-Chip light sources for silicon photonics. Light Sci Appl 2015;4(11):1–13. https://doi.org/10.1038/lsa.2015.131.

[17] Eldada, L.; Member, S.; Shacklette, L. W. Advances in polymer integrated optics. 2000, 6 (1), 54–68.

[18] Paquet, C.; Kumacheva, E. Polymers for photonics. 2008, 11 (4), 48–56.

[19] Search, H.; Journals, C.; Contact, A.; Iopscience, M.; Address, I. P. SU-8: a low-cost negative resist For MEMS. 1997, 121–124.

[20] Eryürek M, Tasdemir Z, Karadag Y, Anand S, Kilinc N, Alaca BE, Kiraz A. Integrated humidity sensor based on SU-8 polymer microdisk microresonator. Sensors Actuators, B Chem 2017;242:1115–20. https://doi.org/10.1016/j.snb.2016.09.136.

[21] Zhao Y, Grischkowsky DR. 2-D terahertz metallic photonic crystals in parallel-plate waveguides. IEEE Trans Microw Theory Tech 2007;55(4):656–63. https://doi.org/10.1109/TMTT.2007.892798.

[22] Ji L, Sun X, He G, Liu Y, Wang X, Yi Y, Chen C, Wang F, Zhang D. Surface plasmon resonance refractive index sensor based on ultraviolet bleached polymer waveguide. Sens Actuators B Chem 2017;244:373–9. https://doi.org/10.1016/j.snb.2017.01.006.

[23] Nitiss E, Bundulis A, Tokmakovs A, Busenbergs J, Rutkis M. All-organic waveguide sensor for volatile solvent sensing. Photonic Sens 2019;9(4):356–66. https://doi.org/10.1007/s13320-019-0543-z.

[24] Malinauskas M, Baltriukiene D, Kraniauskas A, Danilevicius P, Jarasiene R, Sirmenis R, Zukauskas A, Balciunas E, Purlys V, Gadonas R, Bukelskiene V, Sirvydis V, Piskarskas A. In vitro and in vivo biocompatibility study on laser 3D microstructurable polymers. Appl Phys A Mater Sci Process 2012;108(3):751–9. https://doi.org/10.1007/s00339-012-6965-8.

[25] Lorang DJ, Tanaka D, Spadaccini CM, Rose KA, Cherepy NJ, Lewis JA. Photocurable liquid core-fugitive shell printing of optical waveguides. Adv. Mater. 2011;23(43):5055–8. https://doi.org/10.1002/adma.201102411.

[26] Girschikofsky M, Rosenberger M, Förthner M, Rommel M, Frey L, Hellmann R. Waveguide bragg gratings in Ormocer®s for temperature sensing. Sensors (Switzerland) 2017;17(11):1–9. https://doi.org/10.3390/s17112459.

[27] Madani A, Azarinia H, Latifi H. Design and fabrication of a polymer micro ring resonator with novel optical material at add/drop geometry using laser beam direct write lithography technique. Optik (Stuttg) 2013;124(14):1746–8. https://doi.org/10.1016/j.ijleo.2012.06.003.

[28] Liang Y, Zhao M, Wu Z, Morthier G. Bimodal waveguide interferometer RI sensor fabricated on low-cost polymer platform. IEEE Photonics J. 2019;11(2):1–8. https://doi.org/10.1109/JPHOT.2019.2900741.

[29] Zhao WM, Wang Q. Analytical solutions to fundamental questions for lossy mode resonance. Laser Photonics Rev 2023;17(1):1–18. https://doi.org/10.1002/lpor.202200554.

[30] Letko E, Bundulis A, Mozolevskis G. Lossy mode resonance sensors based on planar waveguides: theoretical and experimental comparison. IEEE Photonics J 2024;16 (1):1–7. https://doi.org/10.1109/JPHOT.2023.3348993.

[31] The Lorentz Oscillator Model and Beyond *Extrem. Nonlinear Opt.* 2005, 27–59. 10.1007/3-540-26688-7_3.

[32] Woollam J.A., Spectroscopic Ellipsometers C. *CompleteEASE data acquisition and analysis software for software manual*. 2011.

[33] Wei J, Murray JM, Barnes JO, Krein DM, Schunemann PG, Guha S. Temperature dependent sellmeier equation for the refractive index of GaP. In: Proceedings of the Conference Lasers Electro-Optics. 2; 2017. p. 1–3. https://doi.org/10.1364/CLEO_SI.2017.SW4M.3. *CLEO 2017 - Proc. 2017*-Janua.

[34] Prajzler V, Jašek P, Nekvindová P. Inorganic–organic hybrid polymer optical planar waveguides for Micro-Opto-Electro-Mechanical Systems (MOEMS). Microsyst. Technol. 2019;25(6):2249–58. https://doi.org/10.1007/s00542-018-4105-x.

[35] Piruska A, Bhagat AAS, Zhou K, Peterson ETK, Papautsky I, Seliskar CJ. Characterization of SU-8 optical multimode waveguides for integrated optics and sensing on microchip devices. Microfluid. BioMEMS, Med. Microsyst. IV 2006; 6112:1–9. https://doi.org/10.1117/12.655667. 611207.

[36] Kadhim, R. A.; Yuan, L.; Xu, H.; Wu, J.; Member, S.; Wang, Z. Highly sensitive D-shaped optical fibre surface plasmon resonance refractive index sensor based on Ag- α -Fe2O3 grating. 2020, 1748 (c), 1–11. 10.1109/JSEN.2020.2992854.
[37] Zhang Y, Zhang P, Zhao M, Xu D, Wang J, Li Z, Tang T, Shen J, Li C. A high sensitivity lossy mode resonance refractive index sensor based on SBS structure. Results Phys 2022;36(January):1–10. https://doi.org/10.1016/j.rinp.2022.105454. 105454.
[38] Zhao Y, Wu L, Gan S, Ruan B, Zhu J, Dai X, Xiang Y. High figure of merit lossy mode resonance sensor with graphene. Plasmonics 2019;14(4):929–34. https://doi.org/10.1007/s11468-018-0876-2.

Edvīns Ļetko dzimis 1994. gadā Rīgā. Latvijas Universitātē (LU) ieguvis bakalaura grādu fizikā, Rīgas Tehniskajā universitātē – maģistra grādu materiālu nanotehnoloģijās. Kopš 2020. gada ir LU Cietvielu fizikas institūta Mikro un nanoierīču laboratorijas pētnieks. 2022. gadā līdzdibinājis jaunuzņēmumu SIA "OG Sense", kas specializējas fotonisko čipu izstrādē sensora lietojumiem. Zinātniskās intereses saistītas ar mikroierīču un nanoierīču izstrādi un šo ierīču komercializāciju.

Edvīns Ļetko was born on January 9, 1994, in Riga. He holds a Bachelor's degree in Physics from the University of Latvia and a Master's degree in Materials Nanotechnology from Riga Technical University. Since 2020, he has been a researcher in the Micro and Nanodevices Laboratory at the Institute of Solid State Physics. In 2022, Edvīns co-founded the startup OG Sense SIA, which specializes in the development of photonic chips for sensing applications. His scientific interests are focused on the development of micro and nanodevices and the commercialization of these technologies.